UNIVERSITÀ
DEGLI STUDI
DI PADOVA

UNIVERSITÀ DEGLI STUDI DI PADOVA

DIPARTIMENTO DI INGEGNERIA INDUSTRIALE
CORSO DI LAUREA MAGISTRALE IN INGEGNERIA MECCANICA

Tesi di Laurea Magistrale in Ingegneria Meccanica

DIMENSIONAMENTO DI UN RULLO RISCALDATO AD OLIO DIATERMICO

DESIGN OF A ROLLER HEATED BY DIATHERMIC OIL

Relatore: Prof.ssa Luisa Rossetto

Correlatore: Dott. Ing. Simone Mancin

Tutor Aziendale: Dott. Ing Andreas Lewandowski

Laureando: MARCO MINTO

ANNO ACCADEMICO 2013 – 2014

ACKNOWLEDGEMENTS

I wish to thank my supervisor Prof.ssa Luisa Rossetto for the support and direction that she has given me, along with the assistance of assistant professor Ing. Simone Mancin; he gave me enormous help with understanding and analysing some project issues. To the company directors, Mr. Andreas Lewandowski and Mr. Alex Lewandowski, who gave me the opportunity to start the master thesis project by their company. I want to acknowledge all my job colleagues, who wanted me to learn German and all the wonderful people I was lucky to meet during my experience in Germany….einfach Danke!

I wish to tell all my friends that I am proud to have friends like you: Bivi, Checco, Nico, Massi, Tini, Fede, Conchi, Giuli, Pier, Joy, Lori, Alby, Ale, Boez...and many more that I'm sorry if I don't name; friends I met at the University: Villa, Jack Vettore, Davide, Balla, Gian, Giacomo, Bebo, Alby, Mirco, Bose and I special thank Marce with whom I began and finished these 5 academic years.

I wish to thank my uncle Marcello aunt Maria and my grandpa Bruno, for the interest they conveyed in following my university route.

I thank my family: Dad Claudio, Mum Michela, my two sisters Anna and Silvia, and my brother Giacomo, for their supporting me in everything I do…I like you so much!!

Finally, I would like to thank my girlfriend Silvia and her family, for her patience and encouragement and sacrifice that she has made while I was abroad to study and complete this thesis. The last dutiful thanks I say to Ago...he knows the reason!

I would like to take this opportunity to greet my godfather Stefano...goodbye (R.I.P).

ABSTRACT

This project was developed in a German company, Phoenix Technology Ltd., located in Engen, a little town in the south of Germany, closed to the more famous city of Constance. It is an engineering consulting office, with experience in designing mechanical solutions basically in the field of agriculture machines, but it also ranges over many different engineering branches.

This work attempts to design a heating roller involved in many applications such as textile, paper, plastic, metal, wood technologies and others. The roll is heated by diathermic oil flowing through two helically coiled pipes generated inside it. The oil, in turn, is heated up by two heating cartridges placed at the two roller edges, each one is fed by the oil coming out from one spire and having the minimum temperature after it exchanges the required heat for the process.

A combination of analytical formulations and Finite Element (FEA) software (Ansys Workbench Release 14, Thermal) was used to build up a model to understand the influence of the main parameters effecting the temperature distribution over the outer roller surface. Examples from every project step were modelled using FEA, which was found to accurately simulate theoretical results in most cases. Moreover, the project was developed trying to improve the model quality, step by step, in order to better reproduce process conditions: in undertaking this work, a heating roll in still air was analysed; afterwards the influence of the external web was taken into account, first of all by considering the whole outer roller surface covered by it and, then, only a more realistic partial covering.

SOMMARIO

Il progetto di tesi è stato svolto in un'azienda tedesca, Phoenix Technology Ltd., che si trova nella cittadina di Engen, a sud della Germania, vicino alla più famosa città di Costanza. Si tratta di uno studio di consulenza ingegneristica, con esperienza nella progettazione di soluzioni meccaniche nel settore delle macchine agricole, ma spazia anche in altri campi dell'ingegneria.

Con questo lavoro si tenta di progettare un rullo riscaldante che viene usato in molte applicazioni quali nella tecnologia tessile, della carta, del metallo, del legno e altre ancora. Il rullo viene riscaldato utilizzando olio diatermico che fluisce attraverso due tubi elicoidali generati internamente al rullo stesso. L'olio, a sua volta, è riscaldato da due cartucce elettriche poste alle estremità del rullo; ognuna è alimentata dall'olio stesso proveniente da una delle due spire interne e avente temperatura minima dopo aver ceduto il calore al rullo e al tessuto.

La combinazione di procedure analitiche e semiempiriche e di simulazioni effettuate col software agli elementi finiti (Ansys Workbench Release 14, Termico), ha permesso di comprendere l'influenza dei principali parametri che regolano la distribuzione di temperatura sulla superficie esterna del rullo.

In ogni fase del progetto i casi di studio sono stati modellati attraverso l'analisi agli elementi finiti, che risulta accurata nella simulazione di risultati teorici. Il progetto, inoltre, è stato sviluppato cercando di migliorare la qualità del modello, passo dopo passo, al fine di riprodurre al meglio le condizioni di processo. In una prima fase è stato analizzato il rullo riscaldante posto in aria calma; dopodiché si è tenuta in considerazione l'influenza del tessuto esterno, all'inizio considerando una copertura totale della superficie esterna e, poi, una copertura solo parziale ma più realistica.

TABLE OF CONTENTS

LIST OF TABLES ix

LIST OF FIGURES xiii

CHAPTER 1: Introduzione 1

CHAPTER 2: Introduction 5

2.1 Applications 7

CHAPTER 3: Problem description; roller exposed to the ambient 17

3.1 Step description 17

3.2 Preliminary design of the roller 18

3.2.1 Physical model definition 18

3.2.2 Analytical calculation on the roller surface 22

3.2.3 Analytical calculation on the spires, laminar flow. 23

3.3 Numerical simulation: model and geometry 29

3.4 Results of the first step analysis 33

CHAPTER 4: Project requirement 37

4.1 Step description 37

4.2 Variable project parameters. 38

4.2.1 Analysis 1 38

4.2.2 Analysis 2 45

4.2.3 Analysis 3 48

4.2.4 Analysis 4 51

4.3 Customer requirements 54
4.3.1 Current solution: 55
4.3.2 Oil flow rate selection 55
4.4 Selection of the hydraulic diameter 57
4.5 Variable oil heat transfer coefficient 67
4.6 Selection of the number of turns 72
4.6.1 Effect of the number of turns on the heat flow rate. 72
4.6.2 Variation of heat flow rate with fixed number of turns. 76

CHAPTER 5: Refining of the model: two heat transfer surfaces 83
5.1 Step description 83
5.2 Optimization of q = 30 kW 84
5.2.1 Preparing the analytical model 84
5.2.2 Analytical results 90
5.2.3 Numerical model and results 93
5.2.4 New wall temperature and new results 96
5.3 Check the model 99
5.3 Variation of heat flow rate with fixed number of turns. 106

CHAPTER 6: Rolling roller 119
6.1 Step description 119
6.2 External heat transfer coefficient. 120
6.2.1 Cotton side 121
6.2.2 Ambient side 122
6.3 Heating up of the textile. 123
6.3.1 Piece of textile 124
6.3.2 Optimization of temperature on the outer layer 130

CONCLUSIONS 133

REFERENCES 137

LIST OF TABLES

Table 3.1 Thermo-physical properties of the air at different ambient temperature. 22
Table 3.2 Study cases at different mean oil temperature. 24
Table 3.3 Geometrical properties of the model 27
Table 3.4 Oil properties at the wall temperature and at the mean oil. 28
Table 3.5 Iterations for the calculation of the convection coefficient inside the tube at the average oil temperature. 28
Table 3.6 Results obtained with stainless steel. 34
Table 3.7 Results obtained with Aluminium Alloy. 34
Table 4.1 Parameter setting of the Excel spreadsheet: "Analysis 1" 39
Table 4.2 "Analysis 1": results with q = 3 kW (case 1). For each value of n (number of turns) the results vary as a function of the inlet oil temperature. 40
Table 4.3 Oil properties at 140°C 41
Table 4.4 Oil properties at the average oil temperature. 41
Table 4.5 Oil properties at the average oil temperature and at each step-iteration. 42
Table 4.6 Example of iteration used for the Excel spreadsheet: "Analysis 1". 43
Table 4.7 Parameter setting of the Excel spreadsheet: "Analysis 2" 45
Table 4.8 "Analysis 2": results with Tin = 148 °C (case 1). For each value of n (number of turns) the results vary as a function of the oil flow rate. 46
Table 4.9 Parameter setting of the Excel spreadsheet: "Analysis 3" 48
Table 4.10 "Analysis 3": results with $m = 5\ l\ min - 1$ and q = 3,5 kW (case 2). For each value of n (number of turns) the results vary as a function of outer surface temperature. 49
Table 4.11 Parameter setting of the Excel spreadsheet: "Analysis 4" 52
Table 4.12 "Analysis 4": results with $m = 5\ l\ min - 1$ and $Tsur$ = 140 (case 1). For each value of n (number of turns) the results vary as a function of heat flow rate. 52
Table 4.13 First trial of parameter sets. Focusing on customer requirements. 57
Table 4.14 geometrical properties of the first parameter set. 58
Table 4.15 Results in term of inlet oil temperature and oil flow rate related to the critical Reynolds number. 58
Table 4.16 Results by the turbulent-based analysis of the two models. 59
Table 4.17 General guidelines for limit tube velocities based on tube material. [6] 61
Table 4.18 Results by the turbulent-based analysis of the two models with the new hydraulic diameter. 63
Table 4.19 Pressure drop in one spire calculated for the cases of study with different hydraulic diameter and number of turns. 64
Table 4.20 Results by the turbulent-based analysis of the models characterized by n = 23 and the two different hydraulic diameter. 64
Table 4.21 Pressure drop in one spire calculated for the cases with the two different hydraulic diameter and n=23. 65
Table 4.22 Results obtained from the FEM simulations of the three different number of turns and the first hydraulic diameter dh = 11,93 mm 66
Table 4.23 Results obtained from the FEM simulations of the three different number of turn and the first hydraulic diameter dh =14,27 mm 66

Table 4.24 Average oil temperature at each part of the spire used for calculating the variable heat transfer coefficient. 68
Table 4.25 Oil properties at each average temperature. The oil temperature drop is divided in 10 parts in order to calculate the variable heat coefficient along the spire. 68
Table 4.26 Oil properties at the wall temperature. 68
Table 4.27 Oil flow rate and Reynolds Number for each part of the spire. 69
Table 4.28 Variation of friction factor, Nusselt number and heat transfer coefficient along the spire. 69
Table 4.29 Heat flow exchanged through each part of the spire. The total heat power is referred to only one spire. 70
Table 4.30 First row: Outer roller temperature from FEM simulations; second row: re-calculated wall temperature. 74
Table 4.31 Analytical results with several number of turns. The new wall temperature has been set in the analytical calculations. 74
Table 4.32 Numerical results obtained by the finite element software Ansys, with several number of turns. 75
Table 4.33 Critical oil flow rate from laminar to turbulent. Higher flow rates lead to turbulent conditions. 77
Table 4.34 Analytical and numerical results with three values of heat flow rate and the initial wall temperature set analytically 78
Table 4.35 First row: Outer roller temperature from FEM simulations; second row: re-calculated wall temperature. 79
Table 4.36 Analytical results with several heat flow rates. The new wall temperature has been set in the analytical calculations. 79
Table 4.37 Numerical results obtained by the finite element software Ansys, with several heat flow rates. 80
Table 5.1 Results after the first half a turn: oil features and average heat transfer coefficient. 85
Table 5.2 Oil properties at the average temperature and at the wall temperature, on the ambient-side half a turn. 86
Table 5.3 Calculation of heat transfer coefficient at the ambient side, adopting Gnielinski model. 86
Table 5.4 Oil features and heat flow rates produced by one spire and calculated at each half a turn, starting from the workpiece-side one. 88
Table 5.5 Final results: outlet oil temperature calculated in the last half a turn; total heat flow rate provided by one spire; total heat flow rate of the process. 89
Table 5.6 Ideal constant heat flow rate required by the process and real heat flow rate pro part of the roller. 89
Table 5.7 Final inlet oil temperature. Il provides the required total heat flow rate. 91
Table 5.8 Results from the numerical simulation. Temperature values on the workpiece-side path. 94
Table 5.9 Results from the numerical simulation. Temperature values on the ambient-side path. 95
Table 5.10 Final inlet oil temperature by setting the new wall temperature. It provides the required total heat flow rate. 96
Table 5.11 Equations of oil temperature and heat transfer coefficient distributions over the roller axis, for both spire. 96
Table 5.12 Temperature values on the workpiece-side path. The simulation is made with the new results calculated with the new wall temperature. 98
Table 5.13 Temperature values on the ambient-side path. The simulation is made with the new results calculated with the new wall temperature. 98

Table 5.14 Analytical results of the last analysis, in which the new wall temperature is set. 101
Table 5.15 Oil temperature function over the axial coordinate at each piece of the first spire. 102
Table 5.16 Temperature values on the workpiece-side path. The oil temperature is set at each part of the two spires. 104
Table 5.17 Temperature values on the ambient-side path. The oil temperature is set at each part of the two spires. 104
Table 5.18 Analytical results with q10 kW and setting the old wall temperature. 106
Table 5.19 Analytical results with q20 kW and setting the old wall temperature. 107
Table 5.20 Analytical results with q30 kW and setting the old wall temperature. 107
Table 5.21 Temperature values on the workpiece-side path with four different heat flow rates. 107
Table 5.22 Temperature values on the ambient-side path with four different heat flow rates. 108
Table 5.23 First row: Outer roller temperature from FEM simulations; second row: re-calculated wall temperature. 109
Table 5.24 Analytical results with q = 10 kW and the old wall temperature. 109
Table 5.25 Analytical results with q = 12.5 kW and the old wall temperature. 110
Table 5.26 Analytical results with q = 15 kW and the old wall temperature. 110
Table 5.27 Analytical results with q17.5 kW and the old wall temperature. 110
Table 5.28 Analytical results with q = 20 kW and the old wall temperature. 111
Table 5.29 Analytical results with q = 22.5 kW and the old wall temperature. 111
Table 5.30 Analytical results with q = 25 kW and the old wall temperature. 111
Table 5.31 Analytical results with q = 27.5 kW and the old wall temperature. 112
Table 5.32 Analytical results with q = 30 kW and the old wall temperature. 112
Table 5.33 Analytical results with q = 32,5 kW and the old wall temperature. 112
Table 5.34 Analytical results with q = 35 kW and the old wall temperature. 113
Table 5.35 Analytical results with q = 37.5 kW and the old wall temperature. 113
Table 5.36 Analytical results with q = 40 kW and the old wall temperature. 113
Table 5.37 Temperature values on the workpiece-side path against the heat flow rate. The simulation is made adopting results calculated with the new wall temperature. 115
Table 5.38 Temperature values on the ambient-side path against the heat flow rate. The simulation is made adopting results calculated with the new wall temperature. 115
Table 6.1 Thermo-physical properties of the air at the average temperature 121
Table 6.2 Thermo-physical properties of the air at the average temperature 122
Table 6.3 Temperature distribution over the web thickness, at each substep 126
Table 6.4 Absorbed heat along the thickness after the first substep 128
Table 6.5 Absorbed heat and heat flow rate required at each substep 129
Table 6.6 Final temperature on the outer cotton layer against the process time, varying the outer roller surface temperature 131

LIST OF FIGURES

Figure 2.1 Thermo-oil heated roll [14] 6
Figure 2.2 Cast-film extrusion 8
Figure 2.3 Sheet-Extrusion 9
Figure 2.4 Extrusion-coating 9
Figure 2.5 Laminating and coating. 10
Figure 2.6 Embossing 10
Figure 2.7 Stretching 11
Figure 2.8 Annealing 11
Figure 3.1 Heating roller: the outer cylinder is shown transparent and the two spiral grooves are red and blue (A); A roller end with the heating cartridge: detail of sectioned inner cylinder with milled spiral grooves (B) and assembled inner and outer (green) cylinders (C). 18
Figure 3.2 Exploded view of the heating roller (A); detail of one side components: pump and one heat cartridge (B); detail of the heat cartridge on the other side of the roller (C). The tubes connect the inlet and outer surfaces to the heat cartridge. 19
Figure 3.3: “Shell Heat Transfer Oil S2”. 20
Figure 3.4: Oil thermo-physical properties. 20
Figure 3.5 Cross sectional area. Dimensions are in mm. 26
Figure 3.6 Project Schematic with the eight different models. 29
Figure 3.7 Geometrical model with 6,5 coils: (A)wireframe view with the two spires; (B)model as unique cylinder. 29
Figure 3.8 Temperature distribution of the oil inside the tube for one spire. The other one has the opposite configuration. Case: Tin =155 °C as oil inlet temperature. 31
Figure 3.9 Temperature distribution on the outer roller surface. 31
Figure 3.10 Path created on the outer roller surface to evaluate the temperature distribution along the axis of the roller. 32
Figure 3.11 Surface temperature gradient against the number of turns in case of stainless steel and aluminium alloy. 35
Figure 3.12 Surface temperature against the number of turns in case of stainless steel and aluminium alloy. 35
Figure 4.1 Variation of $\Delta Toil$ against the Tin as a function of n, q, and $Tsur$. 43
Figure 4.2 Variation of m against the Tin as a function of n, q, and $Tsur$ 44
Figure 4.3 Variation of q against the m as a function of n, Tin, and $Tsur$ 47
Figure 4.4 Variation of $\Delta Toil$ against the m as a function of n, Tin, and $Tsur$. 47
Figure 4.5 Variation of Tin against the $Tsur$ as a function of n, q, and m 50
Figure 4.6 Variation of $\Delta Toil$ against the $Tsur$ as a function of n, q, and m. 50
Figure 4.7 Variation of Tin against the q as a function of n, $Tsur$, and m 53
Figure 4.8 Variation of $\Delta Toil$ against the q as a function of n, $Tsur$, and m. 53
Figure 4.9 Pump catalog provided by “Linn-Pumpen Gmbh” 56
Figure 4.10 Variation of $\Delta Tsur, FEM$ against the number of turns. The two curves are related to two hydraulic diameters. 66
Figure 4.11 Variation of heat transfer coefficient along the first spire over the axial coordinate. 70

Figure 4.12 Variation of heat transfer coefficient along the second spire over the axial coordinate. 71
Figure 4.13 Temperature distribution on the outer surface. The values are evaluated at the points of the Path placed on the outer surface and 1,5 m long. 71
Figure 4.14 Outer roller temperature from FEM simulations against the number of turns. 75
Figure 4.15 External temperature gradient from FEM simulations against the number of turns. 76
Figure 4.16 Outer roller temperature from FEM simulations against the heat flow rate by setting the initial value of wall temperature in the analytical calculation. 78
Figure 4.17 Outer roller temperature from FEM simulations against the heat flow rate. 80
Figure 4.18 External temperature gradient from FEM simulations against the heat flow rate. 81
Figure 4.19 Inlet oil temperature to be set while the heat flow rate varies (see table 4.36). 81
Figure 5.1 Difference between the ideal constant heat flow rate and the final provided one over the position of the turn. 90
Figure 5.2 Distribution of convection coefficient within the first spire over the roller axis. 91
Figure 5.3 Distribution of convection coefficient within the second spire over the roller axis. 92
Figure 5.4 Distribution of inlet oil temperature within the first spire over the roller axis. 92
Figure 5.5 Distribution of inlet oil temperature within the second spire over the roller axis. 92
Figure 5.6 Numerical model. Geometry and boundary conditions 93
Figure 5.7 Temperature distribution on the external surface, workpiece and ambient sides 94
Figure 5.8 Temperature distribution on the external surface, workpiece and ambient sides 97
Figure 5.9 Temperature distribution on the outer roller surface, workpiece (left) and ambient (right) sides 97
Figure 5.10 New numerical model. Each spire is divided into 50 parts to better simulate the oil temperature variations 100
Figure 5.11 New numerical model. Paths on the two surfaces to evaluate the results 100
Figure 5.12 Temperature distribution on the outer surface: workpiece and ambient sides. The oil temperature is set at each part of the two spires 104
Figure 5.13 Temperature distribution on the external surface on workpiece side, in case of first and second model 105
Figure 5.14 Temperature distribution on the external surface on ambient side, in case of first and second model 105
Figure 5.15 Mean surface temperature against the heat flow rate by setting the old wall temperature in the analytical calculation 108
Figure 5.16 Temperature distribution on the outer roller surface, workpiece (left) and ambient (right) sides.Case of study: q = 40 kW 114
Figure 5.17 Temperature distribution on the two paths. Case of study: q = 40 kW 114
Figure 5.18 Average and mean surface temperature over the heat flow (see table 5.37) 116
Figure 5.19 External temperature gradient from FEM simulations against the heat flow rate (see table 5.37) 116
Figure 5.20 Inlet oil temperature to be set while the heat flow rate varies (see table 5.37) 117
Figure 6.1 Geometry and path of the piece of cotton 124
Figure 6.2: Temperature distribution over the web thickness; first substep 126
Figure 6.3: Final temperature distribution over the web thickness; last substep 127
Figure 6.4 Final temperature on the outer cotton layer against the process time; the curves are parametric with the temperature on the outer roller surface 131

Figure 6.5 Final temperature on the outer cotton layer against the temperature on the outer roller surface 132

CHAPTER 1: Introduzione

Sono molti i processi che richiedono l'utilizzo di un rullo riscaldato; applicazioni come la laminazione, goffratura, asciugatura, calandratura, per citarne solo alcune. Essi si differenziano molto tra di loro ma hanno anche aspetti in comune e, molto spesso, sono caratterizzati da problemi comuni che devono trovare soluzione in fase di dimensionamento e nella scelta del rullo stesso. Al giorno d'oggi i produttori cercano di aumentar sempre più la velocità di produzione in linea, riducendo contemporaneamente gli scarti; gestendo il tutto attraverso tempi di produzione sempre più corti e utilizzo di macchine o linee di produzione per più prodotti.

Inoltre, i rulli riscaldanti vengono utilizzati in applicazioni che richiedono un riscaldamento temporaneo di substrati al fine di raggiungere ottimi risultati. I processi richiedono elevata precisione e i rulli riscaldati devono fornire il target di temperature in modo affidabile e uniforme.

Per molte decadi, la scelta tipica è stata quella del rullo riscaldato ad olio ed al giorno d'oggi si ha familiarità con questo tipo di tecnologia. L'olio caldo proveniente da un serbatoio viene pompato all'interno di un rullo cavo o a doppio guscio. Al fine di generare flusso di calore dall'olio interno alla superficie del rullo in contatto con il tessuto, l'olio dovrà avere una temperatura maggiore rispetto a quella prevista per la superficie. La maggior parte delle operazioni di riscaldamento che utilizzano rulli caldi riscaldati ad olio prevedono una serie di rulli che portano la temperatura del tessuto al livello voluto. Il più grande carico termico è nel primo rullo e questo rullo avrà il peggior profilo di temperatura superficiale. Il secondo rullo viene normalmente inserito in modo che il flusso sia invertito rispetto al primo. I rulli successivi mantengono la temperatura superficiale desiderata sul tessuto e il carico termico su di essi si riduce molto. All'aumentare della velocità della linea o del il carico termico da trasferire al tessuto, anche la temperatura dell'olio dovrà aumentare. Una buona manutenzione e l'attenzione accurata al profilo di temperatura è necessaria per assicurate una buona produzione. Maggiore è la differenza di temperatura tra l'olio e la superficie del rullo, maggiore sarà anche la differenza rispetto alla temperatura voluta alla fine della linea.

Uno scarso profilo di temperatura provoca scarsa capacità di esecuzione, i problemi comprendono bordi larghi, grinze e pieghe.

Ci sono molti fattori che possono aumentare il trasferimento di calore e l'uniformità della temperatura superficiale influenzando la qualità del prodotto finito. Parte di questi aspetti sono stati affrontati nello sviluppo di questo progetto che vede appunto coinvolto un rullo in acciaio riscaldato ad olio diatermico che fluisce all'interno di due serpentine elicoidali.

Applicazioni

L'industria della carta utilizza i rulli in metallo per imprimere pressione, per asciugare, per la calandratura di trame in carta. L'industria della gomma e della plastica li utilizza per fondere il materiale, per la vulcanizzazione e come rulli pressori. L'industria tessile utilizza i rulli riscaldati, per esempio, in macchine asciugatrici, oppure per la rifinitura del tessuto e per la stampa. Nella pavimentazione si utilizza il rullo per pressare, asciugare, stampaggio e plastificazione del prodotto finito.
Pochi settori dell'industria infatti riescono ad ottenere i loro prodotti senza l'utilizzo di rulli di riscaldamento nelle loro linee di produzione. Ecco una breve lista delle applicazioni:

- **Essicatori** di: carta, adesivi, vernice, tessuti;
- **Stampaggio**: floxografia, rotocalcografia, serigrafia, stampa offset;
- **Rivestimenti**: macchine laminatrici, lastre di zinco, stampa di etichette, rivestimenti adesivi, rivestimento in fusione.
- **Trattamento corona** per macchine per lavorazione della plastica e dei tessuti.

Tra i processi ricordiamo: estrusione di lastre, estrusione di rivestimento, plastificazione, stampa a rilievo, allungamento della trama, riscaldamento per ricottura.
Essi sono accumunati dallo scopo di ottenere una temperatura il più uniforme possibile sulla superficie esterna. Oltre all'utilizzo di olio caldo, ci sono vari altri modi per scaldare il rullo: gas, glicole, acqua, vapore, prodotti chimici speciali, con resistenze elettriche o riscaldamento ad induzione.

Soluzione scelta

Il rullo di riscaldamento che studieremo è formato da due gusci cilindrici coassiali. Sulla superficie esterna del cilindro interno vengono generate, per asportazione di truciolo, due serpentine a spirale ellittica. L'assemblaggio dei due cilindri con calettamento per interferenza, permette alle serpentine di diventare tubi interni di passaggio dell' olio caldo. L'olio, entrando da un lato del rullo, attraversa la prima spira percorrendo l'asse in un verso e cedendo calore. All'uscita dalla prima spira l'olio incontra uno scambiatore a cartucce elettriche di riscaldamento che lo riporta alla temperatura massima, con la quale alimenta la seconda spira fluendo nel verso opposto per poi incontrare il secondo scambiatore posto dall'altra parte del rullo. La circolazione dell'olio è garantita da una pompa che, assieme ai due scambiatori, è posizionata nella cavità interna del rullo stesso. Questa soluzione, rispetto alle precedenti in commercio che vedono una pompa (che preleva da un serbatoio) e scambiatori posti esternamente, ha il vantaggio di ridurre le perdite di calore che avvengono nel trasferimento dell'olio dal serbatoio al rullo, sia perché il tutto è all'interno del rullo e non esposto all'ambiente, sia perché si tratta di un circuito chiuso. Soluzioni precedenti consideravano anche l'utilizzo di un solo scambiatore posto ad un lato del rullo e con un unica serpentina interna al rullo avente l'ingresso e l'uscita posizionate dalla stessa parte; in questo modo l'olio si raffredda percorrendo andata e ritorno rispetto all'asse senza mai venir riscaldato nuovamente. La soluzione con due scambiatori posti nei due lati del rullo comporta sicuramente migliori profili superficiali di temperatura a parità di altri parametri, in quanto cala il salto termico massimo subito dall'olio.

Essendo varie le applicazioni che utilizzano questo prodotto e non avendo un caso specifico da analizzare, questo lavoro verrà studiato partendo da una condizione più generale che vede il rullo completamente avvolto dal tessuto esterno per poi analizzare un caso più preciso secondo alcune specifiche forniteci da un possibile futuro cliente. Sarebbe quindi necessario conoscere l'applicazione che vede coinvolto il rullo di riscaldamento per sviluppare un progetto accurato. Un esempio di studio preliminare dell'applicazione viene affrontato nell'ultimo capitolo.

CHAPTER 2: Introduction

There are many processes that require the use of a heated roller; laminating, embossing, drying, annealing, calendering, and film orientation to name just a few. These processes differ in many ways but there are common needs to be met and problems to solve, when choosing and operating a heat transfer roll. Today's manufacturers are looking to increase line speeds and simultaneously reduce product scrap; while managing through increasingly shorter product runs and frequent changeovers.

Moreover, heating rolls are used in applications that, in order to achieve optimal results, require substrates to be temporarily heated. And today's advanced processes require very precise temperatures, so heat transfer rolls must deliver target temperatures consistently and evenly.

The oil-heated roller have been selected for decades. Nowadays, people are familiar with this technology. Hot oil from a remote reservoir is pumped in and out of a hollow or double shell roller. The oil must be at a higher temperature than the set roller surface temperature. Most heating operations using hot oil rolls are designed with a series of rolls bringing the temperature of the material to the required level. The biggest heat load is on the first roll and this roll will have the worst temperature profile. The second roll will normally be piped so the flow is reversed from the first roll. This helps to even out the temperature profile. The next roll or two rolls maintain the desired web temperature. The heat load on those rolls is reduced dramatically. As the line speed increases, or the thermal load (heat transfer to the web) on the roller gets greater, the oil temperature will have to be higher in order to increase the heat transfer to the roller shell. Good maintenance and careful attention to the temperature profile is mandatory to ensure good product runs. The greater the temperature difference between the oil and the roller surface, the greater will be the temperature overshoot when the line stops. A poor temperature profile causes poor run ability; issues include baggy edges, wrinkles, and poor winds.

There are a number of factors that can increase the heat transfer and temperature uniformity of the roller surface and affect the quality of the product being produced.

Figure 2.1 Thermo-oil heated roll [14]

2.1 Applications

Heating metal rolls are important elements for many manufacturing processes. The paper industry use metal rolls for pressing, drying and calendering of paper webs. The rubber and plastic industries use rolls for melting, vulcanizing and pressing. The textile industry uses heated rolls for drying, sizing and printing. Floor covering industries use roll for pressing, drying, print-transfer and plastification of their end products.
In fact, few industries can produce their goods without the use of heating rolls on their production lines.
A brief list of applications follows below:

- **Dryers:**
  - Paper dryers
  - Adhesive dryers
  - Paint dryers
  - Fabric dryers in textile finishing.
- **Printing**
  - Flexo printing
  - Gravure printing
  - Screen printing
  - Offset printing
- **Coatings**
  - Laminating machines
  - Zinc plates
  - Label printing
  - Adhesive coating
  - hot melt roll coating
- **Corona-treatment**

A brief list of processes follows below:

- Cast-Film-Extrusion: cast films are used for food and textiles packaging, flower wrapping, as photo album page protectors, as coating substrates in extrusion coating processes or laminated to other materials in the formation of more complex films, among others. Typically, the cast film process involves the use of co-extrusion, which is a simultaneous extrusion of two or more materials from a single die to form a multi-layered film. In the cast film extrusion process, the molten polymer travels through a flat die system to adopt its final flat film shape. The die system is formed by the die and feedblock (if the process requires coextrusion) or simply the die, if the process is that of mono-layer extrusion. Immediately after exiting the die, the molten curtain enters the cooling unit where its temperature is lowered with a water cooled chill roll to "freeze" the film. The film is then passed downstream where the edges are trimmed, corona treatment is applied (if a fabrication process such as printing or coating is required) and the film is wound into rolls.

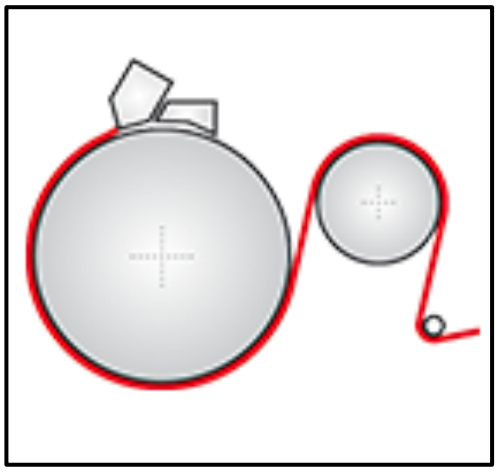

Figure 2.2 Cast-film extrusion

- Sheet-Extrusion: sheet is distinguished from film by its thickness: anything over 0.25-mm is considered sheet. The process closely resembles cast film extrusion. Thinner sheet is typical thermoformed into trays, clam shells, cups or bowls, whereas thick sheet may be used for signage, refrigerator liners and truck bed

liners. Common sheet extrusion materials include PET, high-density polyethylene, polystyrene and ABS. Sheet can be produced in either single or multi-layer formats.

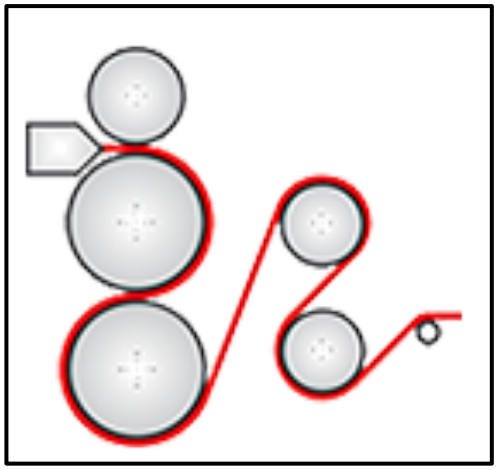

Figure 2.3 Sheet-Extrusion

- Extrusion-Coating: the actual process of extrusion coating involves extruding resin from a slot die at temperatures up to 320°C directly onto the moving web which may then passed through a nip consisting of a rubber covered pressure roller and a chrome plated cooling roll. The latter cools the molten film back into the solid state and also imparts the desired finish to the plastic surface. The web is normally run much faster than the speed at which the resin is extruded from the die, creating a coating thickness which is in proportion to the speed ratio and the slot gap.

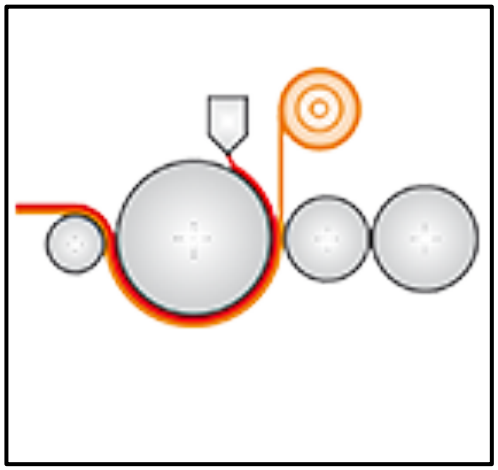

Figure 2.4 Extrusion-coating

- Laminating and Coating: (example of paper) Laminating paper products, such as photographs, can prevent them from becoming creased, faded, water damaged, wrinkled, stained, smudged, abraded, or marked by grease or fingerprints. Photo identification cards and credit cards are almost always laminated with plastic film. Boxes and other containers are also laminated using a UV coating.

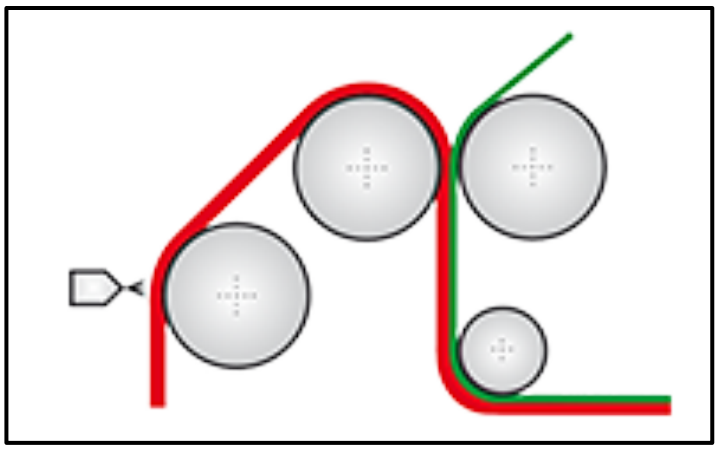

Figure 2.5 Laminating and coating.

- Embossing: Sheet metal (or paper or other materials) embossing is a process for producing raised or sunken designs or relief in sheet metal, paper and other materials. This process can be made by means of matched male and female roller dies, or by passing the sheet between rolls of the desired pattern.

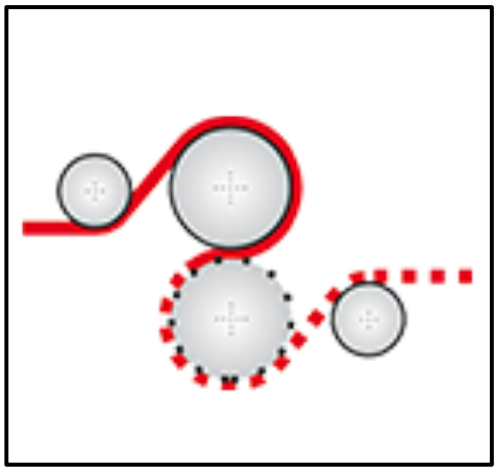

Figure 2.6 Embossing

- Stretching: the film is stretched.

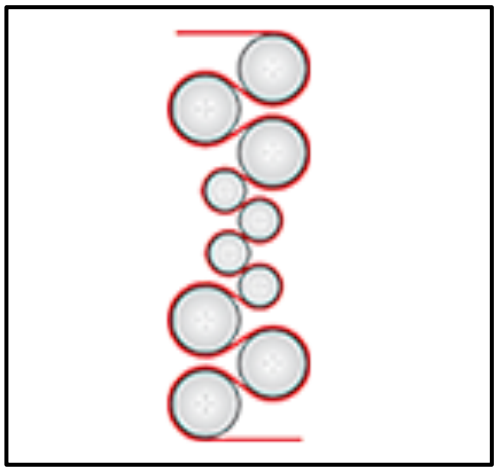

Figure 2.7 Stretching

- Heating, Cooling, Annealing

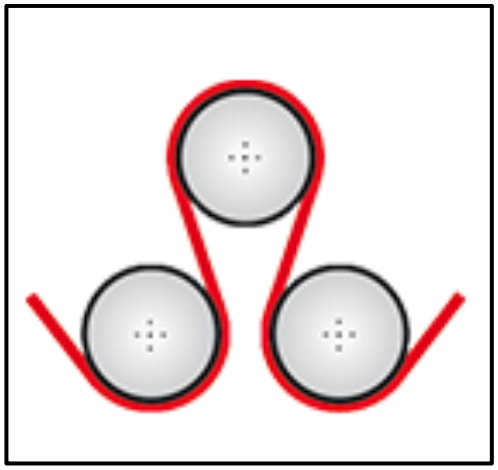

Figure 2.8 Annealing

Whether the roll edges are too cold as in laminators, or too hot as in paper and textile manufacturing, the goal is to provide uniform surface temperature. A heat transfer roll is designed to provide consistent web temperature across entire roll face. There are several ways to heat the roller, especially by selecting the type of thermal transfer mechanism: gas, glycol, hot oil, water, steam, specialty chemicals, electrical and induction heating.
It is possible to classify the roller by the selected material which best suits the application requirements. Here some types:

- Carbon Steels
- stainless steel
- Aluminium
- Combination of steel and stainless steel
- Combination of aluminium and stainless steel

With also examples of surface coatings:

Galvanic:

- Hard chrome plating (single layer or triple layer): rolls are resistant to corrosion in addition to exhibiting excellent wear characteristics with hardness values of up to 950 HV, depending upon the respective plating thickness.
- Nickel plating coatings: as a technical intermediary layer, adhesion promoter or 100% sealed base coat, nickel plating is applied in various coating thicknesses. Typical nickel plating thicknesses/intermediate layers for roll surfaces range from 10µm to 100µm.
- Nickel/Chrome coatings: for surfaces that are subjected to particularly high stresses, e.g. rolls downstream of corona treatment stations or in the area of flame treatment stations.
- Copper plating coatings: The good electrical and excellent thermal conductivity of copper is successfully harnessed for use in the copper plating of roll cores.

Spray:

- Carbide coatings: Carbide coatings are applied to rolls to a professional standard using the HVOF spraying process.
- Ceramic coatings: Ceramic materials are thermally sprayed onto rolls as a wear protection coating for surfaces that are subject to particularly high stresses.
- Cermet coatings: A compound ceramic and metallic material, Cermet coatings are applied as an intermediate layer to compensate for thermal stresses.
- Metal coatings: Spray coatings of various metal alloys and compositions are applied using a thermal spray coating process to protect against wear or for reconditioning journals and shell surfaces during maintenance work.
- Teflon (PFA/PTFE) coatings: Polytetrafluorethylene (PTFE / PFA) is applied to rolls using a spray coating process followed by tempering.
- Paint coatings: Innovative paint systems that range from nano paints and surface sealants through to paints with added filler and hardened particles offer a wide range of options for coating the roll surfaces.

Elastomer:

- Silicon coatings: Polyorganosiloxanes collectively describes a group of synthetic polymers. Silicon coatings can be used in a temperature range of -40°C to + 230°C.
- EPDM Coatings: Ethylene propylene diene monomer (EPDM) is an elastomer (= rubber) or synthetic rubber. Resistance to moisture and ozone together with resistance to high temperatures are among the properties of EPDM coatings.
- PU coatings: Polyurethane (PU) is a plastic or artificial resin that is created in a polyaddition reaction. A high degree of mechanical resistance to cuts, together with high tear strength, means that polyurethane is used in particular to coat web guide rolls on metal machining lines.
- Neoprene coatings: Chloroprene rubber is a synthetic form of rubber that is marketed under the trade name “Neoprene”. Good resistance to organic solvents, ozone and mineral-based oils is a characteristic of Neoprene coatings.

This project involves heat oil as thermovector fluid which flows within the roller and provides heat in order to reach the required temperature on the roller surface.

Liquid heating in textile and plastic industry:

Though most heater rollers are specified to achieve a certain temperature uniformity under no-load conditions, roll-temperature uniformity can vary during operation, depending on line speed (related to thermal load) and web width (related to load distribution).

Liquid-heated roller surfaces will naturally rise close to the internal roller temperature where there is little thermal load outside the web. But without some mechanism such as a heat pipe, the roller tends to be hotter at the ends than in the web path, sometimes causing the web edges to overheat.

Most liquid systems use a remote reservoir and heating element to heat the circulating liquid. They also have a controller and sensor at the tank to set the temperature and operate the system, plus a pump, rotary connector, and plumbing to transfer liquid to the roller.

Liquid-heated rollers consist of either a simple single shell or more commonly of a spiral-baffled, double-walled roll to maintain more consistent thermal transfer across and around the roller. In either case, the roller is heated from the inside out, so the surface is the last part to reach the desired setpoint.

The vast majority of preheating, laminating, and heat-stretching applications use oil-heated systems because of the medium- to high-heat requirements of these processes. However, disposal of carbonized oil after thermal cycling is a continual challenge for users. Carbonized oil also restricts flow and coats the internal surfaces of the roller, hoses, pumps, and filters, which reduces heat transfer. Heat not only causes the oil to break down, it causes hoses and bearings to wear out more quickly. However, hydrocarbon oils reportedly handle higher operating temperatures without degrading.

About 20-25% of heated rollers today use water or steam. Generally, water is used for low-heat applications (below 100 °C), while steam is used for medium- to high-heat applications. In both cases, internal corrosion or scale deposits can reduce heat-transfer

performance. A high-temperature steam system may require a gas-fired boiler to generate sufficient heat, creating a pressure vessel that needs regular inspection and repair.

While some web-processing applications require rollers that can both add or subtract heat (calendering, for example), the downstream converting applications discussed here use rollers for heating only.

Moreover, textile finishing plants (especially those involved in thermo setting of technical woven fabric) as well as the plastics and film industries normally demand cylinder surface temperatures up to 300 °C. Such high temperatures cannot be obtained economically with steam-heating. The steam pressure at a steam temperature of e.g. 250 °C exceeds 40 bars and require an untenable high mechanical capacity. Furthermore these high pressure values are not available in most of the plants of the textile and plastic industries. For this reason the above mentioned processing ranges are preferred to be equipped with thermooil-heated roller and cylinders, which offer a great advantage at high processing temperatures.

A further advantage of thermo oil of the heating is that it offers the possibility of heating below an operating temperature of 100 °C, which is not given with steam-heating because of the specific properties of steam.

Electric-heated rolls in textile and plastic applications:

Electric-heated rollers are currently a minority of the market but offer several advantages. Except for ceramic types, electrically heated rollers are heated internally, resulting in a higher internal temperature than surface temperature. Because these rollers are generally controlled by measuring the shell temperature from a thermocouple embedded near the surface, they are much more easily and quickly controlled than liquid-heated systems. The sensor signal is sent to the temperature controller, which controls power to the heater element.

Thermal losses are limited to normal convection from the roller surface, since all heat is produced internally. Temperature recovery is faster than with liquid heating because of the finer degree of control and higher watt density. Both induction and resistance heating systems can be used.

Induction-heated rollers have been used since about 1970 but have become more popular in the last few years because they provide a high degree of thermal precision and stability.

A combination of induction and heat-pipe technology generates heat on the inside surface of the outer roller shell by exposure to a high-intensity, rapidly changing magnetic field. Induction coils are mounted on a non-rotating shaft, close to the roller shell. The outer shell contains heat pipes to distribute heat across the roller.

Operating temperatures with induction heating go as high as 420 °C , meeting both low- and high-heat application needs. The electrical connection is made to the stationary coil, but a rotary transformer is required for temperature sensing. A high-frequency generator drives the induction-heating coils.

Resistance-heated rollers had a poor performance reputation in the past. Early models used low-end cartridge heaters that had a high rate of failure. However, today resistance-heat technology provides comparable performance to induction heating.

One advanced type of resistance-heated roller incorporates high-performance cartridge heaters in the innermost layer of the roller. A thermal-equalization chamber (or specialized heat pipe) surrounds the inner layer to distribute heat evenly across the roller surface. These rollers can provide temperatures up to 260 °C, suiting them to a wide range of web-heating applications.

Instead of heat pipes, other modern resistance-heating systems use a technology similar to cartridge heaters but with multiple heat zones to control temperature uniformly. These systems reportedly can run at up to 500 °C.

Ceramic heater rolls use a second type of advanced resistance heating, consisting of a variety of ceramic materials applied by thermal spray to the outer surface of the roll core. One of the ceramic layers is actually an electrical resistance heater. When combined, the ceramic materials form a thin, homogeneous insulated heater element that covers the entire roller surface and generates precise levels of radiant heat.

Here, too, a thermal-equalization chamber provides continuous leveling of the surface temperature across the face of the roller. Ceramic systems can provide temperatures up to 180 °C.

With both types of resistance-heated systems, external electrical connections to the roller are normally made through only one journal using a rotary electrical connector.

CHAPTER 3: Problem description; roller exposed to the ambient

3.1 Step description

As already described in the first brief introduction, the system is basically a heating roller, which can be applied to many different applications. The uniform surface temperature distribution represents the common requirement of the different applications. Hence we have to focus most of the design efforts to achieve a uniform surface temperature distribution by fixing a maximum-to-minimum temperature difference.

In order to get into the problem, we start by considering a simplified system running in steady state condition (i.e. not rotating roller) with the roller that exchanges heat only with air at ambient conditions.

Even though the real process is characterized by a high value of the required heat flow rate, on the other hand, under these hypotheses we will be able to figure a simplified case out.

The first step will deal with the analytical calculation of the system by fixing the boundary conditions, the fluids properties (oil and air) and by identifying the most affecting parameters, which must be taken into account in the design process.

Afterwards is possible to set and vary some of them and, then, check the results in order to know what happens to the others. The results can be evaluated by a numerical simulation using the Ansys 14 Workbench software.

Under the hypothesis of a fix heated roller in still air, the problem can be studied using the Steady-State Thermal Analysis for both analytical and numerical calculations. Finally, in this first step, another important hypothesis is to consider negligible the thermal resistance of the roller material. This can be accepted in this general first approach but it will be tuned in the next steps.

3.2 Preliminary design of the roller

3.2.1 Physical model definition

The heating cartridge is characterized by two cylinders, assembled each others. On the external surface of the internal one, two screwed-twisted spires are milled. As shown in Figure 3.1, when the two cylinders are assembled, the two spiral grooves are generated as channels having the same shaped-cross sectional area and length and they are located half a pitch far from each other.

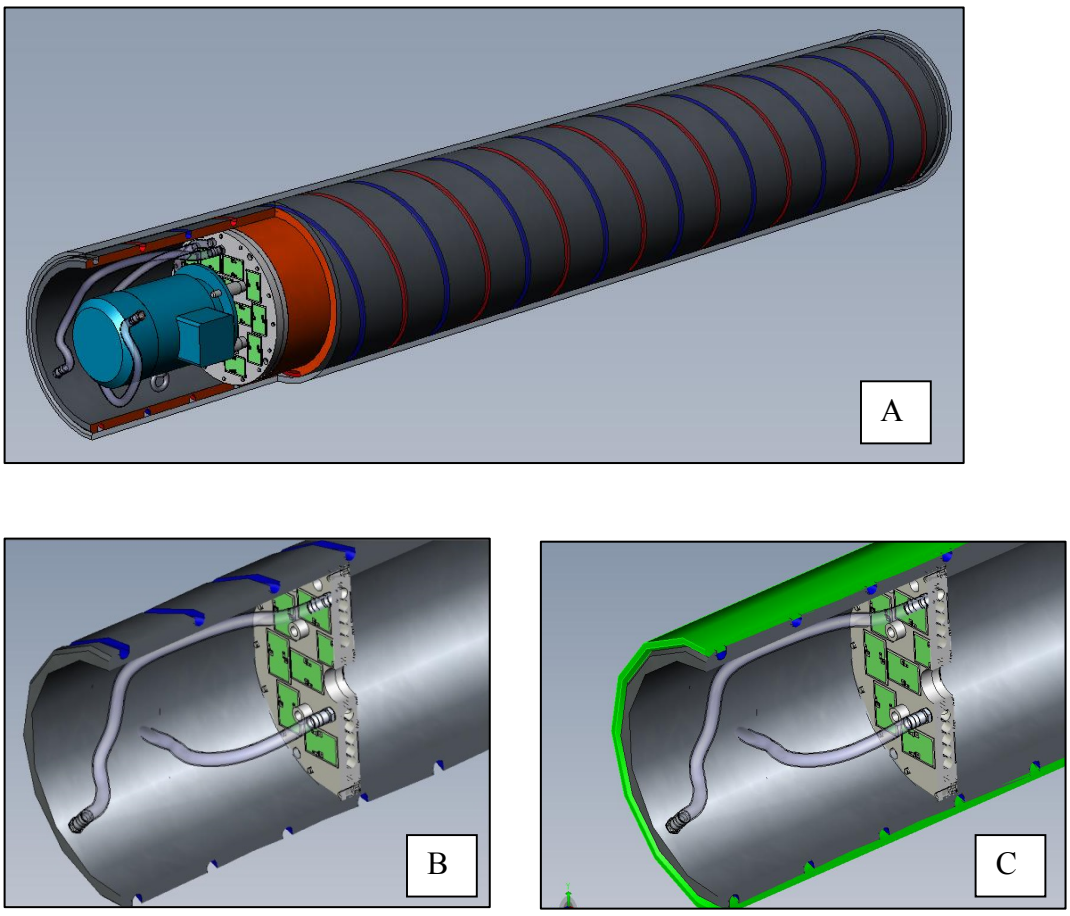

Figure 3.1 Heating roller: the outer cylinder is shown transparent and the two spiral grooves are red and blue (A); A roller end with the heating cartridge: detail of sectioned inner cylinder with milled spiral grooves (B) and assembled inner and outer (green) cylinders (C).

The spires are filled up with heat transfer oil, which is used for heating the roller and maintaining the requested surface temperature. When flowing throughout the cylinder, the oil temperature decreases modifying its thermo-physical properties, which might affect its heat transfer capabilities.

The oil is heated at the two sides of the roller by using two heating cartridges, in this way the oil has the maximum temperature at one side and it reaches the minimum value at the other side of the roller. In fact, the hot oil enters the first spiral channel and flows through it. Meanwhile, it exchanges heat with the surroundings; when it arrives on the other roller side, it is re-heated before flowing backwards and feeding the second spiral groove. The process oil flow rate is assured by a gear pump located in a side compartment. (Figure 5.2)

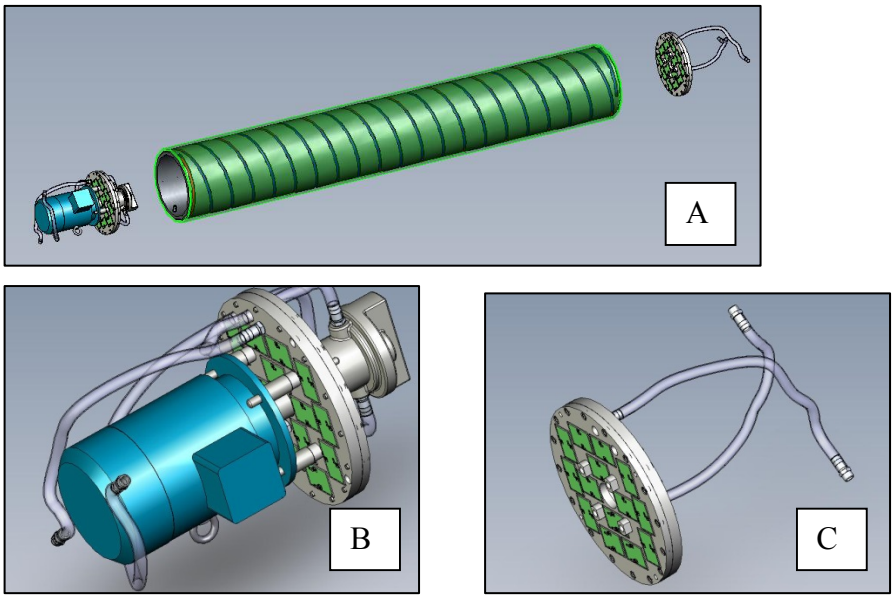

Figure 3.2 Exploded view of the heating roller (A); detail of one side components: pump and one heat cartridge (B); detail of the heat cartridge on the other side of the roller (C). The tubes connect the inlet and outer surfaces to the heat cartridge.

After a review of the different off-the-shelf oils, the following one was chosen: “Shell Heat Transfer Oil S2” (Classified as ISO 6743-12 Family Q), which is a high performance heat transfer fluid (figure 3.3). [1]

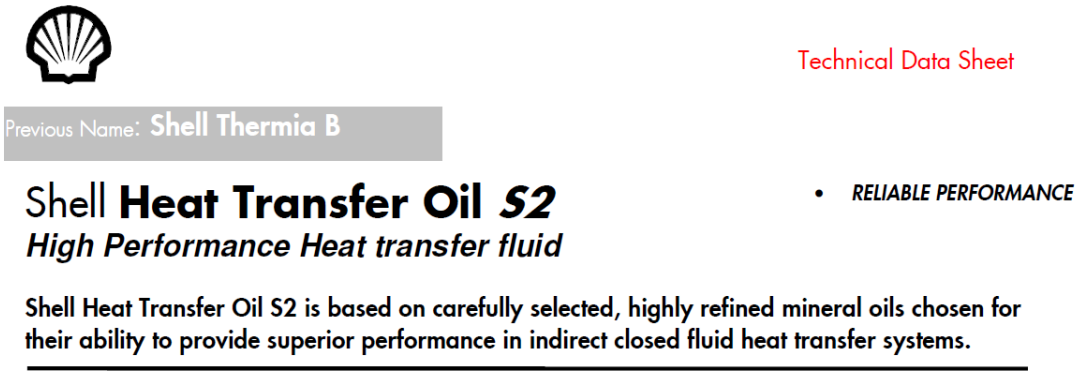

Technical Data Sheet

Previous Name: **Shell Thermia B**

Shell **Heat Transfer Oil *S2***

- ***RELIABLE PERFORMANCE***

High Performance Heat transfer fluid

Shell Heat Transfer Oil S2 is based on carefully selected, highly refined mineral oils chosen for their ability to provide superior performance in indirect closed fluid heat transfer systems.

Figure 3.3: "Shell Heat Transfer Oil S2".

From the data listed in the datasheet, we can derive its most important thermo-physical properties, which will be used in the subsequent thermal analyses. (figure 3.2):

Shell Heat Transfer Oil S2	
Max. film temperature	340°C
Max. bulk temperature	320°C

Typical Physical Characteristics

Density at 15 °C	kg/m3	ISO 12185	866
Flash Point PMCC	°C	ISO 2719	210
Flash Point COC	°C	ISO 2592	220
Fire Point COC	°C	ISO 2592	255
Pour Point	°C	ISO 3016	-12
Kinematic Viscosity		ISO 3104	
at 0 °C	mm2/s		151
at 40 °C	mm2/s		25
at 100 °C	mm2/s		4.7
at 200 °C	mm2/s		1.1
Initial Boiling Point	°C	ASTM D 2887	355
Autoignition Temperature	°C	DIN 51794	360
Neutralisation Value	mgKOH/g	ASTM D974	< 0.05
Ash (Oxid)	%m/m	ISO 6245	< 0.01
Carbon Residue (Conradson)	%m/m	ISO 10370	0.02
Copper Corrosion (3h/100°C)		ISO 2160	class 1

These characteristics are typical of current production. Whilst future production will conform to Shell's specification, variations in these characteristics may occur.

Typical Design Data

Temperature	°C		0	20	40	100	150	200	250	300	340
Density	kg/m3		876	863	850	811	778	746	713	681	655
Specific Heat Capacity	kJ/kg*K		1.809	1.882	1.954	2.173	2.355	2.538	2.72	2.902	3.048
Thermal Conductivity	W/m*K		0.136	0.134	0.133	0.128	0.125	0.121	0.118	0.114	0.111
Prandtl No.			3375	919	375	69	32	20	14	11	9

Figure 3.4: Oil thermo-physical properties.

The assumptions of the first analytical calculation can be summarized as follows:

- Steady-State thermal analysis.
- Natural convection from the external surface to the surroundings.
- We neglect the conduction thermal resistance of the material, i.e. the spiral surface temperature is equal to the external surface temperature.
- We consider an average value of the oil heat transfer coefficient.
- We neglect the thermal contact resistance at the contact area between the two cylinders.

The third assumption permits to bypass the estimation of the temperature drop between the pipe wall and the external roller surface avoiding a cumbersome calculation. Therefore, in this step the conductive resistance of the roller material is neglected.

The input data is the following:

- Required surface temperature T_{sur} = 140 °C
- Ambient temperature T_{amb} = 20 °C
- Max pump flow rate $\dot{V}$ = 30 l min^{-1}

Main roller sizes:

- External diameter 300 mm
- Length 1900 mm
- External diameter of the internal cylinder 280 mm
- cross section 127 mm^2

It is necessary to estimate the required heat flow rate exchanged by the roller with the surroundings through the external surface. At that point, the mean oil temperature is still unknown. Thus, the inlet oil temperature must be set along with the oil temperature change which can be varied to modify the surface wall temperature.

3.2.2 Analytical calculation on the roller surface

As already mentioned, the natural convection is supposed to be the main heat transfer mechanism on the external roll surface.

The heat transfer coefficient has to be calculated. Therefore, the following model can be applied to derive the Nusselt number [2]:

$$Nu = C\ (GrPr)^{1/4} = \frac{\alpha_{free} d}{\lambda}$$

when $10^3 < Ra = GrPr < 10^9$ and $Pr > 0.5$, then C is constant and equal to 0,53 or 0,47.

- Grashof number: $Gr = \frac{D^3 \beta g (T_{sur} - T_\infty)}{\nu^2}$
- Prandtl number: $Pr = \frac{c_p\ \mu}{\lambda}$
- Raylegh number: $Ra = GrPr = \frac{D^3 \beta g (T_{sur} - T_\infty)}{a\nu}$, where *a* is the thermal diffusivity, $a = \frac{\lambda}{c_p\ \rho}$.

The physical air parameters are calculated at the average temperature between the surface and the ambient. Hence $(T_w + T_\infty)/2 = (140+20)/2 = 80$ °C. (table 3.1)

T [°C]	**ρ** [kg m^{-3}]	**c_p** [kJ $kg^{-1}K^{-1}$]	**λ** [10^{-3}W $m^{-1}K^{-1}$]	**μ** [μPas]	**Pr** [-]
20	1,2043	1,0064	25,74	18,25	0,71
30	1,1645	1,0068	26,44	18,73	0,71
40	1,1272	1,0072	27,13	19,21	0,71
50	1,0923	1,0077	27,81	19,68	0,71
60	1,0594	1,0083	28,48	20,15	0,71
70	1,0285	1,009	29,15	20,61	0,71
80	0,9993	1,0097	29,82	21,06	0,71
90	0,9718	1,0106	30,48	21,51	0,71
100	0,9457	1,0115	31,14	21,96	0,71

Table 3.1 Thermo-physical properties of the air at different ambient temperature.

We obtain : Gr = 2,02 10^8 , Ra = Pr Gr = 1,44 10^8 and Nu = $0{,}53(1{,}44\ 10^8)^{1/4}$ = 58,1.

Finally, $\alpha_{free} = \frac{\mathrm{Nu}\,\lambda}{\mathrm{d}} = \frac{58{,}1*0{,}0298}{0{,}3} = 5{,}8$ W $m^{-2}K^{-1}$.

Since the surface of the roller is hot, a non-negligible part of the heat is transferred by radiation. The radiation effect can be accounted by considering a new overall heat transfer coefficient. The new heat transfer coefficient is calculated as follow:

$$\alpha_r = 4\ \sigma\ T_m^3 = 4 * 5{,}67\ 10^{-8} * 353{,}15^3 = 9{,}99\ \mathrm{W\ m^{-2}K^{-1}},$$

where σ is the Stephan-Boltzman constant and T_m the mean value of the temperature between the hot surface and the air.
Adding the two coefficients, we obtain:

$$\alpha_{ext} = \alpha_{free} + \alpha_r = 5{,}8 + 9{,}99 = 15{,}79\ \mathrm{W\ m^{-2}K^{-1}}.$$

With this value is possible now to derive the total heat flow involved in the process:

$$q = \alpha_{ext}\ A_{ext}\ \Delta T_{sur-amb} = 15{,}79*1{,}81*120 = 3430\ \mathrm{W} \sim 3\ \mathrm{kW}$$

where A_{ext} is the external surface A_{ext} = πD*l = 3,14*0,3*1,92 = 1,81 m^2.

3.2.3 Analytical calculation on the spires, laminar flow.

As described before, the oil is heated at the inlet of the first spiral channel and then it flows in the duct where its temperature decreases. The inlet oil temperature and the temperature variation can be assumed and set. Generally speaking, the oil temperature along the spire must be kept higher than the temperature on the roller surface.
We assume four different temperature changes of the oil and two reasonable inlet temperatures for each case.

CASES:

- A) T_{in} = 150 and 146 °C with ΔT_{oil} = 5 °C
- B) T_{in} = 155 and 151 °C with ΔT_{oil} = 10 °C
- C) T_{in} = 160 and 156 °C with ΔT_{oil}= 15 °C
- D) T_{in} = 165 and 161 °C with ΔT_{oil} = 20 °C

Assuming that the entire heat is only transferred to the ambient through the external roller surface, it is possible to calculate for each case the oil flow rate required:

$$\dot{m} = \frac{q}{\left(2cp_{oil}\Delta T_{oil}\right)}$$

where $c_{p_{oil}}$ is the specific heat at the average oil temperature. The total heat flow rate is halved because there are two spirally coiled spires.

If we know the oil flow rates, we can now reject the values incompatible with the maximum pump value (no one is incompatible).

In each previously listed case, we also derive the mean velocity (u) of the oil that flows inside the channels, using the values of the mean oil density (ρ_{oil}) and of the cross-sectional area (A_{sec}) of the channel: $u = \frac{\dot{m}}{\rho_{oil} A_{sec}}$.

T_{in_oil} [°C]	ΔT_{oil} [°C]	average T [°C]	c_p [kJ kg^{-1}K^{-1}]	oil flow $\dot{m}$ [kg s^{-1}]	oil flow $\dot{V}$ [l min^{-1}]	oil velocity u [m s^{-1}]
150	5	147,5	2,34	0,13	9,86	1,294
146	5	143,5	2,33	0,13	9,89	1,298
155	10	150	2,35	0,06	4,92	0,646
151	10	146	2,33	0,06	4,94	0,648
160	15	152,5	2,36	0,04	3,28	0,430
156	15	148,5	2,34	0,04	3,29	0,431
165	20	155	2,37	0,03	2,45	0,322
161	20	151	2,35	0,03	2,46	0,323

Table 3.2 Study cases at different mean oil temperature.

The analytical calculation of the oil heat transfer coefficient within the pipe can now be done. While neglecting the conductive thermal resistance, on tube surface the temperature can be taken equal to the one on the external surface (in this case 140 °C).
The heat transfer coefficient can be calculated using the model proposed by *Gnielinski* [3]

Heat transfer in laminar flow:

The model was validated by using measurements performed on water (2<Pr<5) and oil (100<Pr<200) in coils heated by condensing steam (constant temperature)

$$\mathrm{Nu} = 3{,}66 + 0{,}08\left[1 + 0{,}8\left(\frac{d}{D}\right)^{0{,}9}\right] Re^{m} Pr^{1/3} \left(\frac{Pr}{Pr_w}\right)^{0{,}14}$$

with $\mathrm{m} = 0{,}5 + 0{,}2903\left(\frac{d}{D}\right)^{0{,}194}$

The Prandtl number Pr is evaluated at the mean fluid temperature T_w and Pr_w at the wall temperature.

Heat transfer in Turbulent Flow Re > 2,2 10^4

$$\mathrm{Nu} = \frac{(f/8)\mathrm{RePr}}{1+12{,}7\sqrt{f/8}(\mathrm{Pr}^{2/3}-1)}\left(\frac{\mathrm{Pr}}{\mathrm{Pr_w}}\right)^{0{,}14}$$

The friction factor for turbulent flow in helically coiled tubes is:

$$\mathrm{f} = \left[\frac{0{,}3164}{\mathrm{Re}^{0{,}25}} + 0{,}03\left(\frac{\mathrm{d}}{\mathrm{D}}\right)^{0{,}5}\right]\left(\frac{\mu_w}{\mu}\right)^{0{,}27}$$

μ_w is the dynamic viscosity of the fluid at wall temperature and μ that at mean temperature of the fluid.

The Nusselt number is defined by: $Nu=\alpha*d/\lambda$ with λ the thermal conductivity of the fluid. The Reynolds number is calculated as $Re= G*d/\mu$ where G is the mass velocity ($G= \rho*u = m/A$) and μ the dynamic viscosity of the fluid. The physical properties are evaluated at the mean temperature of the fluid:

$$T_m = \frac{T_{in}+T_{out}}{2}$$

Furthermore, for helically Coiled Tubes the Critical Reynolds number becomes:

$$Re_{crit} = 2300\left[1 + 8{,}6\left(\frac{d}{D}\right)^{0{,}45}\right]$$

This equation is based on a value for the critical Reynolds number or 2300 for the straight tube. The transition from laminar to turbulent flow is shifted to higher Reynolds numbers with increasing relative curvature (d/D).

From the value of the cross-sectional area, we can derive the hydraulic diameter d_h:

$$d_h = \frac{4A_{tube}}{P_w} = 11{,}93 \text{ mm}$$

with A_{tube} the cross-sectional area and P_w the wetted perimeter.

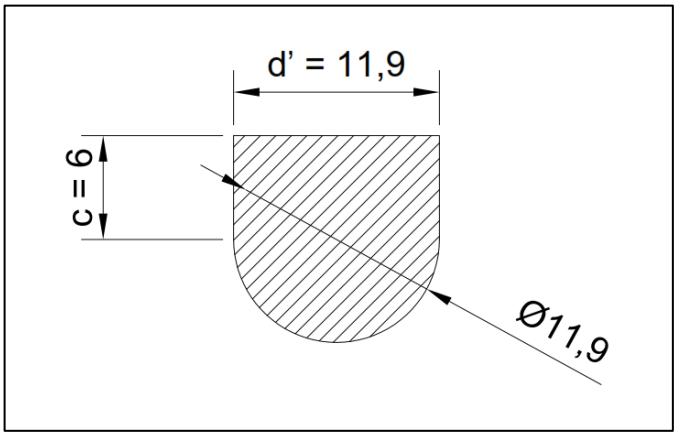

Figure 3.5 Cross sectional area. Dimensions are in mm.

The value $D = D_c \left[1 + \left(\frac{h}{\pi D_c}\right)^2\right]$ depends on the geometry, especially on the pitch h, which has not yet been calculated. Therefore, we do not know neither Nu nor Re_{crit} (D_c is the projected diameter of a winding).

Thus, an iteration process is needed to evaluate the remaining design parameters; starting from an initial value for h, we can calculate D, Nu (we assume a laminar flow, assumption that has to be verified), α_{oil}, and the total length of the pipe:

$$l = \frac{q}{\alpha_{oil} P_w (T_w - T_m)}$$

and the new h:

$$h = \frac{(L-2x)\pi D_c}{l}$$

where L-2x is the axial length of the helically coiled tube, L is the roller length and x the empty length on both sides.

With the new h is possible to start a new iteration. In few steps, the final value of h is achieved.

At this point, we know the value of Nu, so we can also calculate the heat transfer coefficient α_{oil}. We can also derive the critical Reynolds number Re_{crit} and verify if the flow is either laminar or turbulent.

In the following table an example of calculation for the first case of study is shown.

Dc, projected diameter of a winding [m]	0,28
hydraulic diameter d_h [m]	0,012
Wetted perimeter P_w [m]	0,043
Cross-area A_{sec} [m^2]	0,000127
Starting pitch h [m]	0,2
Length of the roller ends [m]	0,05

Table 3.3 Geometrical properties of the model

	Wall	**Mean T oil**
Temperature [°C]	140	147,5
ρ [kg m^{-3}]	784,8	780
$\mathbf{c_p}$ [kJ $kg^{-1}K^{-1}$]	2,31	2,34
μ [10^{-6} kg $m^{-1}s^{-1}$]	2820	2587
λ [10^{-3}W $m^{-1}K^{-1}$]	125,5	125
Pr [-]	51,94	48,41
Re = ṁd/A μ [-]		4654

Table 3.4 Oil properties at the wall temperature and at the mean oil.

iteration	1	2	3	4
h [m]	0,2	0,287	0,283	0,284
n=(L-2x)/h	9,1	6,334	6,424	6,42
D=Dc*[1+(h/πDc)^2]	0,294	0,31	0,309	0,309
d/D [-]	0,041	0,038	0,039	0,039
m	0,656	0,654	0,654	0,654
Nu [-] **(lam)**	80,391	79,258	79,317	79,314
α [W $m^{-2}K^{-1}$]	842	831	831	831
tube length [m]	5,57	5,65	5,65	5,65
new h [m]	0,287	0,283	0,284	0,283
error %	43,673	-1,409	0,075	-0,004

Table 3.5 Iterations for the calculation of the convection coefficient inside the tube at the average oil temperature.

Finally, the laminar assumption for the oil flow has to be verified as:

$$\mathrm{Re}_{crit} = 2300\left[1 + 8{,}6\left(\frac{d}{D}\right)^{0{,}45}\right] = \mathrm{Re}_{crit} = 2300[1 + 8{,}6(0{,}039)^{0{,}45}] = 6894 < \mathrm{Re}$$

Considering the proposed case study, the Re number is lower than the critical one, thus the oil flow can be considered laminar.

Finally, we have 8 solutions related to the 8 cases of oil inlet temperature. The solutions need to be validated using the numerical simulation obtained using Ansys Workbench.

3.3 Numerical simulation: model and geometry

In this section the numerical simulations of the selected case studies are described. The results of this work are the temperature distribution over the roller surface and the surface temperature gradients.

We are not interested in the heating up period, but in the thermal conditions after that period, hence when the system reaches the thermal balance. This hypothesis is quite realistic whether we consider that we are looking at a stationary.

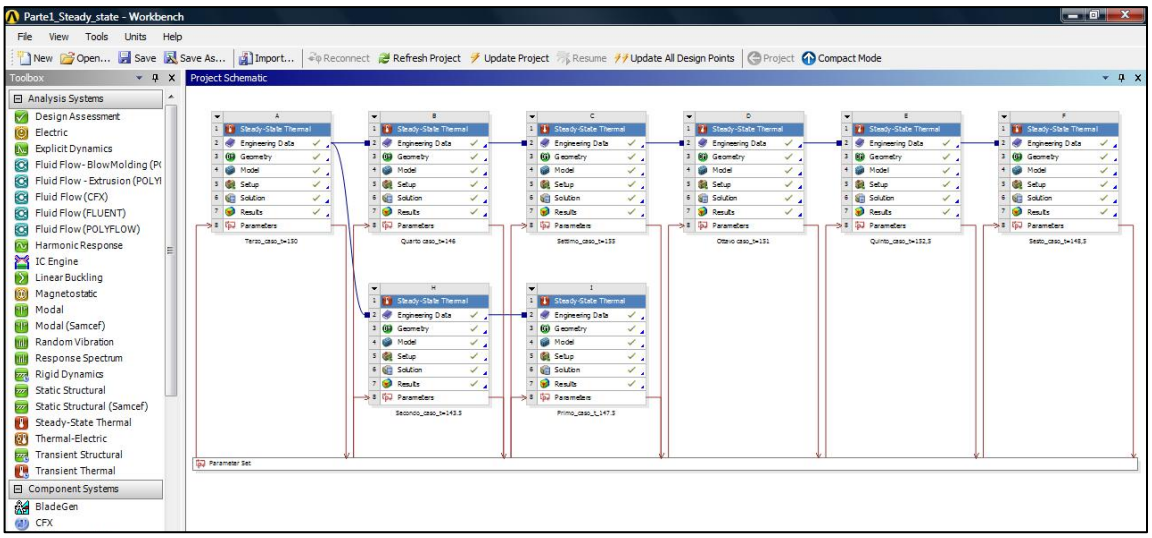

Figure 3.6 Project Schematic with the eight different models.

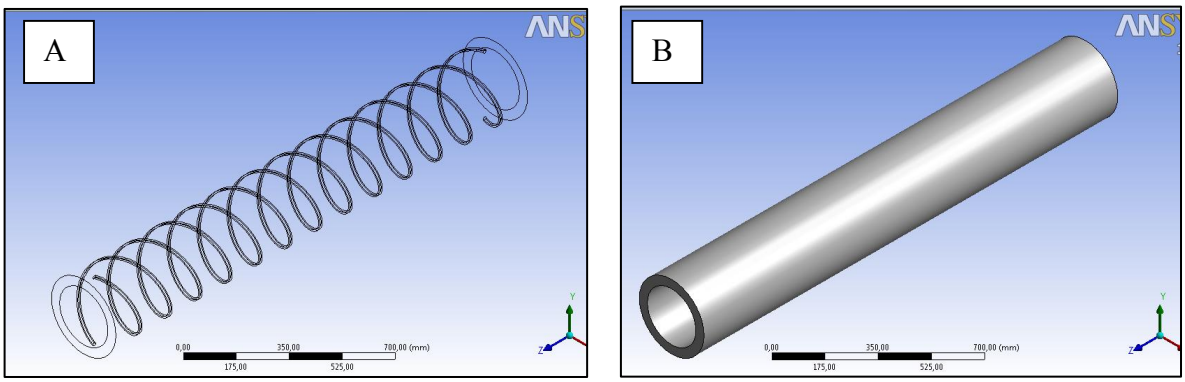

Figure 3.7 Geometrical model with 6,5 coils: (A)wireframe view with the two spires; (B)model as unique cylinder.

Figure 3.6 shows the project schematic in the Ansys Workbench environment. The model can be summarised as follows (Figure 3.7):

- Roller geometry, cross-section of the tube and Dc are known. The number of coils, according to the value of h, depends on the particular case and has already been determined.
- We study the entire model because it has no symmetry, including both the spirally coiled channels.
- We model the roller as a unique cylinder because we neglect the contact thermal resistance.

Material properties:

- We compute the analyses with two different material types: Steel with λ = 16 W $m^{-1}K^{-1}$ and Aluminium with λ= 237 W $m^{-1}K^{-1}$, in order to understand the effect of the material of the cylinder on the thermal performance of the roller.

Boundary conditions:

- Ambient temperature: 20°C.
- External coefficient (free convection and radiation effects) at air side is calculated analytically: α_{ext}=14 W $m^{-2}K^{-1}$.
- Constant oil heat transfer coefficient evaluated at the mean oil temperature.
- The inlet temperature and the oil temperature change are set. Furthermore, the oil temperature through the channel is assumed to linearly vary along the axial axis of the roller.

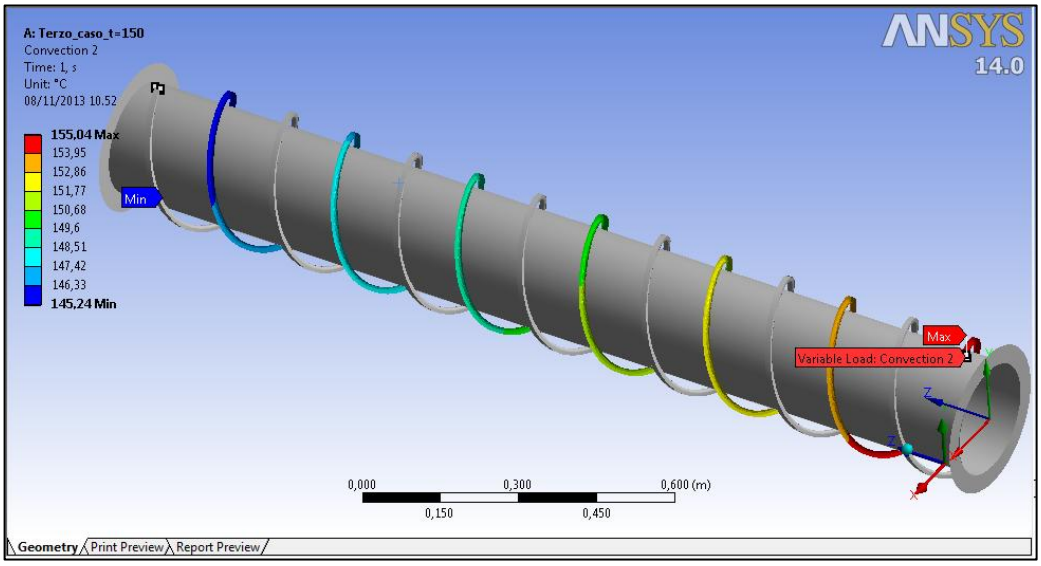

Figure 3.8 Temperature distribution of the oil inside the tube for one spire. The other one has the opposite configuration. Case: T_{in} =155 °C as oil inlet temperature.

As already said, we are interested on verify the temperature distribution over the outer surface of the roller, to:

1. Confirm analytical results. The average surface temperature should be 140 °C.
2. Evaluate the surface temperature gradient. Verify if the maximum temperature gradient is within the requested value.

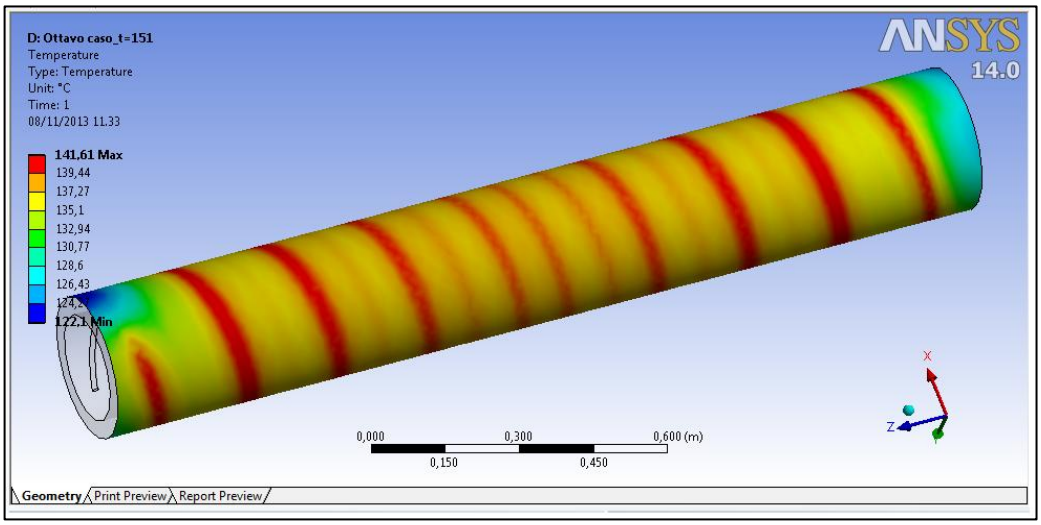

Figure 3.9 Temperature distribution on the outer roller surface.

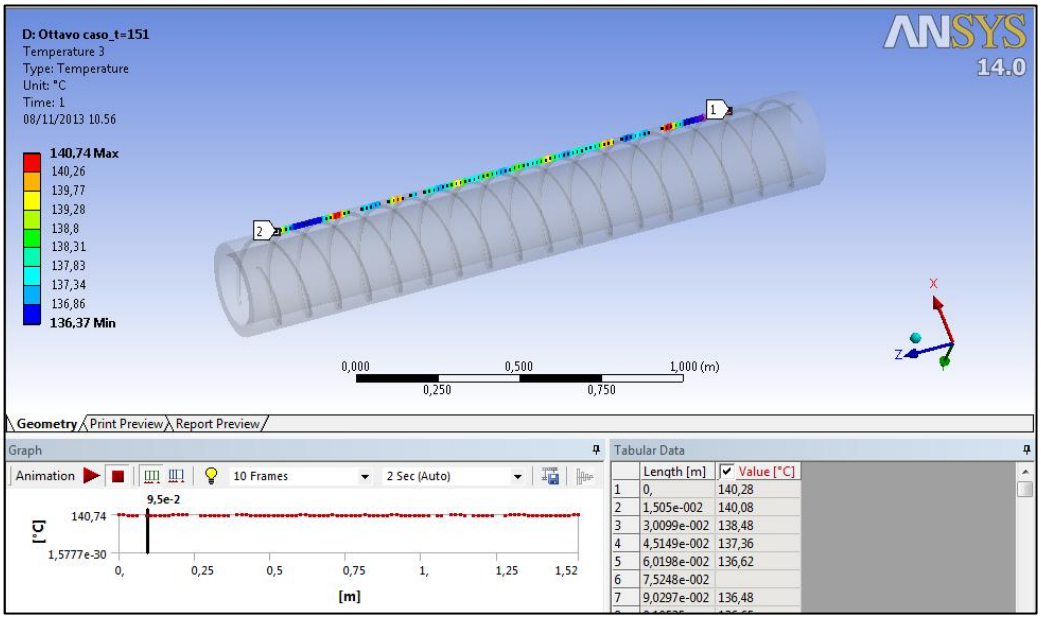

Figure 3.10 Path created on the outer roller surface to evaluate the temperature distribution along the axis of the roller.

1. The temperature distribution is evaluated by displaying the temperature on the outer roller surface, as proposed in figure 3.9. In the example shown in the picture, it is possible to notice the effect of the coils to the temperature distribution. It can also be highlighted that the roller ends are characterized by a significant temperature drop due to the fact that they are not crossed by the oil channels. For this reason, these regions are neglected from the results analyses, as proposed in figure 3.6.

2. To verify the temperature gradient over the surface we define a path, it is a line parallel to the axis and placed on the outer roller surface, as shown in the figure 3.10. The Path is subdivided in 202 points and the mean temperature can be calculated taking into account only the maximum and the minimum value (average temperature) or all the points. For this first project step the average temperature is adopted.

3.4 Results of the first step analysis

As described before each case study was calculated using aluminium and steel as roller material. The parameter tool in Ansys was used for the computation. By enter the engineering data we can set the steel conductivity as an input parameter, which will appear as first design point in the "table of design points" within the "Parameter Set". The "Table of Design Points" initially contains the current project as a design point (DP0), along with its corresponding input and output parameter values. From this table, it is possible to create new design points (or duplicate existing design points) and edit them (by varying one or more input parameters) to create separate analyses for future comparison of data. In our case we adopt the Parameter Set to add the Aluminium conductivity as a design point in addition to the steel one. For each of them is important to set the output parameters; therefore, we enter the "Mechanical Model" and in the "Solution" we click on the result we are interested on and the parameters are simply defined by checking the box between the desired parameter, e.g. minimum and maximum temperature. We have two parameters for each model. The output will then appear in the table of design points. [4]
The results are shown in the next Tables, the first one lists the values obtained in the case of steel whereas the second one those with Aluminium Alloy.
The tables includes:

- Tmax, maximum value of temperature.
- Tmin, minimum value of temperature
- Mean T, average temperature between Tmin and Tmax
- ΔT, maximum temperature gradient along the path.

T_{in_oil} [°C]	ΔT_{oil} [°C]	**calculated number of coils, n**	**n used**	α_{oil} [W $m^{-2}K^{-1}$]	T_{max} **steel** [°C]	T_{min} **steel** [°C]	T_{mean} [°C]	ΔT_{sur} **steel** [°C]
150	5	6,42	6,5	691	139,8	133,3	136,5	6,46
146	5	12,17	12	704	139,4	137,5	138,5	1,91
155	10	6,56	6,5	458	140,2	134,5	137,4	5,72
151	10	10,83	11	462	139,9	137,2	138,6	2,66
160	15	6,64	6,5	361	142,8	135,3	139,1	7,59
156	15	9,72	9,75	363	140,4	136,5	138,4	3,95
165	20	6,52	6,5	307	141,4	134,1	137,7	7,22
161	20	8,86	9	308	140,7	136,4	138,6	4,37

Table 3.6 Results obtained with stainless steel.

T_{in_oil} [°C]	T_{max} **Al** [°C]	T_{min} **Al** [°C]	T_{mean} [°C]	ΔT_{sur} **Al** [°C]
150	140,4	139,1	139,8	1,24
146	139,9	139,4	139,7	0,57
155	140,1	138,8	139,4	1,33
151	140,1	139,3	139,7	0,8
160	141,7	139,4	140,6	2,25
156	140,1	139,1	139,6	1
165	140,2	138,6	139,4	1,64
161	140,2	139,1	139,7	1,04

Table 3.7 Results obtained with Aluminium Alloy.

The results confirm the good quality of the analytical analysis whereas the surface temperature does not deviate from the value required. This fact is probably due to the lower value of heat flow provided by the system. We can also state:

1. the surface temperature gradient increases when decreasing the number of coils. (Figure 3.11)
2. the lower the oil temperature change, the higher the number of coils.
3. the lower the inlet oil temperature, the higher the number of coils.

4. The performance of the Aluminium roller is better than Steel one with regarding both the mean surface temperature and temperature gradient.(Figures 3.11 and 3.12)

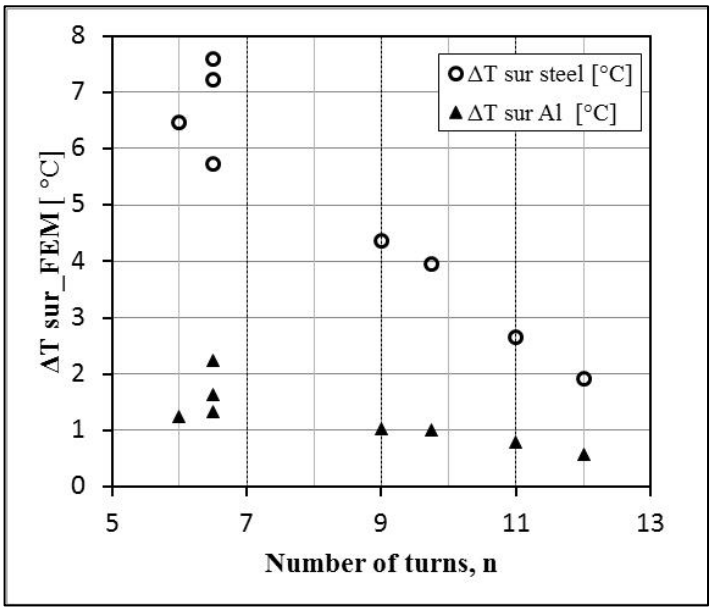

Figure 3.11 Surface temperature gradient against the number of turns in case of stainless steel and aluminium alloy.

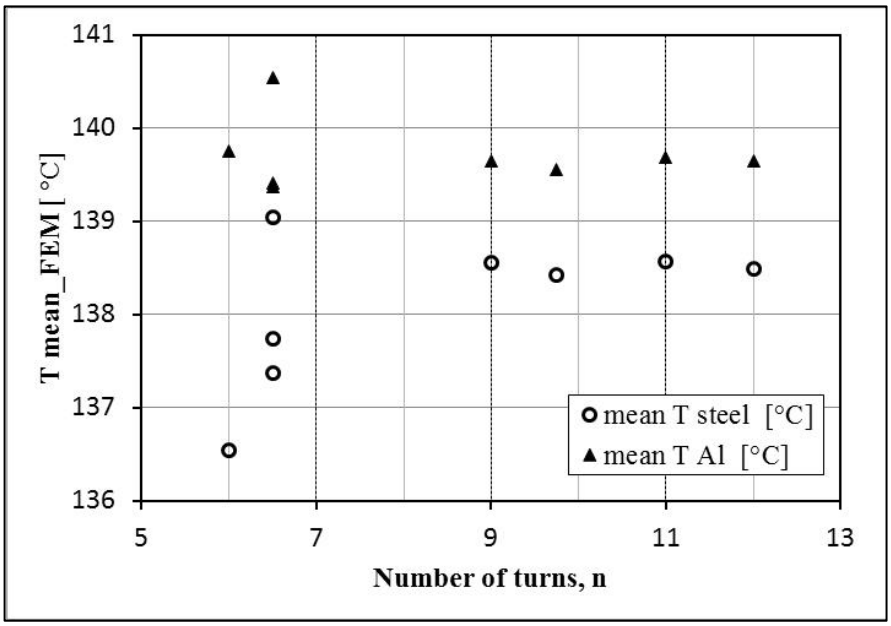

Figure 3.12 Surface temperature against the number of turns in case of stainless steel and aluminium alloy.

CHAPTER 4: Project requirement

4.1 Step description

In the previous chapter, a steady roller exposed to the ambient has been analyzed. However, the applications in which it would be involved commonly require a higher level of heat to be dissipated. Furthermore, in the first step of the project, we suppose the roller blocked, not rotating. Rollers are commonly used to heat up different materials (cotton, plastics..), which are in contact with almost half of the heated surface. This means that the thermal conditions change along the external surface. The piece in contact with the roller surface is heated and its temperature varies affecting the external surface temperature of the roller that in turn is not uniform.

However, in this project step we continue to consider the roller blocked and we assume a uniform distribution of the heat flow rate over the surface. The aim of this project step is to identify the most affecting parameters, which control the heating up process of the roller surface.

As already mentioned, the piece to be heated up does not touch the whole surface of the roller but it is usually in contact with almost half of that. A partial contact area has a strong influence on the modeling and analysis. However, in this chapter we consider simplified model with the heat flow rate uniformly distributed over the outer roller surface.

The following analysis would study the roller under a real, design heat flow rates, which are commonly required by the process. We identify the parameters affecting the proper design of the roller to achieve the required heat flow rate (i.e. inlet oil temperature, oil flow rate, hydraulic diameter of the tube, etc.), which would lead to the possibility of an optimized design of the system.

4.2 Variable project parameters.

In order to understand the effects of each parameter on the performance of the roller, we developed a general spreadsheet using the Microsoft Excel application. It permits to analyze several cases but it also allows for preliminary calculations useful at the first rough design of the roller for a specific heat flow rate requirement. Afterwards it can be precisely used to meet the requirements of the customer.
The parameters considered in the spreadsheet are the following:

- Heat flow, q [W]
- Number of turns per spire, n
- Inlet oil temperature, T_{in} [°C]
- oil temperature change, ΔT_{oil} [°C]
- Oil flow rate, $\dot{m}$ [kg s^{-1} or l min^{-1}]
- External surface temperature of the roller, T_{sur} [°C]

These 6 parameters are not independent one to each other; in fact, two of them are defined by setting the other 4. Thus, we created four spreadsheets trying to describe the effects of the dependent variables by defining four different groups of four parameters, which are supposed to represent different type of project requirements.
The first release of the spreadsheets is done by keeping the roller geometry equal to the one been used up to this step and still considering a laminar oil flow. Later on, a turbulent-based analysis was implemented when necessary.

4.2.1 Analysis 1

The first analysis can be summarized as follows:

Fixed parameters:

- Heat flow, q [W]
- External surface temperature of the roller, T_{sur} [°C].

- Number of turns per spire, n

Three cases are created, for each one we fix one value of q and T_{sur} and four values of n.

Variable parameter:

- Inlet oil temperature, T_{in} [°C] with 20 values.

Dependent parameters:

- oil temperature change, ΔT_{oil} [°C]
- Oil flow rate, $\dot{m}$ [l min^{-1}]

In the end we set 252 calculations of the dependent parameters.

Analysis 1	case 1	case 2	case 3
q [W]	3500	3000	2500
n1	9	9	9
n2	10	10	10
n3	12	12	15
n4	15	15	20
$\mathbf{T_{sur}}$ [°C]	140	140	140

Table 4.1 Parameter setting of the Excel spreadsheet: "Analysis 1".

The spread sheet allows for an easy continuous analysis by changing the values of the tables. In this way we can optimize each considered parameter for any given costumer requirement. by assure the project requirements.

Is necessary to remark that the External surface temperature of the roller, T_{sur}, is considered as the average value along the surface of the coil, T_w.

The next table shows the results of the first case connected to the previous table.

T_{in_oil} [°C]	ΔT_{oil} **(n1)**	**oil flow** $\dot{m}$ [l min^{-1}] **(n1)**	ΔT_{oil} **(n2)**	**oil flow** $\dot{m}$ [l min^{-1}] **(n2)**	ΔT_{oil} **(n3)**	**oil flow** $\dot{m}$ [l min^{-1}] **(n3)**	ΔT_{oil} **(n4)**	**oil flow** $\dot{m}$ [l min^{-1}] **(n4)**
145	2,75	20,97	3,02	19,11	3,52	16,41	4,17	13,85
146	3,52	16,36	3,86	14,96	4,47	12,92	5,26	10,98
147	4,34	13,28	4,74	12,17	5,46	10,57	6,38	9,04
148	5,19	11,10	5,65	10,19	6,49	8,88	7,55	7,64
149	6,08	9,47	6,60	8,72	7,55	7,63	8,75	6,59
150	7,00	8,23	7,59	7,59	8,65	6,66	9,97	5,78
151	7,94	7,24	8,60	6,70	9,77	5,90	11,22	5,13
152	8,92	6,45	9,63	5,97	10,91	5,28	12,50	4,61
153	9,91	5,80	10,69	5,38	12,08	4,76	13,80	4,17
154	10,93	5,26	11,77	4,88	13,27	4,34	15,11	3,81
155	11,97	4,80	12,88	4,46	14,48	3,97	16,44	3,50
156	13,03	4,41	14,00	4,11	15,71	3,66	17,79	3,23
157	14,11	4,07	15,14	3,80	16,95	3,39	19,16	3,00
158	15,20	3,78	16,30	3,52	18,22	3,16	20,54	2,80
159	16,32	3,52	17,47	3,29	19,49	2,95	21,93	2,62
160	17,44	3,29	18,66	3,08	20,78	2,76	23,34	2,46
161	18,59	3,09	19,86	2,89	22,09	2,60	24,76	2,32
162	19,75	2,90	21,08	2,72	23,41	2,45	26,19	2,19
163	20,92	2,74	22,32	2,57	24,74	2,32	27,64	2,08
164	22,11	2,59	23,56	2,43	26,08	2,20	29,09	1,98
165	23,30	2,46	24,82	2,31	27,44	2,09	30,55	1,88

Table 4.2 "Analysis 1": results with q = 3 kW (case 1). For each value of n (number of turns) the results vary as a function of the inlet oil temperature.

In what follows, we show an example of calculation; considering the case:

q = 3500 W; n = 9; T_{sur} = 140 [°C]; T_{in} = 165 [°C]

The geometrical characteristics of the roller are those reported in chapter 3.2 and we adopt the Gnielinski model (see paragraph 3.2.3) to compute the heat transfer coefficient inside the channel.

First of all, we calculate the size of the pitch and the average diameter of the curvature D of the coil:

$$h = \frac{L-2x}{n} = \frac{1920-2*50}{9} = 200 \text{ mm}$$

$$D = D_c \left[1 + \left(\frac{h}{\pi D_c}\right)^2\right] = 280\left[1 + \left(\frac{200}{\pi 280}\right)^2\right] = 295 \text{ mm}$$

$$\frac{d}{D} = \frac{12}{295} = 0{,}04$$

The mean surface temperature of the tube is set at 140 °C; therefore, we can define the oil properties which are:

T_w [°C]	ρ [kg m^{-3}]	c_p [kJ kg^{-1} K^{-1}]	μ [10^{-6}kg $m^{-1}s^{-1}$]	λ [mW m^{-2} K^{-1}]	Pr_w [-]
140	784,87	2,313	2820	125,56	51,94

Table 4.3 Oil properties at 140°C .

The procedure requires some iterations because the heat transfer coefficient depends on the average temperature of the oil, which is unknown because at this stage we don't know the oil temperature variation.
Thus, we start from a first tentative value of temperature change, for example: $\Delta T_{oil,0}$ = 10 °C.

First iteration (laminar oil flow):

- Average $T_{oil,0}$= T_{in} - $\Delta T_{oil,0}$/2 = 165-10/2=160 °C, oil properties at $T_{oil,0}$:

$\rho_{,0}$ [kg m^{-3}]	$c_{p,0}$ [kJ $kg^{-1}K^{-1}$]	$\mu_{,0}$ [10^{-6}kg $m^{-1}s^{-1}$]	$\lambda_{,0}$ [mW $m^{-2}K^{-1}$]	$Pr_{,0}$ [-]	$\dot{m}_{,0}$ [kg s^{-1}]	$Re_{,0}$ [-]
771,87	2,3847	2197,87	124,12	42,23	0,07338	3135

Table 4.4 Oil properties at the average oil temperature.

- $m = 0{,}5 + 0{,}2903\left(\frac{d}{D}\right)^{0{,}194} = m = 0{,}5 + 0{,}2903(0{,}04)^{0{,}194} = 0{,}656$
- $Nu_{,0} = 3{,}66 + 0{,}08\left[1 + 0{,}8\left(\frac{d}{D}\right)^{0{,}9}\right] Re^{m} Pr^{1/3}\left(\frac{Pr}{Pr_w}\right)^{0{,}14} =$

  $= 3{,}66 + 0{,}08[1 + 0{,}8(0{,}04)^{0{,}9}]\ 3135^{0{,}656} 42{,}23^{1/3}\left(\frac{42{,}23}{51{,}94}\right)^{0{,}14} = 59{,}15$
- $\alpha_{,0} = \frac{Nu\ \lambda}{d} = \frac{59{,}15\ 124{,}12\ 10^{-3}}{0{,}012} = 615{,}47\ \mathrm{W\ m^{-2}K^{-1}}$
- $T_{oil,1} = \frac{q}{2\alpha A_{tube}} + T_w = \frac{3500}{2*615{,}47*0{,}3586} + 140 = 147{,}93\ °C$
- $\Delta T_{oil,1} = (T_{in} - T_{oil,1})*2 = (165\text{-}147{,}93)*2 = 34{,}14\ °C$
- $\text{error } \% = \frac{T_{oil,1} - T_{oil,0}}{T_{oil,0}}*100 = \frac{147{,}93 - 160}{160}*100 = -7{,}54\ \%$
- $\Delta T_{oil,1,new} = \frac{\Delta T_{oil,1} - \Delta T_{oil,0}}{2} = \frac{34{,}14 + 10}{2} = 22{,}07\ °C$

With this value of oil temperature change, we can start the new iteration by repeating the calculations reported before. We will iterate till the deviation between two iteration is less than 0,005%.

step	**mean T oil** [°C]	**ρ** [kg m^{-3}]	**c_p** [kJ kg^{-1} K^{-1}]	**μ** [10^{-6}kg m^{-1}s^{-1}]	**λ** [mW m^{-2} K^{-1}]	**ṁ** [kg s^{-1}]	**Re** [-]	**Pr** [-]
1	147,93	779,72	2,34	2573,39	124,99	0,03387	1236	48,20
2	153,03	776,40	2,36	2414,68	124,62	0,03224	1254	45,72
3	153,25	776,25	2,36	2407,76	124,60	0,03189	1244	45,61
4	153,33	776,20	2,36	2405,33	124,60	0,03183	1242	45,57
5	153,34	776,19	2,36	2404,92	124,60	0,03181	1242	45,57

Table 4.5 Oil properties at the average oil temperature and at each step-iteration.

step	**ΔT_{new}** [°C]	**mean T_{oil}** [°C]	**Nu** [-]	**α_{oil}** [W m^{-2} K^{-1}]	**mean $T_{oil,new}$** [°C]	**ΔT_i** [°C]	**error %**
1	22,1	147,9	35,74	374	153,0	23,9	3,449
2	23,0	153,0	35,24	368	153,3	23,5	0,145
3	23,3	153,3	35,04	366	153,3	23,3	0,051
4	23,3	153,3	35,01	366	153,3	23,3	0,009
5	23,3	153,3	35,00	366	153,4	23,3	0,002

Table 4.6 Example of iteration used for the Excel spreadsheet: "Analysis 1".

The results can be finally summarized as:

- Final ΔT_{oil} = 23,3 °C
- outlet oil temperature, T_{out} = T_{in} - ΔT_{oil} = 165-23,3 = 141,7 °C
- oil flow rate $\dot{V}$= 60000*$\frac{\dot{m}}{\rho}$ = 60000* 0,032/776,19 = 2,46 l min^{-1}

Finally, we can create the table of results (table 4.2) , which permits to create the diagram reported in Figures 4.1 and 4.2 that show the variation of ΔT_{oil} and $\dot{V}$ plotted against the T_{in} as a function of q, T_{sur} and n (4 diagrams per graph).

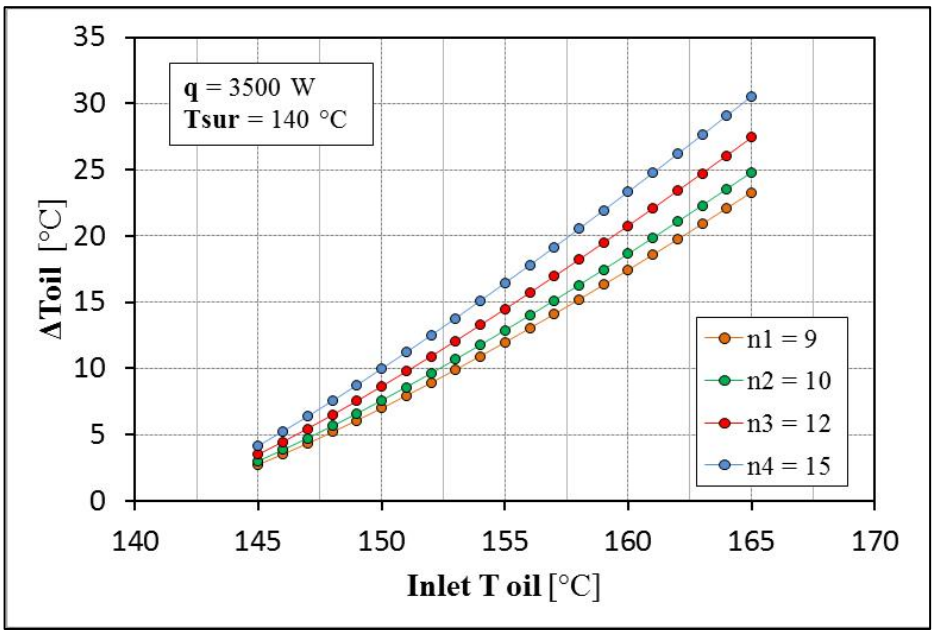

Figure 4.1 Variation of ΔT_{oil} against the T_{in} as a function of n, q, and T_{sur}.

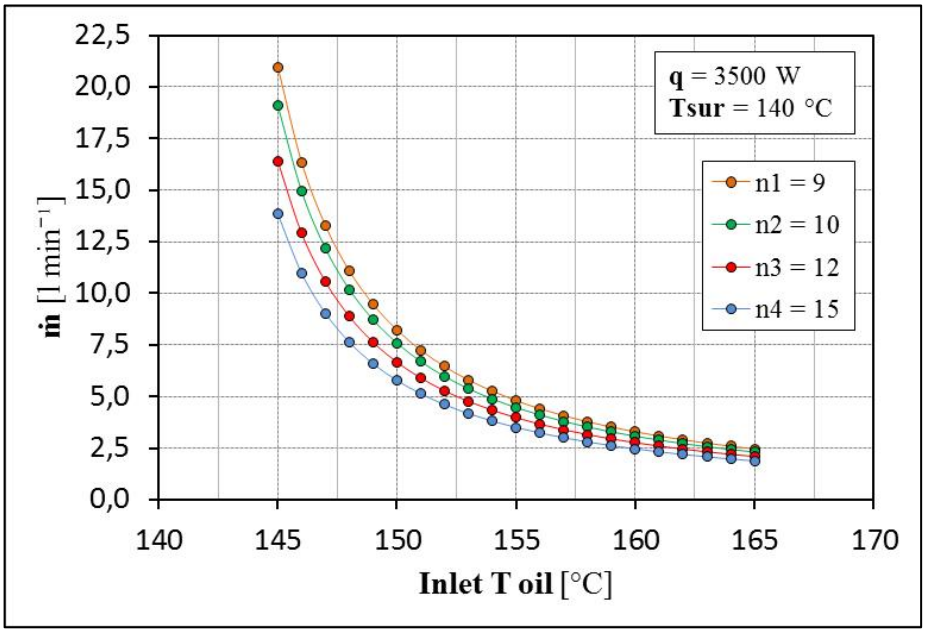

Figure 4.2 Variation of $\dot{m}$ against the T_{in} as a function of n, q, and T_{sur}.

The two graphs are also useful to check if every loop is successfully converged. In fact each diagram has to provide a mostly continuum trend, without any particular discontinuity.

With this Analysis we can get a first rough idea on the effects of each parameters on the performance of the roller. Keeping constant the values of heat flow rate (q) and external surface temperature (T_{sur}), from the analysis of the results we can state that:

- The lower the inlet oil temperature, the better results; in fact, the oil temperature change decreases with T_{in}. This leads to a better temperature distribution on the outer roller surface.
- A low inlet oil temperature implies a high oil flow rate, which leads to higher oil velocity, inlet pressure, and pressure drop. The problem can be solved by increasing the number of turns since the oil flow rate decreases as n increases. Meanwhile the oil temperature change increases and this does not provide any benefit to the outer surface temperature distribution but we have also to consider that the increase of n leads to a lower value of pitch (distance between 2 turns), which is surely helpful for the results.

4.2.2 Analysis 2

The "Analysis 2" considers the following configuration:

Fixed parameters:

- Inlet oil temperature, T_{in} [°C]
- External surface temperature of the roller, T_{sur} [°C].
- Number of turns per spire, n

Three cases are generated; for each one we fix one value of T_{in} and T_{sur} and two values of n.

Variable parameter:

- Oil flow rate, $\dot{m}$ [l min^{-1}] with 7 values.

Dependent parameters:

- oil temperature change, ΔT_{oil} [°C]
- Heat flow, q [W]

Finally, we set 42 calculations of the dependent parameters.

Analysis 2	case 1	case 2	case 3
$\mathbf{T_{in}}$ [°C]	148	148	148
n1	9	10	12
n2	15	16	17
$\mathbf{T_{sur}}$ [°C]	140	140	140

Table 4.7 Parameter setting of the Excel spreadsheet: "Analysis 2".

$\dot{m}$ [l min^{-1}]	ΔT_{oil} **(n1)**	**q** [W] **(n1)**	ΔT_{oil} **(n2)**	**q** [W] **(n2)**
2	7,76	942	9,65	1171
3	7,09	1292	9,00	1638
5	6,30	1914	8,20	2487
7	5,82	2473	7,68	3263
9	5,47	2991	7,30	3990
11	5,20	3478	7,01	4681
13	4,99	3941	6,77	5341

Table 4.8 "Analysis 2": results with T_{in} = 148 °C (case 1). For each value of n (number of turns) the results vary as a function of the oil flow rate.

The procedure implemented is similar to the proposed in the "Analysis 1". At the beginning, we have to set a first tentative value for $\Delta T_{oil,0}$.

At each step we can calculate the $\Delta T_{oil,i}$ (at which the oil properties are estimated) because T_{in} is known. Then m, Nu_i, and α_i. The heat flow is computed as:

$$q_i = 2\alpha_i A_{tube} (T_{oil,i} - T_w)$$

then the new temperature drop:

$$\Delta T_{oil,new} = \frac{q_i}{2\, c_p \dot{m}}$$

where $\dot{m}$ is the oil flow rate [kg s^{-1}]. The oil temperature change for the next step iteration:

$$\Delta T_{oil,i+1} = (\Delta T_{oil,i} + \Delta T_{oil,new})/2;$$

and

$$\text{error\%} = \frac{\Delta T_{oil,i+1} - \Delta T_{oil,i}}{\Delta T_{oil,i}} * 100.$$

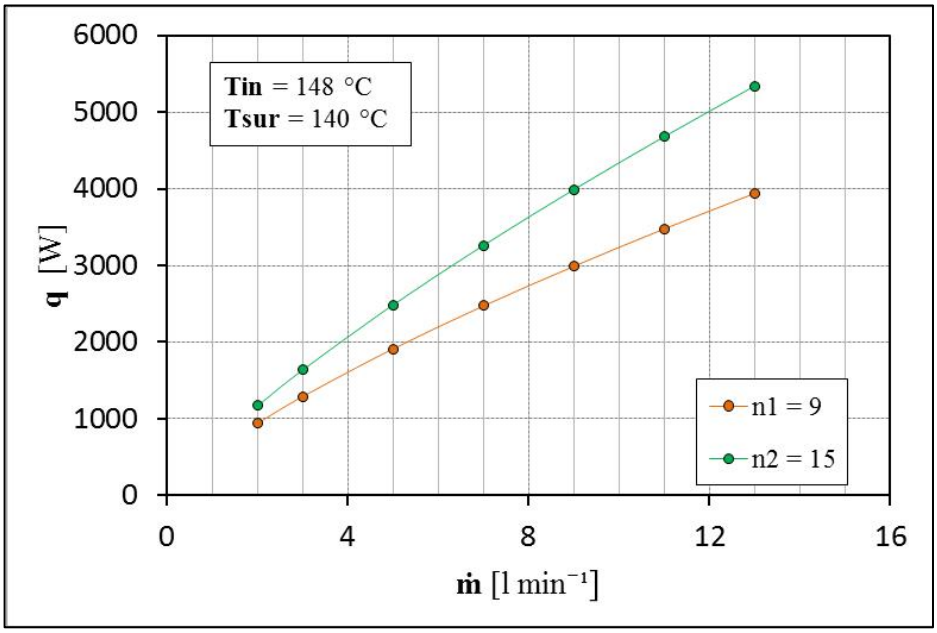

Figure 4.3 Variation of q against the ṁ as a function of n, T_{in}, and T_{sur}.

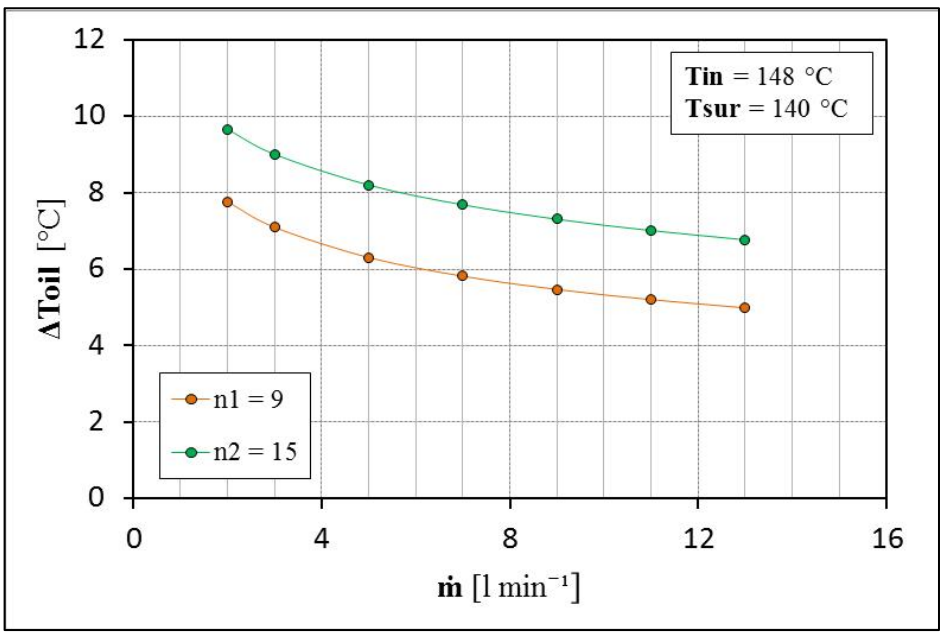

Figure 4.4 Variation of ΔT_{oil} against the ṁ as a function of n, T_{in}, and T_{sur}.

As shown in the figures 4.3 and 4.4 we can plot the results; in this case, q and ΔT_{oil} *are plotted as a function of* the oil flow rate. From the analysis of the results we can state that:

- For a certain value of inlet oil temperature, the higher the oil flow rate, the higher the heat flow.
- The higher the number of turns, the higher q and ΔT_{oil}
- This analysis could be very useful if we want to regulate the process by changing the oil flow rate while keeping the inlet oil temperature almost constant.

4.2.3 Analysis 3

The "Analysis 3" considers the following configuration:

Fixed parameters:

- Oil flow rate, $\dot{m}$ [l min^{-1}]
- Heat flow, q [W]
- Number of turns per spire, n

Three cases are generated, for each one we fix one value of $\dot{m}$ and q and two values of n.

Variable parameter:

- External surface temperature of the roller, T_{sur} [°C] with 13 values.

Dependent parameters:

- oil temperature change, ΔT_{oil} [°C]
- Inlet oil temperature, T_{in} [°C]

Finally, we set 78 calculations of the dependent parameters.

Analysis 3	case 1	case 2	case 3
$\dot{m}$ [l min^{-1}]	5	5	5
n1	9	9	9
n2	15	15	15
q [W]	3000	3500	4000

Table 4.9 Parameter setting of the Excel spreadsheet: "Analysis 3".

T surface [°C]	**ΔT_{oil} (n1)**	**T_{in_oil}** [°C] **(n1)**	**T_{out_oil}** [°C] **(n1)**	**ΔT_{oil} (n2)**	**T_{in_oil}** [°C] **(n2)**	**T_{out_oil}** [°C] **(n2)**
80	12,05	96,1	84,0	12,09	92,3	80,2
85	11,99	101,0	89,0	12,03	97,2	85,2
90	11,94	105,9	94,0	11,98	102,2	90,2
95	11,89	110,8	98,9	11,93	107,1	95,2
100	11,84	115,7	103,9	11,88	112,0	100,2
105	11,80	120,7	108,9	11,83	117,0	105,2
110	11,75	125,6	113,8	11,78	121,9	110,1
115	11,70	130,5	118,8	11,74	126,9	115,1
120	11,66	135,4	123,7	11,69	131,8	120,1
125	11,62	140,3	128,7	11,65	136,7	125,1
130	11,57	145,2	133,6	11,60	141,7	130,0
135	11,53	150,1	138,6	11,56	146,6	135,0
140	11,49	155,0	143,5	11,52	151,5	140,0

Table 4.10 "Analysis 3": results with $\dot{m}$ = 5 $l\,min^{-1}$ and q = 3,5 kW (case 2). For each value of n (number of turns) the results vary as a function of outer surface temperature.

The procedure implemented is similar to the proposed in the "Analysis 1". At the beginning, we have to set a first tentative value for $T_{oil,0}$.

At each step we can calculate the oil properties. Then m, Nu_i, and α.

And then the new oil temperature $T_{oil,i}$:

$$T_{oil,i} = \frac{q}{2\alpha A_{tube}} + T_w \quad \text{where } A_{tube} \text{ is the internal area of one spire,}$$

and the error:

$$error\% = \frac{T_{oil,i} - T_{oil,i-1}}{T_{oil,i-1}} * 100.$$

Figures 4.5 and 4.6 report the obtained results; in this case T_{in} and ΔT_{oil} *are plotted against* the required temperature on the roller surface.

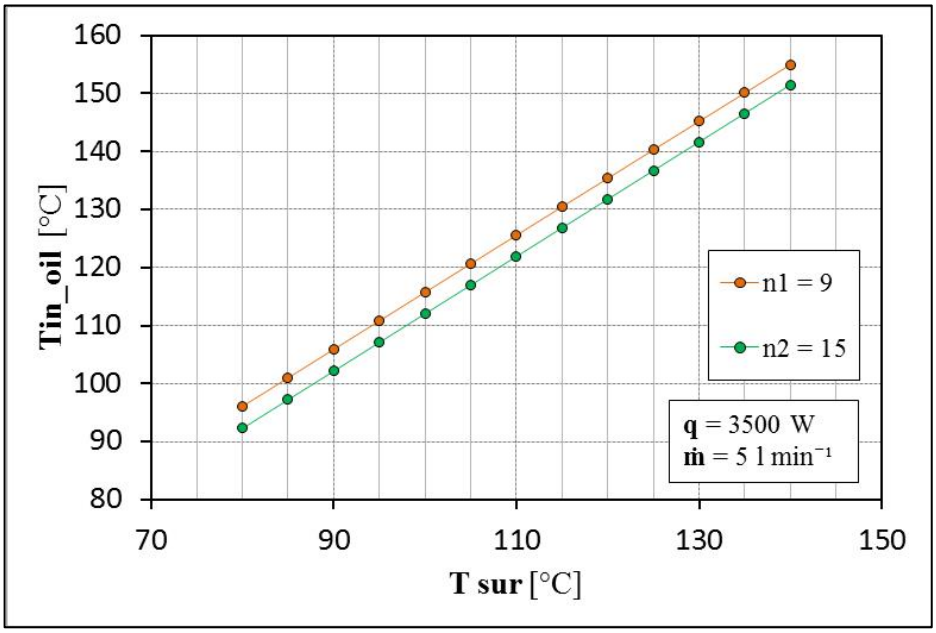

Figure 4.5 Variation of T_{in} against the T_{sur} as a function of n, q, and $\dot{m}$.

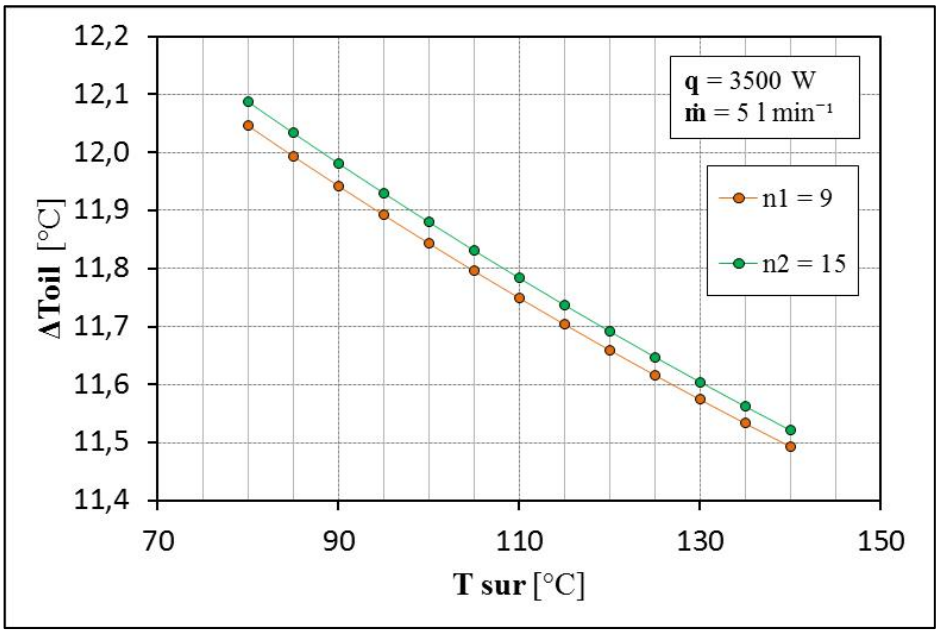

Figure 4.6 Variation of ΔT_{oil} against the T_{sur} as a function of n, q, and $\dot{m}$.

From the analysis of the diagrams we can state that:

- For a certain value of oil flow rate, an increasing of the surface temperature requires higher inlet oil temperature, the relationship between these two variables is almost linear.
- The higher the number of turns, the lower the inlet oil temperature to be provided.
- For a certain value of oil flow rate, the higher the required surface temperature, the lower the value of oil temperature change, while the number of turns does not exhibit a noticeable influence on the results.

4.2.4 Analysis 4

The "Analysis 4" considers the following configuration:

Fixed parameters:

- Oil flow rate, $\dot{m}$ [l min^{-1}]
- External surface temperature of the roller, T_{sur} [°C]
- Number of turns per spire, n

Three cases are created, for each one we fix one value of $\dot{m}$ and q and two values of n.
Variable parameter:

- Heat flow, q [W] with 13 values.

Dependent parameters:

- oil temperature change, ΔT_{oil} [°C]
- Inlet oil temperature, T_{in} [°C]

Finally, we set 78 calculations of the dependent parameters.

Analysis 4	case 1	case 2	case 3
$\dot{\mathbf{m}}$ [l min^{-1}]	5	5	5
n1	9	9	9
n2	15	15	15
$\mathbf{T_{sur}}$ [°C]	140	130	150

Table 4.11 Parameter setting of the Excel spreadsheet: "Analysis 4".

q [W]	$\mathbf{\Delta T_{oil}}$ **(n1)**	$\mathbf{T_{in\_oil}}$ [°C] **(n1)**	$\mathbf{T_{out\_oil}}$ [°C] **(n1)**	$\mathbf{\Delta T_{oil}}$ **(n2)**	$\mathbf{T_{in\_oil}}$ [°C] **(n2)**	$\mathbf{T_{out\_oil}}$ [°C] **(n2)**
3500	11,50	154,6	143,0	11,52	151,2	139,7
4000	13,13	156,6	143,5	13,16	152,8	139,7
4500	14,76	158,6	143,9	14,80	154,4	139,6
5000	16,38	160,7	144,3	16,44	156,0	139,6
5500	18,00	162,7	144,7	18,07	157,6	139,5
6000	19,63	164,7	145,1	19,70	159,2	139,5
6500	21,24	166,7	145,5	21,33	160,7	139,4
7000	22,86	168,7	145,9	22,96	162,3	139,4
7500	24,47	170,7	146,3	24,59	163,9	139,3
8000	26,08	172,7	146,6	26,21	165,5	139,2
8500	27,69	174,7	147,0	27,84	167,0	139,2
9000	29,30	176,7	147,4	29,46	168,6	139,1
9500	30,90	178,6	147,7	31,08	170,1	139,1

Table 4.12 "Analysis 4": results with $\dot{m}$ = 5 $l\ min^{-1}$ and T_{sur} = 140 (case 1). For each value of n (number of turns) the results vary as a function of heat flow rate.

The procedure implemented is similar to the proposed in the "Analysis 1".

Figures 4.7 and 4.8 reports the results; in this case, T_{in} and ΔT_{oil} *are plotted as a function of* the required heat flow rate. From the analysis of the two diagrams we can infer:

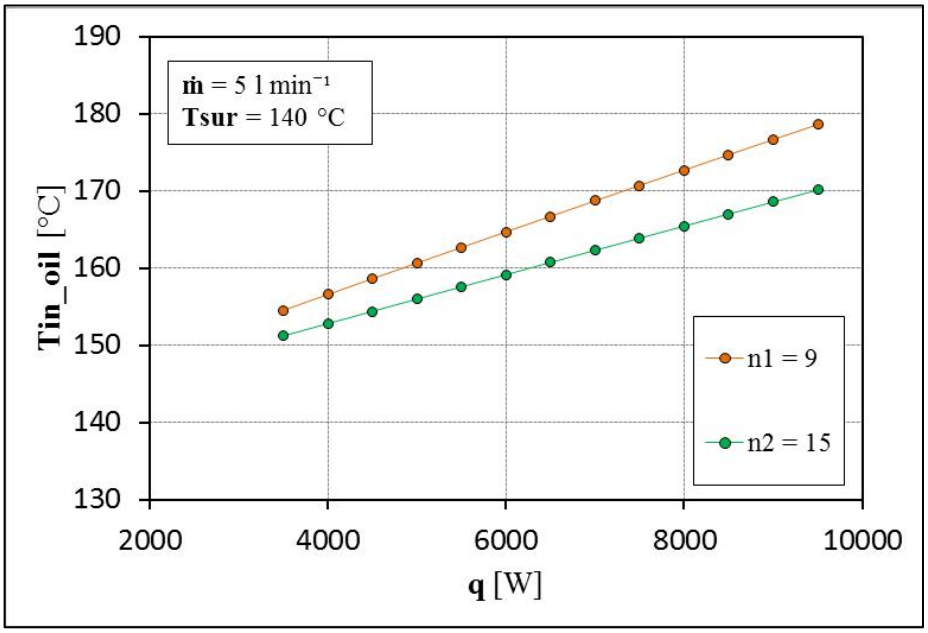

Figure 4.7 Variation of T_{in} against the q as a function of n, T_{sur}, and $\dot{m}$.

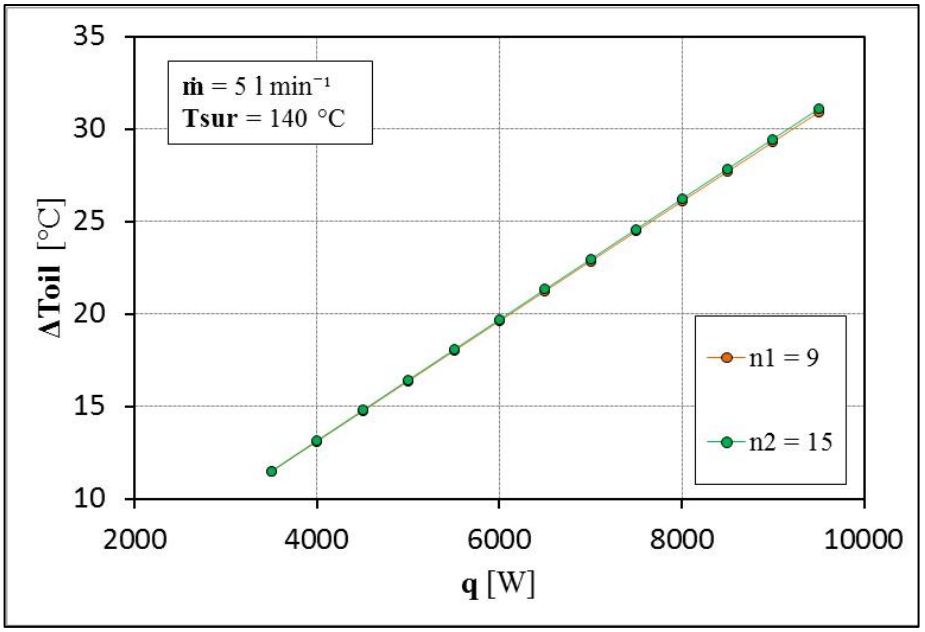

Figure 4.8 Variation of ΔT_{oil} against the q as a function of n, T_{sur}, and $\dot{m}$.

- For a certain values of oil flow rate and surface temperature of the roller, an increasing of heat flow rate requires higher inlet oil temperature; the relationship

between these variables is almost linear. The higher the number of turns, the lower the inlet oil temperature to be provided.

- For a certain values of oil flow rate and surface temperature of the roller, the higher the required heat flow rate, the higher the value of oil temperature change, while the number of turns does not show to strongly affect the results.

4.3 Customer requirements

At this point of the project, it is important to focus our attention on specific values of the parameters. Thanks to the appointment with a possible interested customer, we had the opportunity to discuss about some design data involved in a particular application.
We studied the solution currently used by the customer in order to design a new version that would include the present technology meeting the process requirements, which can be listed as follows:

1. The solution would be a preheating roller. It is a roller used in coating and laminating machines and not directly involved in the coating process, but rather used for the applications where a preheating process of the materials is needed in order to reach a suitable temperature for the following process-steps.
2. Required heat flow rate, q = 30 kW.
3. Temperature on the outer roller surface, T_{sur} = 140 °C
4. Maximum surface temperature gradient: ± 2,5 °C. ΔT_{sur} = 5 °C.
5. The external piece of textile covers only a semicircle of the outer surface of the roller. Hence, during the rotation, it touches 180 ° of the angular coordinate.
6. Process speed: 40 m min^{-1}. From this value we can derive the rotational speed of the roller.
7. Material: cotton textile. Weighing = 200 g m^{-2}

4.3.1 Current solution:

The current solution uses two concentric cylinders separated by a small gap along all the roller length. Within the gap a coiled-designed metal slice is inserted. The slice is welded to the internal cylinder and the external one is placed on it. It creates an internal coiled-shaped tube, rolled between the two cylinders, fed with the hot oil. The inlet and outlet sections are placed at the same cylinder end. It means that the oil flows in one direction to the other cylinder end, and comes directly back through the opposite way. An external heat exchanger heats the oil coming from a tank where it arrives after flowing through the cylinder. An external pump is used to ensure the oil flow.
The main geometrical characteristics of the roller are:

- length, L= 2000 mm
- external diameter, D = 300 mm

The current solution seems to present a big weakness: the oil temperature decreases during the heating process and the pipe configuration leads to a maximal oil temperature gradient on one cylinder side (where the inlet and outlet sections are located). However, the temperature difference decreases along the axis till a minimum value at the opposite cylinder side. The problem was solved by choosing a suitable high oil flow rate (60 – 70 $\mathrm{l\,min^{-1}}$) in order to reduce the oil temperature change, leading to a more uniform surface temperature on the outer roller surface. However, that high oil flow rate requires a pumping power. The selection of the pump has a strong influence on the final product cost, which increases with the pump size.

4.3.2 Oil flow rate selection

According to what previously described, the proper selection of the oil flow rate can lead to a cost reduction. In our project sketch, the pump is placed in an internal bay of the roller. In order to select the oil flow rate, we have to take into account two important points:

- as already explained, a high flow rate requires a pumping power (i.e. high cost) but leads to better results
- a high pumping power means a big-size pump.

Looking at the catalog offered by "Linn-Pumpen Gmbh" [5] we can have an idea on the several gear pumps produced by the company (Figure 4.9)

Performance n ≈ 1450 1/min

Typ	cm³/U	Pressure											
		bar	5	10	15	20	30	40	50	60	70	80	90	100
		Capacity / required drive power (kW*)												
F 310	5,1	l/min	7,40	7,35	7,30	7,25	7,20	7,10	7,00	6,90	6,80	6,70	6,60	6,50
		kW*	0,09	0,18	0,26	0,35	0,53	0,71	0,88	1,06	1,24	1,41	1,59	1,77
F 314	7,1	l/min	10,20	10,15	10,10	10,00	9,90	9,70	9,40	9,10	8,80	8,50	8,00	7,40
		kW*	0,12	0,24	0,37	0,49	0,73	0,97	1,22	1,46	1,70	1,95	2,19	2,43
F 318	9,1	l/min	13,20	13,10	13,00	12,80	12,60	12,40	12,10	11,80	11,50	11,20	10,80	10,40
		kW*	0,16	0,31	0,47	0,63	0,94	1,26	1,57	1,89	2,20	2,52	2,83	3,15
F 323	11,7	l/min	16,70	16,60	16,50	16,40	16,20	16,00	15,60	15,20	14,80	14,40	14,00	13,60
		kW*	0,20	0,40	0,60	0,80	1,20	1,59	1,99	2,39	2,79	3,19	3,59	3,98
F 328	14,1	l/min	20,30	20,20	20,10	20,00	19,80	19,60	19,40	19,00	18,60	18,20	17,70	17,20
		kW*	0,24	0,48	0,72	0,96	1,45	1,93	2,41	2,89	3,37	3,86	4,34	4,82
F 333	16,7	l/min	24,10	24,00	23,90	23,80	23,60	23,40	23,20	22,90	22,50	22,10	21,60	21,10
		kW*	0,28	0,57	0,85	1,14	1,70	2,27	2,84	3,41	3,97	4,54	5,11	5,68

Valid for hydraulic oil with 35 mm²/s at 50 °C
Tolerance of capacity: +/- 3%
Oil-Speed: max. 1,5 m/s suction side, max. 4,5 m/s pressure side
* **kW** = required drive power in kW (without dissipation)

Figure 4.9 Pump catalog provided by "Linn-Pumpen Gmbh"

The pump choice is based on the oil flow rate: instead of 60-70 $\mathrm{l\,min^{-1}}$, which is the solution currently adopted by the customer, in our project we reduce that value up to more suitable one which should be the best tradeoff between performance and costs:

- Oil flow rate, $\dot{m}$= 24 $\mathrm{l\,min^{-1}}$.

As shown in the figure 4.9, that oil flow rate is related to pressure p = 10 bar. The required pressure is still unknown because the geometry and the components are not yet known. However, we can assume that the pressure drop won't be greater than 10 bar.

4.4 Selection of the hydraulic diameter

Considering the customer requirements we can start an analytical analysis using the Excel spreadsheets described is paragraph 4.2. The project is characterized by high heat flow rate and a fixed value of average temperature on the external surface. We proceed as follows:

1. *Selection of two values of number of turns.*
   Up to now we considered low values of heat flow rates due to the assumption that the roller exchanges heat only with the surroundings. In this case, the requirements are different, thus we start the project by choosing two different values of number of turns: n=15 and n=30, which obviously are greater than before.

   The two sets of parameters are the following:

set number	**q** [kW]	$\dot{\mathbf{m}}$ [l min $^{-1}$]	$\mathbf{T_{sur}}$ [°C]	**n**
1	30	24	142	15
2	30	24	142	30

Table 4.13 First trial of parameter sets. Focusing on customer requirements.

   In the analytical calculation the surface temperature is taken as the average value on the internal wall of the spire. Since the concept is already argued, we can directly set a assumed value which has to be higher than the required temperature on the external surface: T_w = 142 °C > 140 °C.

2. *Check the flow features. Laminar or turbulent flow (paragraph 3.2.3).*

   For each set of parameters we can calculate the Critical Reynolds number (paragraph 3.2.3) and derive the related oil flow rate and inlet oil temperature as:
   - geometrical properties:

D_c, projected diameter of a winding [m]	0,28
Hydraulic diameter d [m]	0,012
Wetted perimeter P_w [m]	0,043
Cross-area A_{sec} [m^2]	0,000127
D, average diameter of the curvature of the coil [m]	0,29
Spire length (**l** = $D_c \pi$ n) [m]	13,5
Internal spire surface (A_{tube}= P_wl) [m^2]	0,58
Starting pitch h [m]	0,2
Ratio d/D [-]	0,042
Length of the roller ends [m]	0,05

Table 4.14 geometrical properties of the first parameter set.

The Critical Reynolds number for the first parameter set is: Re_{cr} = 7040.

- Set a first tentative mean oil temperature (i.e. 150 °C), and derive the oil properties at this temperature and at the T_w = 142 °C (density, specific heat capacity, dynamic viscosity, thermal conductivity, Prandtl number)
- Calculate $\dot{m} = \frac{Re_{cr} A_{sec} \mu_{oil}}{d}$; $\xi = f(Re_{cr}, \frac{d}{D}, \mu_w, \mu_{oil})$; $Nu = f(Re_{cr}, \xi, Pr_w, Pr_{oil})$ and $\alpha = \frac{Nu\, \lambda}{d}$.
- Compute the new oil temperature $T_{oil,new} = \frac{q}{2\alpha A_{tube}} + T_w$ and temperature change $\Delta T_{oil,new} = \frac{q}{2 c_p \dot{m}}$.
- error % = $\frac{T_{oil,new} - T_{oil}}{T_{oil}} * 100$, start the next iteration.

Finally, we obtain the final inlet oil temperature and the oil flow rate.

	q = 30 kW	
	inlet oil T [°C]	**oil flow rate** [l min^{-1}]
n = 15	179,4	12,8
n = 30	168,0	14,4

Table 4.15 Results in term of inlet oil temperature and oil flow rate related to the critical Reynolds number.

In case of design oil flow rate lower than the critical one (shown in the table above) the oil flow will be laminar, otherwise it will be turbulent. It means that our design flow rate ($\dot{m}$ 24 l min^{-1}) leads to a turbulent flow of the oil.
That means that the formula for heat transfer in turbulent flow has to be used to calculate the Nusselt number.

3. *Enter the "Analysis 4" and set the values of oil flow rate (4.3.2) and required surface temperature, for each analyzed number of turns. Evaluate the results: inlet and outlet oil temperature, oil temperature drop. Compare the results.*

We can now set the input parameters and check the analytical results at the required heat flow rate and outer surface temperature.

Analysis 4 **q = 30** kW $\mathbf{T_w}$ **= 142** °C $\dot{\mathbf{m}}$ **= 24** l min^{-1}		
n	15	30
$\Delta\mathbf{T_{oil}}$ [°C]	20,5	20,5
$\mathbf{T_{in}}$ [°C]	163,2	158,1
$\mathbf{T_{out}}$ [°C]	142,7	137,5
$\boldsymbol{\alpha_{oil}}$ [W m^{-2} K^{-1}]	2371	2293

Table 4.16 Results by the turbulent-based analysis of the two models.

The oil temperature change is almost the same because it depends on the oil flow rate, heat flow rate, and specific heat capacity: the first two parameters are fixed and the third one has a very little influence on the temperature.
The results improve as the number of turn increases because the pitch of the spires decreases and, as shown in the table 4.16, it leads to a decreasing of inlet oil temperature, which means that the oil temperature is closer to the one required on the external surface.

Moreover, higher the number of turns, lower the heat transfer coefficient. However, it does not decrease too much and its decreasing is compensate by the increasing of the total heat transfer area.

4. *Check the mean oil velocity*

In both cases the mean oil velocity is:

$$v = \frac{\dot{m}}{60000 A_{sec}} = \frac{24}{60000 * 0{,}000127} = 3{,}15 \text{ m s}^{-1}.$$

The oil velocity have an impact on the heat transfer coefficients but it also can affect the vibration, pressure drop, propensity for fouling and overall service life of the component. For most fluids, in most applications, the higher tube velocity, the higher the heat transfer coefficient, however tubes have limits to the maximum velocity they can handle with. There is also a limit to the minimum velocity. In addition to make designs more complex, is it possible to design with an ideal tube velocity for heat transfer and longevity, however if the fluid flow is varied during the operational life of the product it can have a great impact on the maintenance of that heat exchanger.

Maximum recommended tube velocity.

Recommended maximum tube velocities will vary by source, not necessarily due to differing opinions, but mostly due to the fact that fluid temperature, chemistry and other factors might have different effects as a function of the tube material.

Factors effecting acceptable tube velocities:

- Type of fluid and temperature
- Fluid make-up (suspended solids, treatment, chemistry)
- Tube material

General effects of excessive tube velocity

- Erosion (abrasion)

- Corrosion
- Pressure drop
- Vibration

General guidelines for limit tube velocities based on tube material

Tube Material	**Velocity Limit** $[\mathrm{m\ s^{-1}}]$
Aluminium, Copper, Brass	1,8
Copper-Nickel (70/30%)	4,6
Copper-Nickel (90/10%)	3
Carbon Steel	3
Austenitic Stainless Steel	4,6
Titanium	> 15

Table 4.17 General guidelines for limit tube velocities based on tube material. [6]

Low tube velocity:

For most fluids, in most applications a low tube velocity means low heat transfer coefficient, therefore the heat transfer is less effective, so thermal designers will typically try to keep the velocity as high as the tube material and pressure drop will allow. Similar to high tube velocities, what is considered to be too low of a tube velocity also depends on: fluid temperature, chemistry, and construction. For clean pure fluids, with little or no suspended solids which are not prone to fouling, the goal is to avoid laminar flow.

.

Effects of too low of a tube velocity:

- Fouling
- Corrosion
- Deposition
- Low heat transfer coefficient

Observing the values shown in the Table 4.17, we notice that the maximum velocity limit in the case of carbon steel is v_{lim} = 3 m s^{-1}. In both cases the oil velocity is higher, therefore we may:

- reduce the oil flow rate
- increase the cross-section of the tube

The first possibility will lead to worst results due to the consequent increase of oil temperature change. Thus, we modified the channel diameter considering an optimal velocity of:

v_{oil} = 2,2 m s^{-1}.

Is it now possible to calculate the new cross-sectional area:

$$A_{sec,new} = \frac{v_{oil,old}}{v_{oil,new}} A_{sec,old} = \frac{3,15}{2,2} 0,000127 = 0,000182 \text{ m}^2 = \frac{\pi d'^2}{8} + d'c.$$

where ***d'*** is the width of the tube corresponding to the diameter of the semicircle which forms the area, and ***c*** is the height of the rectangle (see Figure 3.5). We keep the same **c**, hence, we can derive the new value of **d'**.

$$d'_{new} = \frac{-c+\sqrt{c^2+4\frac{\pi A_{sec,new}}{8}}}{\frac{\pi}{4}} = 15,23 \text{ mm}$$

$$P_{w,new} = \frac{\pi d'_{new}}{2} + 2c + d'_{new} = 51,15 \text{ mm}$$

and the new hydraulic diameter: $d_{h,new} = \frac{4A_{sec,new}}{P_{w,new}} = 14,27$ mm

5. *Check the results with the new channel configuration*

We enter the "Analysis 4" with the turbulent formulations and set the same inputs as before.

We find the following results (Table 4.18):

Analysis 4 **q = 30** kW **T_w = 142** °C **$\dot{m}$ = 24** l min^{-1} **d_h2 = 14,27** mm		
n	15	30
$\dot{m}$ lam-tur [l min^{-1}]	14,97 (tur)	17,8 (tur)
ΔT_{oil} [°C]	20,5	20,5
T_{in} [°C]	164,9	159
T_{out} [°C]	144,4	138,4
α_{oil} [W m^{-2} K^{-1}]	1720	1653

Table 4.18 Results by the turbulent-based analysis of the two models with the new hydraulic diameter.

Comparing the table 4.16 and 4.18, we can make some considerations about the influence of the new hydraulic diameter on the analytical results. It does not affect the inlet oil temperature and the oil temperature change. The heat transfer area increases whereas the heat transfer coefficient decreases

We have to calculate, in both cases of study and with the two different cross-section configurations, the pressure drop on one spire. We consider only the distributed pressure loss due to friction but, later on, we have to calculate the local pressure drops involved in the process in order to choose the proper hydraulic pump to be used.

$\Delta p = \rho \, \xi \frac{l}{d_h} \frac{v^2}{2}$ [Pa],

where ρ is the oil density [kg m^{-3}], ξ is the friction factor for turbulent flow in helically coiled tubes, l is the length of the tube, d_h is the hydraulic diameter and *v* is the mean oil velocity.

ξ is given by [4] as: $\xi = \left[\frac{0,3164}{Re^{0,25}} + 0,03 \left(\frac{d_h}{D}\right)^{0,5}\right] \left(\frac{\mu_w}{\mu}\right)^{0,27}$

n	$\mathbf{d_h}$ [mm]	**ρ** [kg m^{-3}]	**l** [m]	**v** [ms^{-1}]	**Re** [-]	**ξ**	**Δp** [Pa]	**Δp** [bar]
15	11,93	776	13,50	3,15	12071	0,0376	164121	1,641
30	11,93	780	26,54	3,15	11361	0,0375	322870	3,229
15	14,268	775	13,50	2,2	10255	0,0398	70605	0,706
30	14,268	779	26,54	2,2	9558	0,0396	138868	1,389

Table 4.19 Pressure drop in one spire calculated for the cases of study with different hydraulic diameter and number of turns.

Is it now possible to say that an increasing of cross-sectional area provides better results even in terms of pressure drops. However, an increasing of number of turns gives worst results due to the consequent increase of the tube length.

6. *FEM simulations: distribution of surface temperature.*

Before focusing on the FEM simulations, we decide to add a case considering a intermediate value of number of turns: n = 23.
Repeating the previous steps for this new value, we get the following results (Table 4.20 and 4.21):

Analysis 4 **q = 30** kW $\mathbf{T_w}$ **= 142** °C $\dot{\mathbf{m}}$ **= 24** l min^{-1} **n = 23**		
$\mathbf{d}_h$ [mm]	11,928	14,268
$\dot{m}$ **lam-tur** [l min^{-1}]	13,15 (turb)	16,99 (turb)
$\Delta\mathbf{T_{oil}}$ [°C]	20,52	20,5
$\mathbf{T_{in}}$ [°C]	159,67	160,83
$\mathbf{T_{out}}$ [°C]	139,18	140,33
$\boldsymbol{\alpha_{oil}}$ [W m^{-2} K^{-1}]	2316,7	1673,15

Table 4.20 Results by the turbulent-based analysis of the models characterized by n = 23 and the two different hydraulic diameter.

n	$\mathbf{d_h}$ [mm]	**ρ** [kg m^{-3}]	**l** [m]	**v** [ms^{-1}]	**Re** [-]	**ξ**	**Δp** [Pa]	**Δp** [bar]
23	11,928	778,74	20,43	3,15	11576	0,0375	248508	2,485
23	14,268	777,99	20,43	2,2	9769	0,0396	106892	1,069

Table 4.21 Pressure drop in one spire calculated for the cases with the two different hydraulic diameter and n=23.

In order to get the distribution of temperature on the roller surface, we set the numerical calculation with the finite element method by adopting the software Ansys workbench 14.

How to create the geometry and set the boundary conditions of the model is explained in the chapter 3.3. There is basically one difference: on the outer surface of the roller is not set anymore a value of free heat transfer coefficient to the ambient. In this case, we have a higher heat flow rate and also the heat flux changes over the surface. For these simulations we set a value of heat flow rate as uniformly distributed over the entire outer surface of the roller, q = 30 kW. It means that we simulate a situation in which the piece to be heated up touches all the roller surface. The case is not realistic but gives interesting information to make some rough considerations.

Material properties: [7]

The material is a not specified Alloy Steel, which commonly has:

λ_{steel} = 26 ÷ 48,6 W m^{-2} K^{-1}.

For this reason we select a value of λ_{steel} = 35 W m^{-2} K^{-1}.

Postprocessing:

After running the simulations for each case of study we obtain the following results:

d_h1	n15	n23	n30
T_{min} [°C]	129,6	131,5	132,1
T_{max} [°C]	138,0	137,4	137,0
average T [°C]	133,8	134,5	134,5
ΔT_{sur} [°C]	8,4	5,9	4,9

Table 4.22 Results obtained from the FEM simulations of the three different number of turns and the first hydraulic diameter d_h = 11,93 mm

d_h2	n15	n23	n30
T_{min} [°C]	130,33	132,01	132,87
T_{max} [°C]	137,82	136,94	136,48
average T [°C]	134,08	134,48	134,68
ΔT_{sur} [°C]	7,49	4,93	3,61

Table 4.23 Results obtained from the FEM simulations of the three different number of turn and the first hydraulic diameter d_h =14,27 mm

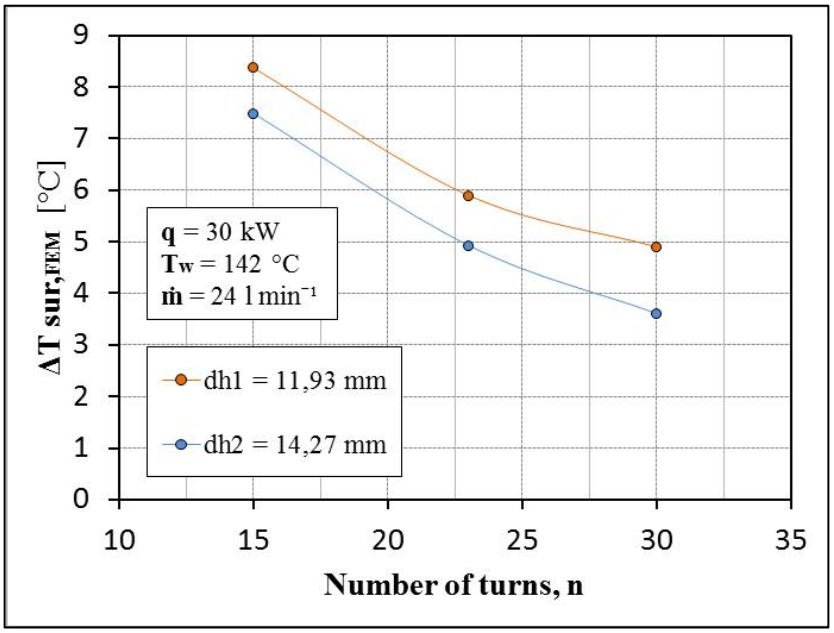

Figure 4.10 Variation of $\Delta T_{sur,FEM}$ against the number of turns. The two curves are related to two hydraulic diameters.

The average value of the temperature on the outer roller surface is lower than the one we set in the analytical calculation (142 °C) due to the assumption done.

Looking at the final results, we can make the following conclusion:
The temperature distribution on the outer surface improves when increasing both the number of turns and the cross-sectional area.

4.5 Variable oil heat transfer coefficient

Up to now we derived from the analytical calculation the average value of heat transfer coefficient along the entire spire. This value is then set as constant in the numerical calculation with the aid of the finite element software. The geometry remains the same, however, the oil properties change while it flows through the spire. This leads to a variation of the heat transfer coefficient and, in turn, to a variation of heat transferred. Therefore, it could be interesting to verify how a variable heat transfer coefficient along the channel would affect the outer surface temperature distribution.
We will consider an example where we set some parameters and then calculate the new temperature distribution on the outer surface of the roller once the heat transfer coefficient is varied along the channel.
We take a set of parameters already analyzed (table 4.18 in case of 15 number of turns).
The results obtained by setting a constant value of heat transfer coefficient along the spire in the FEM simulation are shown in the Table 4.23.
To calculate a variable heat transfer coefficient we proceed as follows:

1. Considering a linear distribution of oil temperature along the axial coordinate of the roller, we divide it in 10 parts and then we calculate the average oil temperature in each part.

$\mathbf{T_{in}}$ [°C]	1	2	3	4	5	6	7	8	9	10	$\mathbf{T_{out}}$ [°C]
164,86	163,8	161,8	159,8	157,7	155,7	153,6	151,6	149,5	147,5	145,4	144,41

Table 4.24 Average oil temperature at each part of the spire used for calculating the variable heat transfer coefficient.

2. We can derive the oil properties at each average temperature (density, specific heat capacity, kinematic viscosity, thermal conductivity, Prandtl number)

part	$\boldsymbol{\rho}$ [kg m^{-3}]	$\boldsymbol{c_p}$ [kJ kg^{-1} K^{-1}]	$\boldsymbol{\mu}$ [10^{-6}kg $m^{-1}s^{-1}$]	$\boldsymbol{\lambda}$ [mW m^{-2} K^{-1}]
1	769	2,40	2079	124
2	771	2,39	2142	124
3	772	2,38	2206	124
4	773	2,38	2269	124
5	775	2,37	2333	124
6	776	2,36	2397	125
7	777	2,35	2460	125
8	779	2,35	2524	125
9	780	2,34	2587	125
10	781	2,33	2651	125

Table 4.25 Oil properties at each average temperature. The oil temperature drop is divided in 10 parts in order to calculate the variable heat coefficient along the spire.

3. We can derive the oil properties at the wall temperature (density, specific heat capacity, kinematic viscosity, thermal conductivity, Prandtl number)

$\mathbf{T_w}$ [°C]	$\boldsymbol{\rho}$ [kg m^{-3}]	$\boldsymbol{c_p}$ [kJ kg^{-1} K^{-1}]	$\boldsymbol{\mu}$ [10^{-6}kg $m^{-1}s^{-1}$]	$\boldsymbol{\lambda}$ [mW m^{-2} K^{-1}]
142	784	2,32	2758	125

Table 4.26 Oil properties at the wall temperature.

4. We can derive Reynolds number Re = $\frac{\dot{m} d_h}{A_{sec} \mu_{oil}}$.

	1	2	3	4	5	6	7	8	9	10
$\dot{m}$ [kg s^{-1}]	0,308	0,308	0,309	0,309	0,31	0,31	0,311	0,312	0,312	0,313
Re = ṁ*d/ A*μ [-]	11578	11253	10948	10659	10386	10128	9883	9650	9429	9219

Table 4.27 Oil flow rate and Reynolds Number for each part of the spire.

5. After computing the friction factor for turbulent flow ξ, we derive the Nusselt number Nu for each part and then the heat transfer coefficient.

part	ξ	**Nu** [-]	α_{oil} [W m^{-2} K^{-1}]
1	0,0402	212,2	1841
2	0,0401	208,5	1812
3	0,0400	205,1	1784
4	0,0399	201,7	1757
5	0,0398	198,6	1731
6	0,0397	195,5	1707
7	0,0396	192,6	1683
8	0,0396	189,8	1661
9	0,0395	187,1	1639
10	0,0394	184,4	1618

Table 4.28 Variation of friction factor, Nusselt number and heat transfer coefficient along the spire.

6. To assure that the entire heat flow rate is almost equal to the set one, we derive the value for each part and then we sum the results. If we multiply the total heat flow rate through one spire by two, we will obtain almost the total one required by the process, 30 kW.

1	2	3	4	5	6	7	8	9	10	**q tot** [W]
2777	2477	2186	1905	1633	1369	1112	863	620	384	15326

Table 4.29 Heat flow exchanged through each part of the spire. The total heat power is referred to only one spire.

To set the variable film coefficient in the FEM simulation, we decide to derive the formula of α_{oil} over the axial coordinate of the roller in both directions. In both spires the heat transfer coefficient decreases while the oil flows, but the flow directions are opposite. The distribution of the heat transfer coefficient is almost linear, therefore we derive two linear equations as shown in the following figures:

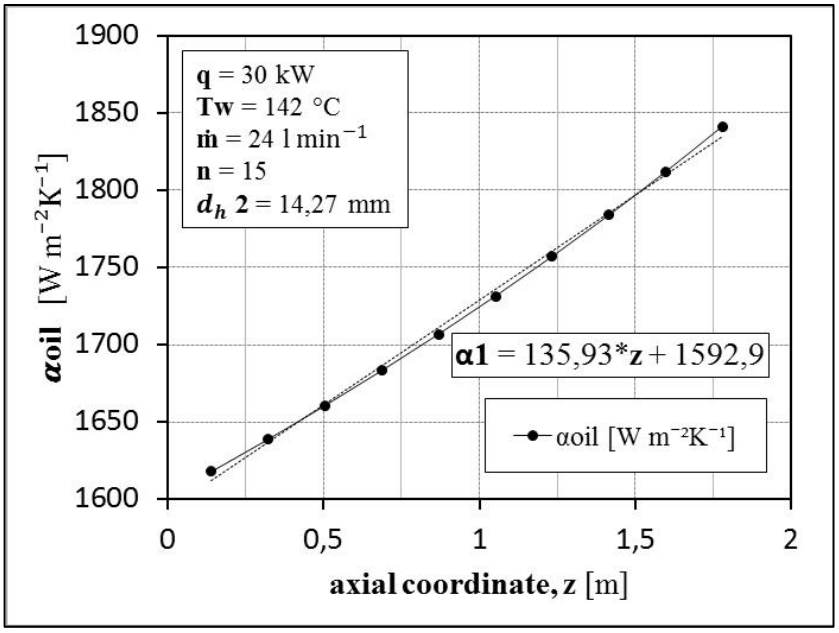

Figure 4.11 Variation of heat transfer coefficient along the first spire over the axial coordinate.

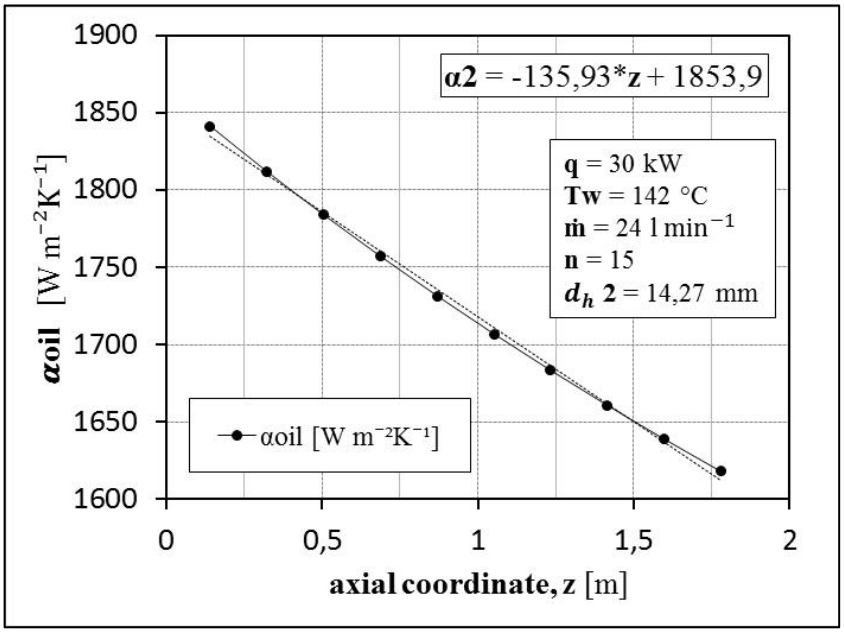

Figure 4.12 Variation of heat transfer coefficient along the second spire over the axial coordinate.

Finite element simulation: we keep the same model and change only the heat transfer coefficient by filling the boxes with the new linear equations. Evaluating the result of the surface temperature on the Path placed on the outer surface (see Figure 4.13), we see the two temperature distributions not significantly varying each other. It means that the assumption of constant heat transfer coefficient does not strongly affect the final results.

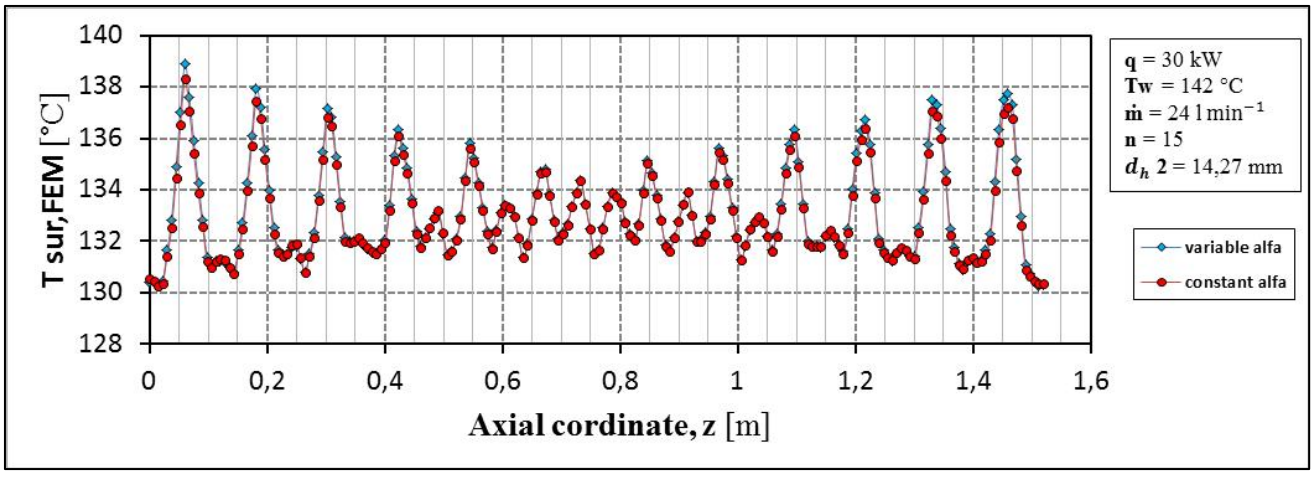

Figure 4.13 Temperature distribution on the outer surface. The values are evaluated at the points of the Path placed on the outer surface and 1,5 m long.

4.6 Selection of the number of turns.

4.6.1 Effect of the number of turns on the heat flow rate.

In this paragraph we study how to select the more suitable number of turns to meet the customer's requirements. We fix the cross-sectional area as obtain from the previous study, see Chapter 4.4. We will vary the number of turns and compute analytically the values of oil temperature change, inlet oil temperature and average heat transfer coefficient. Afterwards we will run the simulations in order to find out the values of temperature variation on the outer roller surface. We expect that an increasing of the number of turns leads to a decreasing of temperature gradient. The customer fixed a threshold on the temperature gradient equal to 5 °C. The number of turns plays a crucial role in the achievement of such result.
We proceed through the following steps:

1 *Choose a set of number of turns and obtain the analytical results by setting a initial value of surface temperature.*

We choose three values of number of turns: n=15, n=23, and n=30. In fact, we have already analytically studied these three number of turns by setting a value of wall temperature on the tube equal to 142 °C (neglecting the thermal resistance of the material).

2 *Check the flow: laminar or turbulent.*

It is important to check the flow condition. We have already found that in every case the oil flow is turbulent (see Table 4.18 and 4.20).

3 *Find out the analytical and numerical results.*

Considering the three values of number of turns we can calculate the values of inlet and outlet oil temperatures and of the heat transfer coefficient. Afterwards we can deal with the FEM simulations and derive the average value of outer temperature

and its variations along the Path used to evaluate the results (see Table 4.18 an 4.20 for the analytical results and Table 4.23 for the simulation results).

4 Find the relationship between the wall temperature and the number of turns.

We can immediately recognize that the mean external surface is less than 140 °C, temperature required by the customer; that means that the wall temperature used for the analytical calculation was too low. We have to define now the realistic value to be set analytically as wall temperature of the tube in order to get, in the end, the required external temperature. We set an initial value of the temperature wall, the mean temperature on the outer surface changes by varying the number of turns or the inlet oil temperature (here we focus on the number of turns). Therefore, we can make a linear interpolation of $T_{sur,FEM}$ considering a pair of n:

$$\mathbf{T_{sur,FEM}\ (n)} = T_{sur,FEM}\ (15) + \frac{T_{sur,FEM}(30) - T_{sur,FEM}(15)}{30-15}\ (\mathbf{n}\text{-}15)$$

We choose n15 and n30 because they give the lower error as compared to n23.

5 Choose of other values of n to be analyzed in order to create the final graphs.

The following values of number of turns are chosen:

9, 11, 13, 15, 17, 19, 21, 23, 25, 27, 29, 30. We run the numerical simulations changing the number of turns up to the value that permits a temperature gradient lower than 5 °C.

6 Calculation of $T_{sur,FEM}$ and $T_{w,new}$.

We can derive the $T_{sur,FEM}$ for each number of turns. It is useful to avoid other simulations to be run involving different number of turns, which lead to a high time consuming. In every case the value of $T_{sur,FEM}$ will be less than 140 °C. Afterwards we can make a simple proportion and finally obtain the $T_{w,new}$ to be set in the analytical calculation ($T_{w,old}$= 142 °C)

$$T_{w,new} = \frac{T_{w,old}}{T_{sur,FEM}} * 140$$

Finally, we obtain the following values:

n	9	11	13	15	17	19	21	23	25	27	29	30
$T_{sur,FEM}$	133,9	134,0	134,0	134,1	134,1	134,2	134,2	134,5	134,3	134,3	134,4	134,7
$T_{w,new}$	148,4	148,4	148,3	148,3	148,2	148,2	148,2	147,8	148,1	148,0	148,0	147,6

Table 4.30 First row: Outer roller temperature from FEM simulations; second row: re-calculated wall temperature.

7 *Set the input parameters in the "Analysis 4" and find out the analytical results.*

For each case of study is it possible to set the number of turns, the oil flow rate, and the new wall temperature and see the results at the required heat flow rate. The results are the inlet and outlet oil temperature and the heat transfer coefficient (Table 4.31).

n	$\mathbf{T_{in\_oil}}$ [°C]	$\mathbf{T_{out\_oil}}$ [°C]	$\mathbf{\Delta T_{oil}}$ [°C]	$\mathbf{\alpha_{oil}}$ [W m^{-2} K^{-1}]
9	177,1	156,8	20,28	1881
11	174,3	154,0	20,32	1840
13	172,3	151,9	20,35	1811
15	170,6	150,2	20,37	1789
17	169,3	148,9	20,39	1772
19	168,2	147,8	20,40	1758
21	167,3	146,9	20,41	1747
23	166,3	145,9	20,43	1734
25	165,9	145,5	20,43	1729
27	165,4	144,9	20,44	1722
29	164,9	144,4	20,45	1716
30	164,3	143,9	20,45	1710

Table 4.31 Analytical results with several number of turns. The new wall temperature has been set in the analytical calculations.

8 *Run the simulations with different model geometry and find out the mean temperature on the surface for each case of study.*

After running the simulations, we evaluate the numerical results:

n	T_{min} [FEM]	T_{max} [FEM]	T_{mean} [FEM]	T_{mean} of 202 values	ΔT_{sur} [FEM]
9	127,7	144,05	135,9	133,9	16,35
11	132,2	144,5	138,4	136,4	12,3
13	135,1	144,5	139,8	138,2	9,38
15	136,5	144,7	140,6	139,3	8,13
17	137,5	143,9	140,7	140,0	6,41
19	138,1	144,1	141,1	140,5	6,02
21	138,2	144,1	141,2	140,7	5,89
23	138,1	143,2	140,6	140,5	5,1
25	138,7	143,1	140,9	140,8	4,42

Table 4.32 Numerical results obtained by the finite element software Ansys, with several number of turns.

The results are taken from the Path placed on the outer surface of the roller. The path is characterized by 202 values. The results listed in the Tables are the average values of the computed data.. The temperature gradient is calculated considering the maximum and the minimum temperatures over the points of the path. N = 25 leads to a temperature gradient of ΔT_{sur} = 4,42 °C, which meets the requirement. This number is used in the next calculations and for the next project steps.

Hence, 25 number of turns becomes a fixed parameter for the rest of the project.

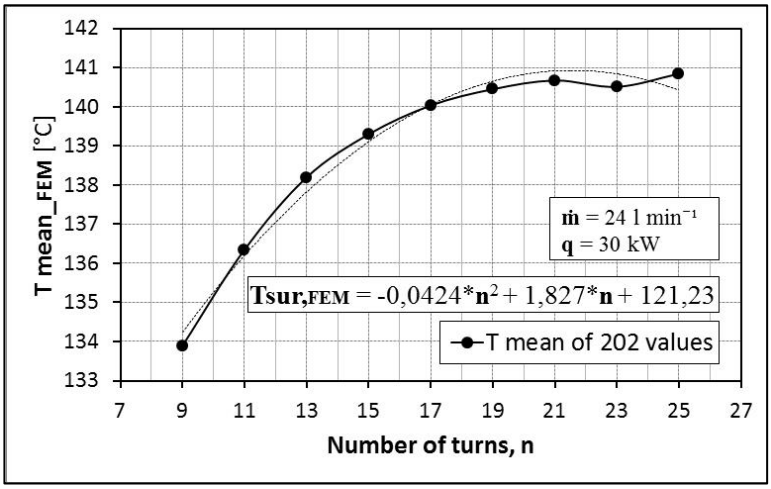

Figure 4.14 Outer roller temperature from FEM simulations against the number of turns.

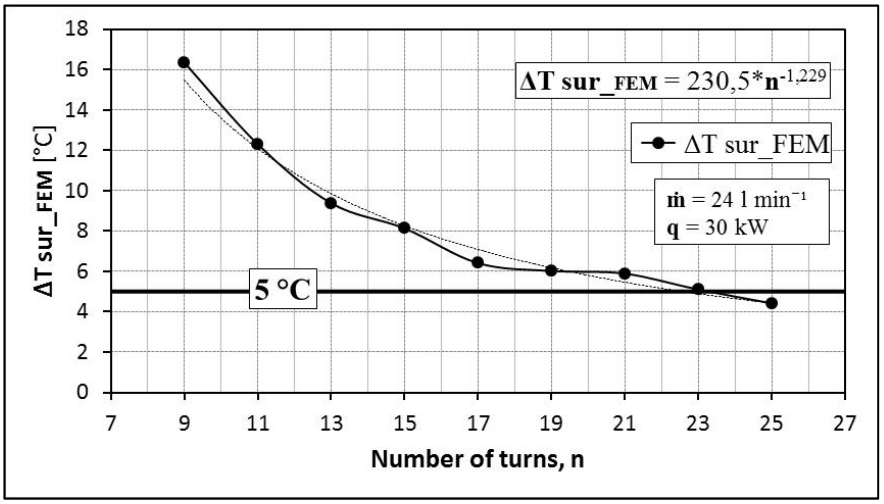

Figure 4.15 External temperature gradient from FEM simulations against the number of turns.

The Figure 4.14 shows the variation of mean temperature calculated with all the points of the external path. The graph confirms an almost constant value of mean temperature with different number of turns involved in the model. This values has to be closed to the one required by the customer, T_{sur} = 140 °C. In case of number of turns lower than 15 we can see that the mean temperature goes down. In fact we made the interpolation between the numerical results obtained with n = 15 and n = 30, to derive the real wall temperature to be set in the analytical calculation. Hence, It can be that the interpolation has worst effect on number of turns lower than 15.
The Figure 4.15 shows the variation of external temperature gradient over the number of turns. The higher the number of turns, the lower the temperature gradient. N = 25 ensures a temperature gradient lower than 5 °C.

4.6.2 Variation of heat flow rate with fixed number of turns.

In the paragraph above we define the suitable number of turns to be considered for the rest of the project. However, it can happen that, during the process, a different heat flow rate is required or also that the final designed roller is used in different applications

characterized by different required heat flow rate, even though the required outer surface temperature will remain the same. The roller geometry is already defined, therefore we are now looking for a solution to be used in order to let the process reach the desired heat flow rate. We can vary:

- The oil flow rate, keeping the same inlet oil temperature
- The inlet oil temperature, keeping the same oil flow rate
- Both inlet oil temperature and oil flow rate.

We consider here the second solution. Hence, we study how the inlet oil temperature should vary in order to obtain defined heat flow rate. Therefore we are going to follow the procedure described above to adjust the T_w to be set in the analytical calculation. However, now we fix the number of turns and we find $T_{sur,FEM}$ as a function of the heat flow rate.

1) Three values of heat flow rate: q = 20, q = 30, q = 40 kW were selected. For the calculation, we start with the initial T_w calculated in case of q = 30 and n = 25: T_w = 148,06 °C. At the beginning, we use this value even for the other two cases: q = 20 and q = 40 kW.

2) Check the oil flow, laminar or turbulent:
   According to the Table 4.33 an oil flow rate equal to 24 l min^{-1} leads to a turbulent flow.

T_w = 148.1 °C **n = 25**			
q [kW]	20	30	40
ṁ lam-tur [l min^{-1}]	17,42	16,65	15,85

Table 4.33 Critical oil flow rate from laminar to turbulent. Higher flow rates lead to turbulent conditions.

3) Find out the analytical and numerical results.

$T_{w,an}$ [°C]	q [kW]	T_{in_oil} [°C]	T_{out_oil} [°C]	ΔT_{oil} [°C]	α_{oil} [W m^{-2} K^{-1}]	T_{min} [FEM]	T_{max} [FEM]	T_{mean} [FEM]	ΔT_{sur} [FEM]
148,06	20	160,1	146,4	13,6	1700	141,8	144,8	143,3	2,9
148,06	30	165,9	145,5	20,4	1729	138,7	143,1	140,9	4,4
148,06	40	171,7	144,5	27,2	1759	135,6	141,5	138,5	6,0

Table 4.34 Analytical and numerical results with three values of heat flow rate and the initial wall temperature set analytically

4) Find the function between the wall temperature and the heat flow rate.

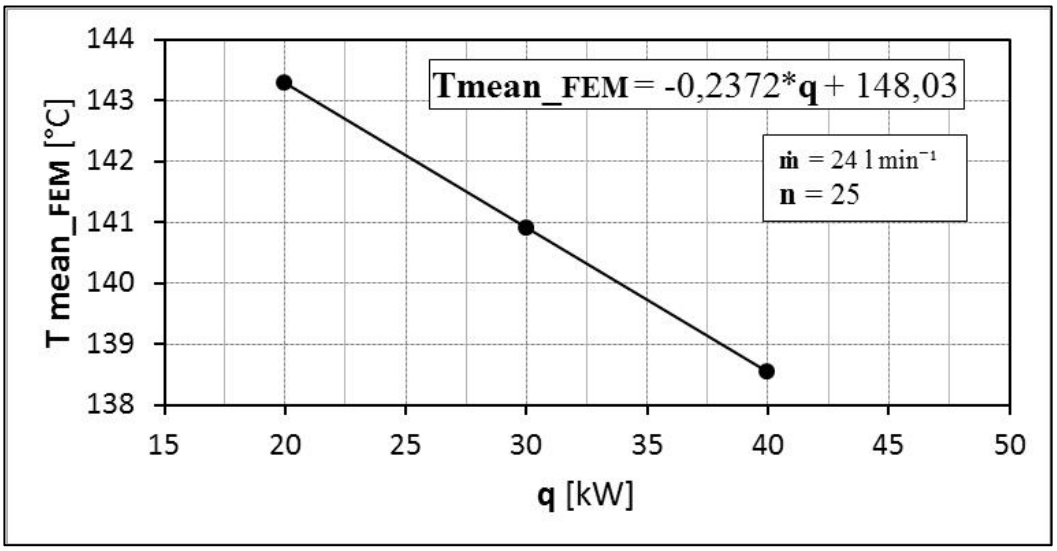

Figure 4.16 Outer roller temperature from FEM simulations against the heat flow rate by setting the initial value of wall temperature in the analytical calculation.

The figure 4.16 shows the variation of the mean temperature on the outer roller surface over the heat flow rate. We can derive the following function:

$$T_{sur,FEM}(q) = -0{,}2372*q + 148.03.$$

5) Choose of other values of q to be analysed in order to create the final map.
The following values of heat flow rate are chosen [kW]:
10; 12,5; 15; 17,5; 20; 22,5; 25, 27,5; 30; 32,5; 35; 37,5; 40.

6) Calculation of $T_{sur,FEM}$ and $T_{w,new}$.

Adopting the derived equation, we can calculate the $T_{sur,FEM}$ for each number of turns. Afterwards we can make a simple proportion and, finally, obtain the $T_{w,new}$ to be set in the analytical calculation ($T_{w,old}$= 148,06 °C)

$$T_{w,new} = \frac{T_{w,old}}{T_{sur,FEM}} * 140$$

We obtain in the end the following values:

q [kW]	10	12,5	15	17,5	20	22,5	25	27,5	30	32,5	35	37,5	40
$\mathbf{T_{sur,FEM}}$	145,6	145,0	144,4	144,9	143,3	142,7	142,1	141,5	140,9	140,3	139,7	139,1	138,5
$\mathbf{T_{w,new}}$	142,3	142,9	143,5	144,1	144,7	145,3	145,9	146,5	147,1	147,8	148,4	149,0	149,7

Table 4.35 First row: Outer roller temperature from FEM simulations; second row: re-calculated wall temperature.

7) Set the input parameters in the "Analysis 4" and find out the analytical results.

q [kW]	$\mathbf{T_{in\_oil}}$ [°C]	$\mathbf{T_{out\_oil}}$ [°C]	$\mathbf{\Delta T_{oil}}$ [°C]	$\boldsymbol{\alpha_{oil}}$ [W m^{-2} K^{-1}]
10	148,4	141,5	6,86	1614
12,5	150,5	141,9	8,57	1626
15	152,6	142,3	10,27	1639
17,5	154,8	142,8	11,98	1652
20	156,8	143,2	13,68	1665
22,5	158,9	143,5	15,37	1678
25	161,0	144,0	17,06	1693
27,5	163,1	144,3	18,75	1706
30	165,1	144,7	20,44	1720
32,5	167,3	145,2	22,13	1736
35	169,3	145,5	23,81	1750
37,5	171,3	145,8	25,49	1765
40	173,5	146,3	27,17	1782

Table 4.36 Analytical results with several heat flow rates. The new wall temperature has been set in the analytical calculations.

8) Run the simulations with different model geometry and find out the mean temperature on the surface at every case of study.

q [kW]	**T_{min} [FEM]**	**T_{max} [FEM]**	**T_{mean} [FEM]**	**T_{mean} of 202 values**	**ΔT_{sur} [FEM]**
10	139,1	140,5	139,8	139,8	1,42
12,5	138,9	140,7	139,8	139,8	1,79
15	138,7	140,9	139,8	139,8	2,15
17,5	138,7	141,2	139,9	139,9	2,52
20	138,5	141,4	139,9	139,9	2,90
22,5	138,3	141,6	139,9	139,9	3,27
25	138,2	141,9	140,0	140,0	3,65
27,5	138,0	142,1	140,0	140,0	4,04
30	137,9	142,3	140,1	140,0	4,41
32,5	137,9	142,7	140,3	140,2	4,80
35	137,7	142,9	140,3	140,2	5,20
37.5	137,5	143,1	140,3	140,2	5,60
40	137,5	143,5	140,5	140,3	6,00

Table 4.37 Numerical results obtained by the finite element software Ansys, with several heat flow rates.

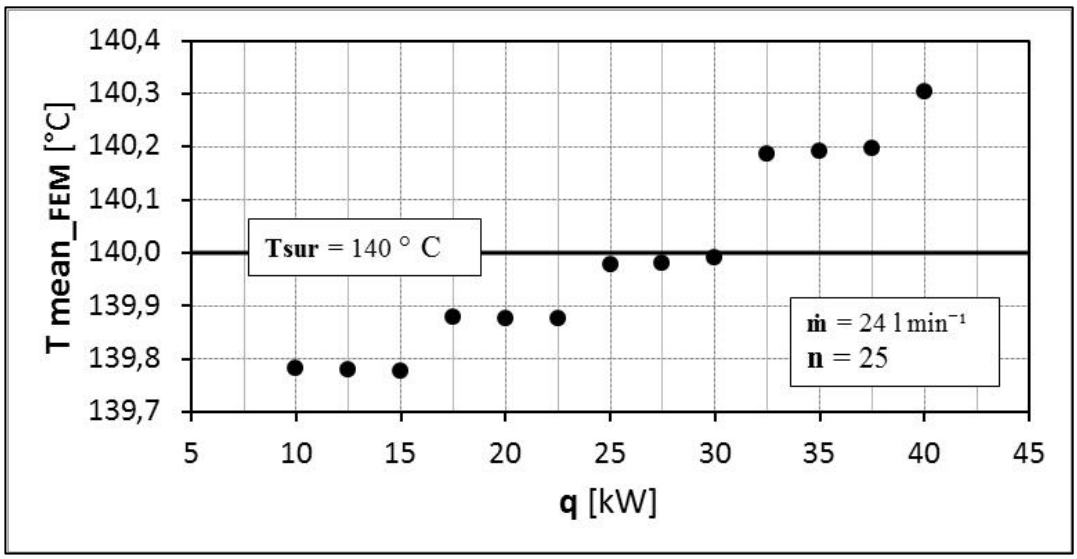

Figure 4.17 Outer roller temperature from FEM simulations against the heat flow rate.

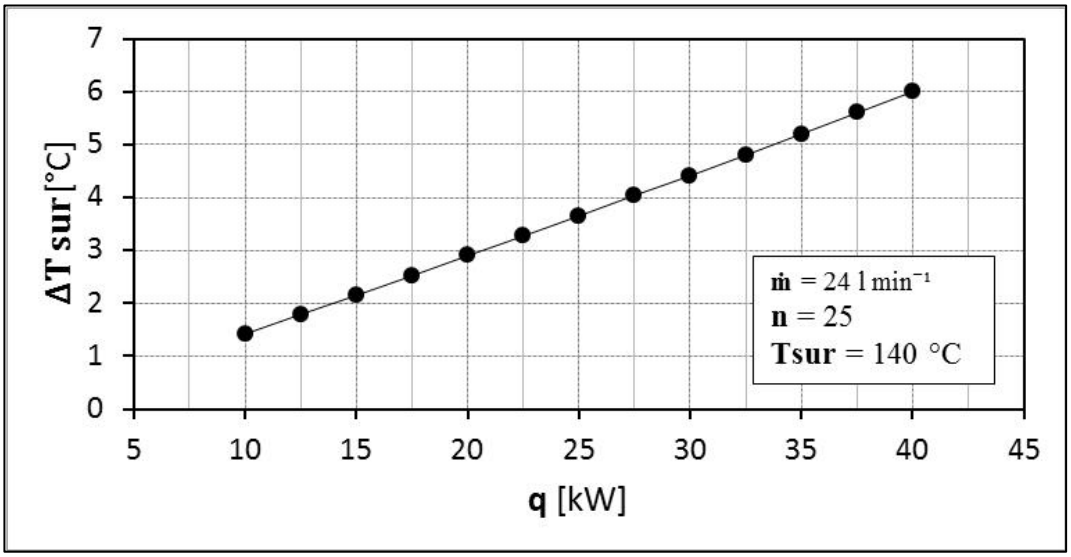

Figure 4.18 External temperature gradient from FEM simulations against the heat flow rate.

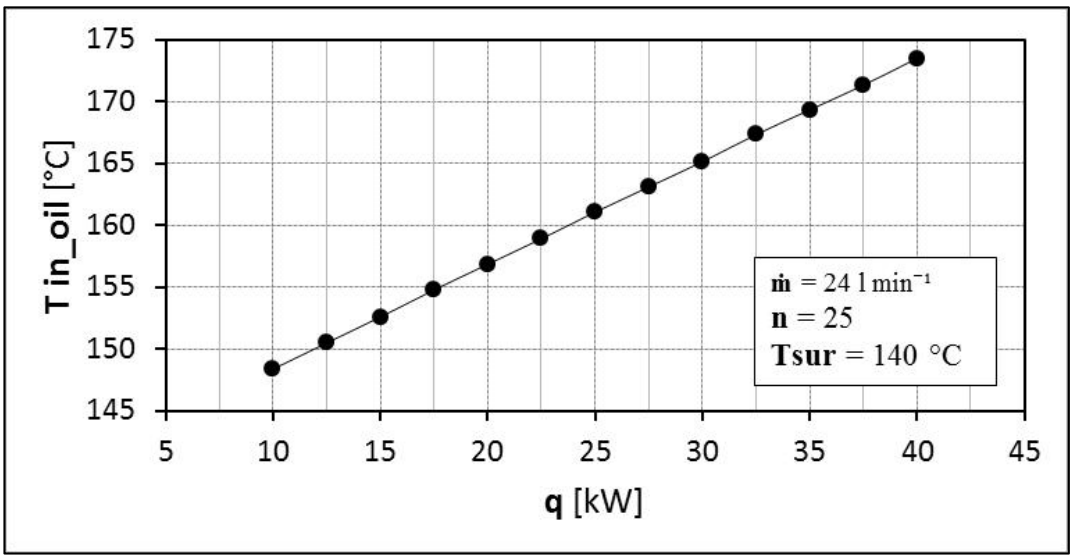

Figure 4.19 Inlet oil temperature to be set while the heat flow rate varies (see table 4.36).

The Figure 4.17 shows the variation of mean temperature calculated with all the points of the external path. The graph confirms an almost constant value of mean temperature with different heat flow rates involved in the model. This values has to be closed to the one required by the customer, T_{sur}= 140 °C.

The Figure 4.18 shows the variation of external temperature gradient over the heat flow rate. The relationship is almost linear and when the heat flow rate becomes greater than 35 kW, the temperature variation overcomes the required threshold of 5 °C. We can deduce that the roller has to be designed with the highest heat flow rate, in this way when the load will be lower the temperature gradient won't be greater than the maximum value.

The figure 4.19 shows how the inlet oil temperature should be set in order to obtain a defined amount of heat flow rate from the process. The relationship is almost linear and the oil temperature increases with the heat flow rate.

CHAPTER 5: Refining of the model: two heat transfer surfaces

5.1 Step description

In this chapter we will simulate and create a more realistic model, in order to better reproduce the process conditions. In fact, so far we have considered a blocked roller in which the entire outer surface was involved in the heat transfer. Now we still make the assumption that the roller rotates with a low angular velocity. In the paragraph 4.3.1 is explained the current solution of the customer and the speed process of the textile is v = 40 m min^{-1}. This means the angular velocity will be:

$$\omega = \frac{v}{R} = \frac{40}{0{,}15}\ \text{rad min}^{-1} = \frac{40}{0{,}15\ 60}\ \text{rad sec}^{-1} = 4{,}44\ \text{rad sec}^{-1}$$

We still neglect the rotational effects and consider a stationary roller. However, in this chapter we are going to take into account the effect of two different heat transfer surfaces. During the process, the external piece covers half of the outer roller surface, while the rest of the surface exchanges directly to the surroundings. Therefore, we study analytically and numerically a cylinder with the same geometry parameter but considering two different heat transfer conditions. Both surfaces will have a defined boundary condition, which is uniformly distributed over them. After defining the way to create the new model and study, we will find the results with the same set of input parameters we considered in the previous chapter in order to check how different are the results with the new model. Afterwards, we re-make the map which shows how should be set the inlet oil temperature to provide different heat flow rates required by the application and the process.

5.2 Optimization of q = 30 kW

5.2.1 Preparing the analytical model

The set of input parameters is:

- Heat flow rate, q = 30 kW
- Number of turns per spire, n = 25
- Oil flow rate, $\dot{m}$ = 24 l min^{-1}
- External surface temperature of the roller, T_{sur} = 140 °C.

The total heat flow rate is 30 kW and it has to be divided in two parts: one to the ambient side and one to the workpiece side; therefore, we will compute the first amount of power in order to derive the second one with a simple subtraction.

- Ambient side: we calculate the heat transfer coefficient with the formula previously adopted (see Chapter 3.2.2), which is referred to the external heat transfer to the ambient in case of horizontally tube with equal surface temperature.
  We obtain: α_{ext} = 15 W m^{-2} K^{-1}, which provides:

  $q_{amb} = \alpha_{ext}\ A_{amb}\ \Delta T_{sur-amb} = \alpha_{ext}\ \pi RL\ \Delta T_{sur-amb}$ = 15 π 0,15 1,92 (140–23) = 1588 W

  The surface that we considered is obviously only half of the entire one and the T_{sur} has to be 140 °C on the workpiece side. On the ambient side we keep this value for the calculation even if, in the end, it will be higher due to the lower heat flow rate required.

- Workpiece side: $q_{w-p} = q_{tot} - q_{amb}$ = 30 – 1,59 = 28,41 kW

We consider now only one spire. We suppose to know the inlet oil temperature to be set in order to meet the requirements. At each turn, the oil flows first to the workpiece-side

and, then, to the ambient side. The first piece of tube where the oil starts flowing through, is characterized by high heat flux exchanged. It settles on this side till it overpasses half a turn. On the other half there is the ambient side and we have to consider different boundary conditions, which influence the changing of oil features. The analytical calculation is done in a spreadsheet, named "Analysis 2_bis", and it is based on the following steps:

1. ***Workpiece-side:*** for the first half a turn the input parameters can be summarized us follow:
   - Oil flow rate, $\dot{m} = 24\ l\ min^{-1}$.
   - Initial value of the wall temperature, T_w : we don't know this value but it has to be set to carry on with the calculation. We start setting the same value we found in the previous analysis (*Paragraph 4.6.2, Table 4.35, q30*):
     $T_w = 147{,}13\ °C$.
   - Inlet oil temperature, T_{in} : this value will be the final result for the calculation but, at the beginning, it has to be set to compute the total heat flow rate. We start from T_{in} = 165,12 (see *Table 4.36*). In order to find the final result, this value has to be changed till the required total heat flow rate is achieved.

   The geometrical parameters have already been defined and we can derive the heat flow rate exchanged in the first half a turn, the oil temperature change and the heat transfer coefficient. The calculation procedure is the same as in the "Analysis 2" (see *paragraph 4.2.2*), here considering only half a turn.

final ΔT_{oil} [°C]	0,99
T_{out} [°C]	164,1
$\dot{m}$ [kg s^{-1}]	0,308
q [W]	734,4
α_{oil} [W m^{-2} K^{-1}]	1850

Table 5.1 Results after the first half a turn: oil features and average heat transfer coefficient.

2. ***Ambient side:*** the results obtained from the first half of a turn become the initial parameters for the second half. Moreover, the total amount of heat flow rate

exchanged with the ambient may be divided into 25 in order to get the real flow rate on a single part of the roller, considering both directions, and also by 2 counting only one of them.

$q_{half-turn} = \frac{q_{amb}}{50} = \frac{1588}{50} = 31{,}76$ W = $\dot{m}c_p\Delta T_{oil}$,

we can derive the outlet oil temperature:

$T_{out} = T_{in} + \frac{q_{half-turn}}{\dot{m}c_p} = 164{,}13 + \frac{31{,}76}{0{,}308*2{,}4*10^3} = 164{,}08$ °C.

With c_p calculated at the initial oil temperature of the analyzed part. The oil temperature change on the ambient side of the tube is very low because low is the heat flow rate.

We can even calculate, in one iteration and with Gnielinski model, the heat transfer coefficient.

	T [°C]	**ρ** [kg m^{-3}]	**c_p** [kJ kg^{-1} K^{-1}]	**μ** [10^{-6}kg $m^{-1}s^{-1}$]	**λ** [mW m^{-2} K^{-1}]	**Pr** [-]
wall	163,34	769,3	2,40	2094	123,9	40,51
oil	164,10	769,2	2,40	2070	123,8	40,12

Table 5.2 Oil properties at the average temperature and at the wall temperature, on the ambient-side half a turn.

$\dot{m}$ [l min^{-1}]	**$\dot{m}$** [kg s^{-1}]	**ΔT_{oil}** [°C]	**h** [m]	**D** [m]	**Re** [-]	**d/D** [-]	**ξ**	**Nu** [-]	**α_{oil}** [W m^{-2} K^{-1}]	**q** [W]
24	0,308	0,04	0,07	0,28	11622	0,05	0,04	210,97	1830,8	31,74

Table 5.3 Calculation of heat transfer coefficient at the ambient side, adopting Gnielinski model.

The wall temperature is unknown and we set it in order to obtain an heat flow rate almost equal to 31,76 W (we can also observe that the T_w influences mostly the q value but not too much the α_{oil}):

q = $\alpha_{oil} T_{half-turn}$ (T_{oil}-T_w) = 1830,8 *0,02269*(164,10-163,34)= 31,74 W.

It is important to change the wall temperature for every half-turn on the ambient side, every time that we start a new analysis with a new set of input parameters.

The outlet oil features from the first turn have to be considered as inlet ones for the second turn and the previous calculations have to be repeated till the end of the spire.

3. ***Summation of the heat flow rates and final results:*** we make the previous calculations for each turn at the ambient-side and workpiece-side. In this way we can reach the last turn of the spire and finally derive the outlet oil temperature of the entire spire. We have now the heat flow rate at every single piece of tube. Therefore, it is possible to compute the whole heat flow rate exchanged during the process (the sum is made considering a constant value for the ambient-side parts and the calculated value for the workpiece-side parts). We suppose the oil conditions to be the same between the two spires.

$\dot{\mathbf{m}}$ [l min^{-1}]	$\mathbf{T}_{in}$ [°C]	$\Delta\mathbf{T}_{oil}$ [°C]	$\mathbf{q}$ [W]	$\boldsymbol{\alpha}_{oil}$ [W m^{-2} K^{-1}]
24	165,1	0,99	734,38	1850
24	164,1	0,04	31,76	1831
24	164,1	0,93	686,61	1836
24	163,2	0,04	31,76	1817
24	163,1	0,87	642,50	1822
24	162,2	0,04	31,76	1805
24	162,2	0,82	601,68	1809
24	161,4	0,04	31,76	1794
24	161,3	0,76	563,82	1798
24	160,6	0,04	31,76	1783
24	160,5	0,72	528,65	1787
24	159,8	0,04	31,76	1774
24	159,8	0,67	495,93	1777
24	159,1	0,04	31,76	1765
24	159,1	0,63	465,43	1768
24	158,4	0,04	31,76	1757
24	158,4	0,59	436,97	1760
24	157,8	0,04	31,76	1749
24	157,7	0,56	410,38	1752
24	157,2	0,04	31,76	1742
24	157,1	0,53	385,51	1744

Table 5.4 First part of the table. It continues in the next page.

$\dot{\mathbf{m}}$ [l min^{-1}]	$\mathbf{T}_{in}$ [°C]	$\Delta\mathbf{T}_{oil}$ [°C]	$\mathbf{q}$ [W]	$\boldsymbol{\alpha}_{oil}$ [W m^{-2} K^{-1}]
24	156,6	0,043	31,76	1735
24	156,6	0,493	362,22	1737
24	156,1	0,043	31,76	1729
24	156,0	0,464	340,39	1731
24	155,6	0,043	31,76	1723
24	155,5	0,436	319,91	1725
24	155,1	0,043	31,76	1717
24	155,0	0,410	300,69	1719
24	154,6	0,043	31,76	1712
24	154,6	0,385	282,62	1714
24	154,2	0,043	31,76	1707
24	154,2	0,362	265,63	1709
24	153,8	0,043	31,76	1703
24	153,8	0,341	249,65	1704
24	153,4	0,043	31,76	1699
24	153,4	0,320	234,60	1700
24	153,1	0,043	31,76	1695
24	153,0	0,301	220,42	1696
24	152,7	0,043	31,76	1691
24	152,7	0,283	207,05	1692
24	152,4	0,043	31,76	1687
24	152,3	0,265	194,45	1688
24	152,1	0,043	31,76	1684
24	152,0	0,249	182,56	1685
24	151,8	0,043	31,76	1681
24	151,7	0,234	171,33	1682
24	151,5	0,043	31,76	1678
24	151,5	0,220	160,73	1679
24	151,2	0,043	31,76	1675

Table 5.4 Oil features and heat flow rates produced by one spire and calculated at each half a turn, starting from the workpiece-side one.

With the last calculation we derive also the final outlet oil temperature and, in turn, the oil temperature change. Moreover, is it possible to sum the heat flow rates and derive the total heat flow rate provided by one spire and then multiply it by two.

$\mathbf{T_{out}}$ [°C]	151,2
Heat flow rate, one spire [W]	10238
Total heat flow rate [W]	20476

Table 5.5 Final results: outlet oil temperature calculated in the last half a turn; total heat flow rate provided by one spire; total heat flow rate of the process.

We divide the roller into 25 parts which is the number of turns and calculate for each part we calculate the amount of heat flow rate by adding the power provided by the parts of the two spires placed on it. This value should be constant and theoretically equal to:

$$q_{half-turn} = \frac{q_{tot}}{25} = \frac{20476}{25} = 819{,}05 \text{ W}$$

$$\text{error\%} = \frac{q_{provided} - q_{half-turn}}{q_{half-turn}} * 100$$

required q pro part [W]	**Position of the turn first spire + second one**	**Provided q pro part** [W]	**Error** [%]
819,05	1+25	958,63	17,04
	2+24	921,46	12,50
	3+23	888,58	8,49
	4+22	859,65	4,96
	5+21	834,39	1,87
	6+20	812,59	-0,79
	7+19	794,04	-3,05
	8+18	778,60	-4,94
	9+17	766,12	-6,46
	10+16	756,52	-7,63
	11+15	749,72	-8,46
	12+14	745,66	-8,96
	13+13	744,31	-9,13

Table 5.6 Ideal constant heat flow rate required by the process and real heat flow rate pro part of the roller.

The table above and the following figure show how big is the gap between the ideal heat flow rate, which should be constant, and the generated one over the position of the turn. The first turn of the first spire is in combination with the last turn of the second spire (1+25) and, so on, for the other parts of the roller. In the table 5.6 are

shown only the first 13 parts of the roller because the rest is symmetric (see figure 5.1).

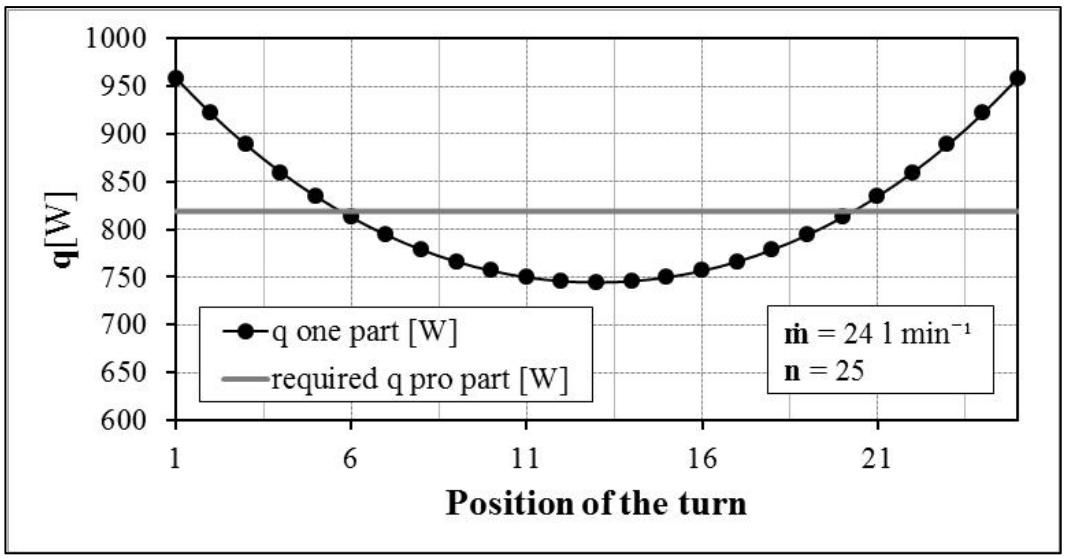

Figure 5.1 Difference between the ideal constant heat flow rate and the final provided one over the position of the turn.

In our calculations, the heat flow rate is not uniform over the roller length. This error can be avoided by changing the pitch between the turns along the spire envelopment, but in this project we don't consider this solution.

5.2.2 Analytical results

Adopting the analytical model described above, we can find the results: final inlet oil temperature, oil temperature change, and heat transfer coefficient variations along the tube. The last two equations are used for the numerical model. In the Excel we set the same wall temperature as before:

T_w = 147,13 °C.

1. *Derive the inlet oil temperature* T_{in} : The inlet oil temperature is an input parameter to be set in order to carry on with the project but it is also the final result of the analysis. The final total heat flow rate is very important to determinate the inlet oil temperature to be set. In fact, in the example above we calculated:
   q = 20476 W which is not the required one (q = 30 kW). However, with all the necessary linked boxes in the spreadsheet, we can change the inlet oil temperature till we achieve the required value. After some attempts, we find the following results:

$\boldsymbol{T_{in}}$ [°C]	173,4
q [W]	30000
$\mathbf{T_{out}}$ [°C]	153,1
$\Delta\mathbf{T_{oil}}$ [°C]	20,33

Table 5.7 Final inlet oil temperature. Il provides the required total heat flow rate.

2. *Distributions of oil temperature and heat transfer coefficient along the tube:* considering the table 5.4, we can create the graphs of heat transfer coefficient and oil temperature derived with the new inlet oil temperature. The x-axis corresponds to the roller axis and it starts from the beginning of the roller, which is the zero of the main coordinate system in the numerical model. It is, then, important to interpolate the graph points with a suitable equation. The formulas will be used in the numerical model to simulate the process.

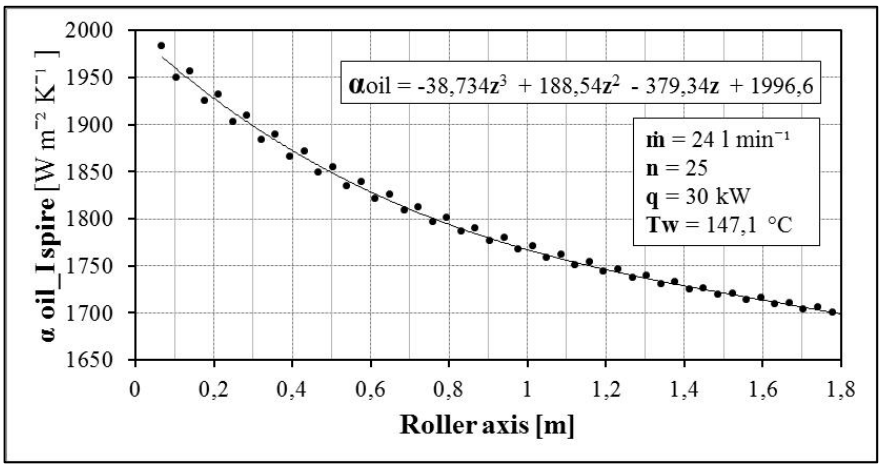

Figure 5.2 Distribution of convection coefficient within the first spire over the roller axis.

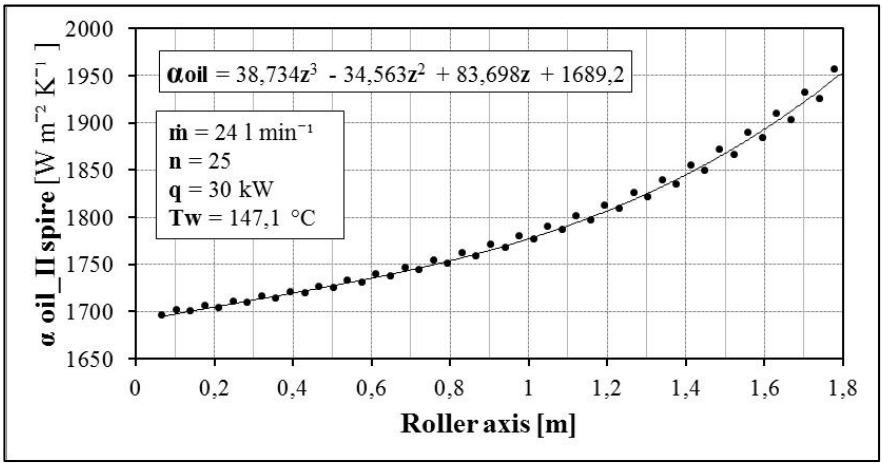

Figure 5.3 Distribution of convection coefficient within the second spire over the roller axis.

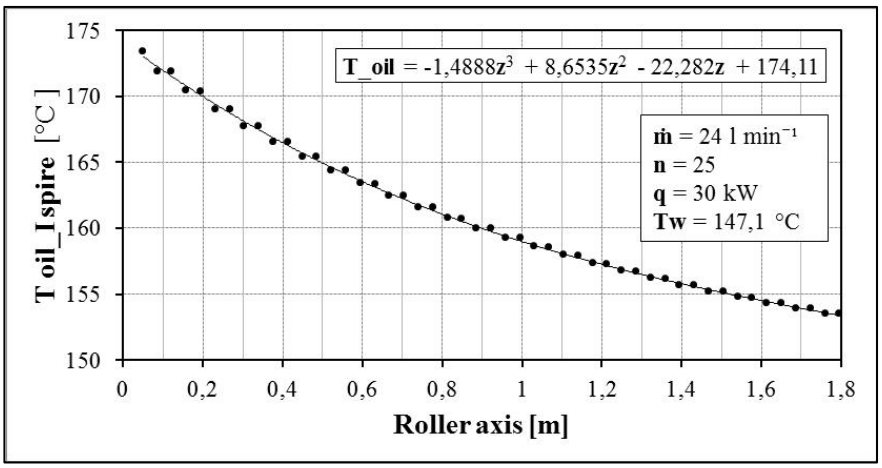

Figure 5.4 Distribution of inlet oil temperature within the first spire over the roller axis.

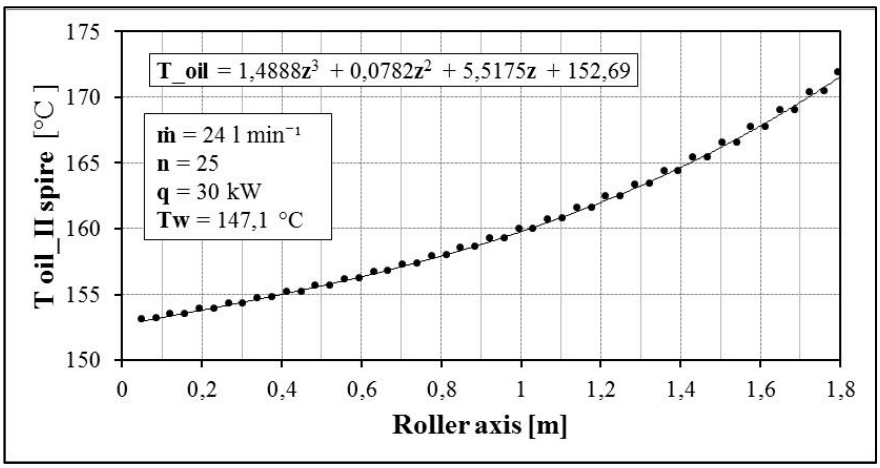

Figure 5.5 Distribution of inlet oil temperature within the second spire over the roller axis.

A third-degree polynomial equation characterizes in every case the distribution of values over the axial coordinate. The equations are useful for the numerical simulation.

5.2.3 Numerical model and results

Numerical model

The model geometry development is explained in chapter 3.3. We additionally divide the outer roller surface into two parts, red and blue shown in the figure 5.6.

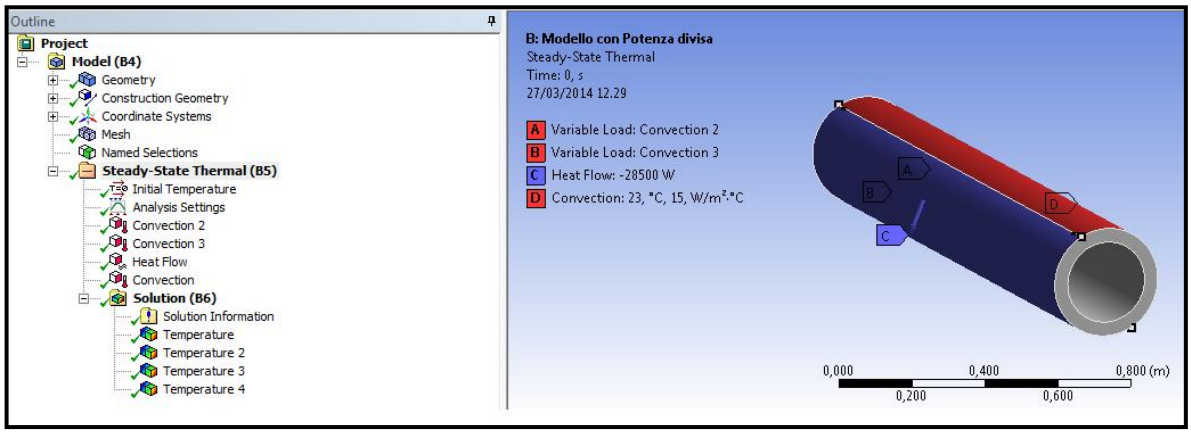

Figure 5.6 Numerical model. Geometry and boundary conditions.

The steel thermal conductivity is (see chapter 4.4) : λ_{steel} = 35 W m^{-1} K^{-1}.

Boundary conditions:

- Ambient temperature: 23 °C
- On one surface (blue in the figure above) a negative heat flow rate is set, q = 27,5 kW. It represents the effect of the external workpiece.
- On the other surface (red in the figure above) a convection is set: ambient temperature T_{amb}= 23 °C and α_{amb} = 15 W m^{-2} K^{-1}.

- Convection within the two spires using the formulations analytically calculated. The box called “ambient temperature” has to be filled up with the corresponding equation of the oil temperature change along the axial coordinate.

Post processing:

To evaluate the results we create two paths, in the middle of both external surfaces and in the axial direction. They are created by excluding the two roller edges. One of those represents the results on the ambient side and the other the ones on the workpiece side. Both of them are subdivided in 202 points.

Numerical results:

We run the simulation and find the following results:

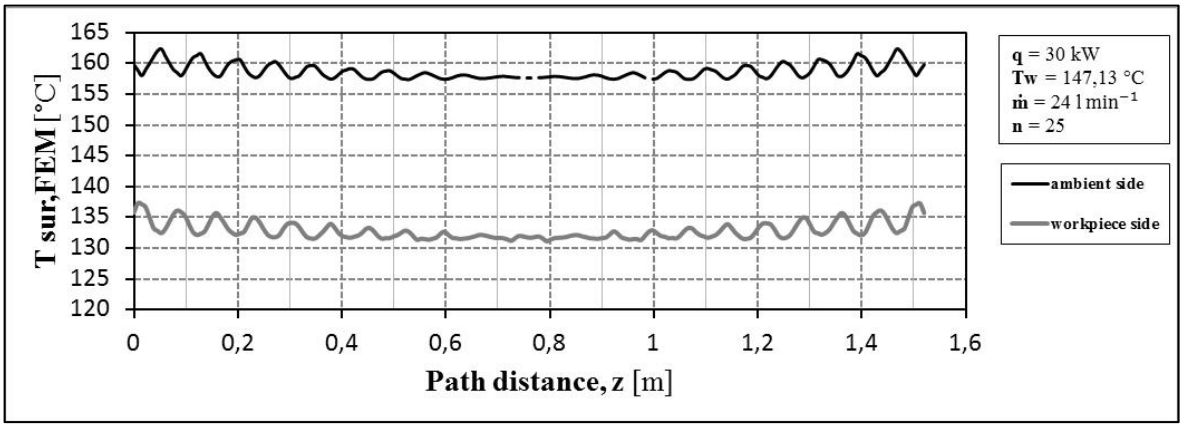

Figure 5.7 Temperature distribution on the external surface, workpiece and ambient sides.

- Temperature at the path points on the workpiece side

T_{in} [°C]	T_{min_sur} [°C]	T_{max_sur} [°C]	ΔT_{sur} [°C]	average T [FEM] [°C]	T_{mean} of 202 values [°C]
173,4	131,2	137,3	6,2	134,2	132,7

Table 5.8 Results from the numerical simulation. Temperature values on the workpiece-side path.

The temperature gradient is calculated as a subtraction between the maximum and minimum surface temperatures. The mean temperature is calculated by considering all the 202 points of the path.

- Temperature at the path points on the ambient side

$\mathbf{T_{min\ \_sur}}$ [°C]	$\mathbf{T_{max\ \_sur}}$ [°C]	$\mathbf{\Delta T_{sur}}$ [°C]	**average T [FEM]** [°C]	$\mathbf{T_{mean}}$ **of 202 values** [°C]	$\mathbf{\Delta T_{sur-amb}}$ [°C]	**q** [W]
157,37	162,32	4,95	159,85	158,64	135,64	1840

Table 5.9 Results from the numerical simulation. Temperature values on the ambient-side path.

The $\Delta T_{sur-amb}$ is the temperature difference between the surface on the ambient side and the ambient. We can calculate the heat flow rate exchanged through the roller surface to the ambient (only considering the surface directly exposed to the ambient).

$\Delta T_{sur-amb} = T_{sur} - T_{amb} = 158,64-23 = 135,64$ °C

$q_{amb} = \alpha_{amb}\ \pi RL\ \Delta T_{sur-amb} = 15*\pi*0,15*1,92*135,64 = 1840$ W

This value is a little bit higher than what we calculated before, because the temperature on the roller surface is higher too.

The mean temperature on the workpiece side is lower than the one on the ambient side due to an higher exchanged heat flow rate. However it is less than the required temperature:

$T_{sur\_FEM\_wp} = 132,85 < 140$ °C.

It means that the wall temperature set in the analytical calculation was lower than the real one.

5.2.4 New wall temperature and new results

It is now possible to calculate the new wall temperature to be set in the analytical calculation in order to gain the required one on the external surface before running the new simulation. We use a simple proportional law:

$$T_{w,new} = 140 \frac{T_{w,old}}{T_{sur\_FEM\_wp}} = 140 \frac{147,13}{132,85} = 155,05\ °C$$

1. *Analytical calculation of the inlet oil temperature and results*: setting the new wall temperature in the spreadsheet, we change the inlet oil temperature till the total heat flow rate reaches the required value.

$\boldsymbol{T_{in}}$ [°C]	180,7
q [kW]	30
$\mathbf{T_{out}}$ [°C]	160,4
$\Delta\mathbf{T_{oil}}$ [°C]	20,23

Table 5.10 Final inlet oil temperature by setting the new wall temperature. It provides the required total heat flow rate.

From the results we have to create new maps of the oil temperature and heat transfer coefficient change along the axial coordinate of the cylinder (see 5.2.2).

$\boldsymbol{\alpha_{oil}}$ **first spire** [W m^{-2} K^{-1}]	α_{oil} = -51,612 z^3 + 244,98 z^2 - 470,53 z + 2139,4
$\boldsymbol{\alpha_{oil}}$ **second spire** [W m^{-2} K^{-1}]	α_{oil} = 51,612 z^3 - 52,302 z^2 + 100,58 z + 1773,8
$\mathbf{T_{oil}}$ **first spire** [°C]	T_{oil} = -1,6561 z^3 + 9,329 z^2 - 22,913 z + 181,34
$\mathbf{T_{oil}}$ **second spire** [°C]	T_{oil} = 1,6561 z^3 - 0,2103 z^2 + 5,4056 z + 160,01

Table 5.11 Equations of oil temperature and heat transfer coefficient distributions over the roller axis, for both spire.

2. *Numerical simulation and results:* we set the analytical results in the numerical model. We keep the same model as before but we edit the convective terms within the two spires by changing the old equations with the new calculated ones. We run the simulation and obtain the following results:

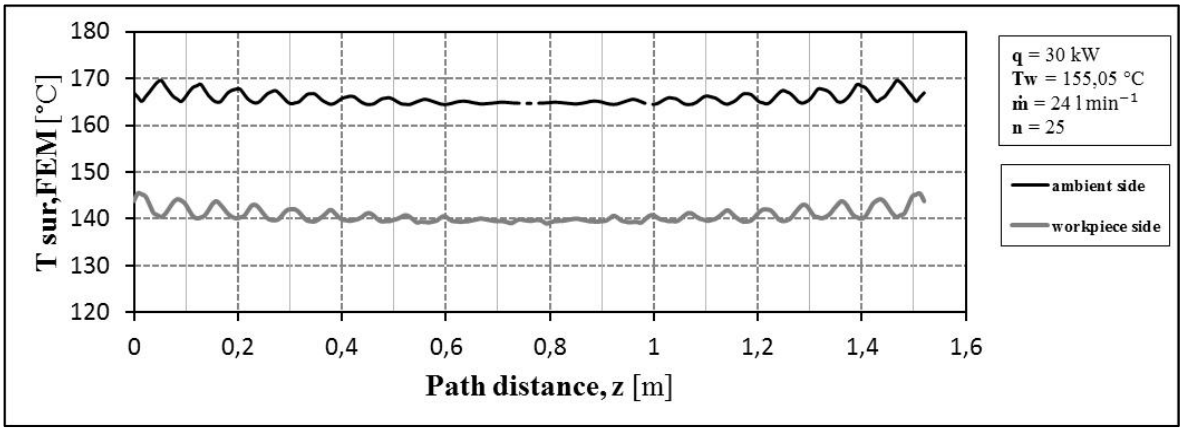

Figure 5.8 Temperature distribution on the external surface, workpiece and ambient sides.

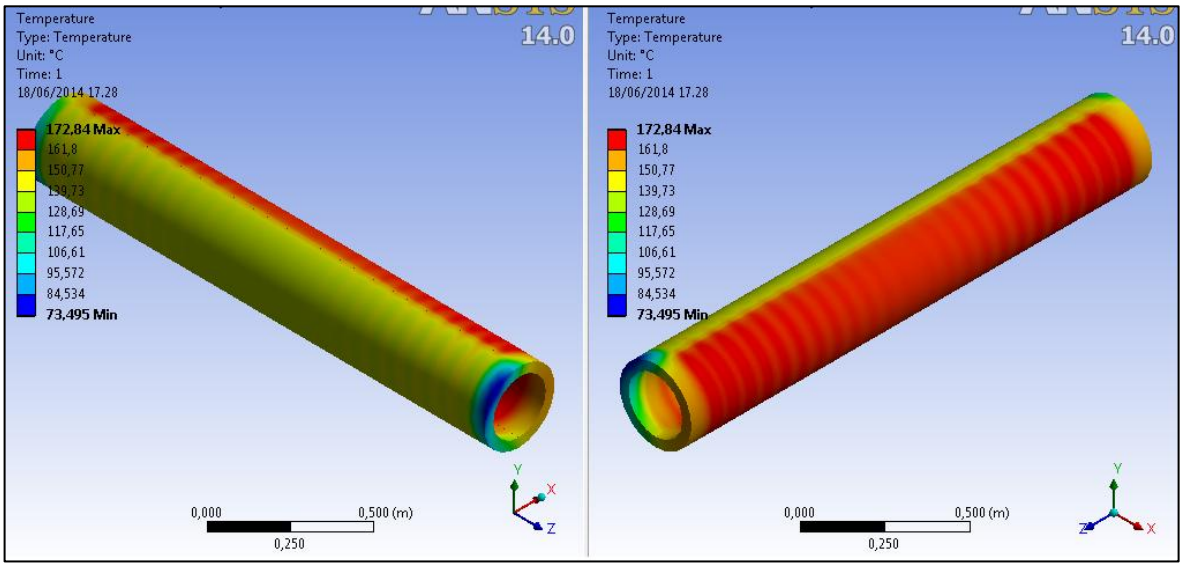

Figure 5.9 Temperature distribution on the outer roller surface, workpiece (left) and ambient (right) sides.

- Temperature at the path points on the workpiece side

$\mathbf{T_{in}}$ [°C]	$\mathbf{T_{min\ \_sur}}$ [°C]	$\mathbf{T_{max\ \_sur}}$ [°C]	$\mathbf{\Delta T_{sur}}$ [°C]	**average T [FEM]** [°C]	$\mathbf{T_{mean}}$ **of 202 values** [°C]
180,6	139,0	145,5	6,5	142,3	140,8

Table 5.12 Temperature values on the workpiece-side path. The simulation is made with the new results calculated with the new wall temperature.

- Temperature at the path points on the ambient side

$\mathbf{T_{min\ \_sur}}$ [°C]	$\mathbf{T_{max\ \_sur}}$ [°C]	$\mathbf{\Delta T_{sur}}$ [°C]	**average T [FEM]** [°C]	$\mathbf{T_{mean}}$ **of 202 values** [°C]	$\mathbf{\Delta T_{sur-amb}}$ [°C]	**q** [W]
164,4	169,6	5,13	167,0	165,7	142,7	1936

Table 5.13 Temperature values on the ambient-side path. The simulation is made with the new results calculated with the new wall temperature.

$\Delta T_{sur-amb}$ = T_{sur}- T_{amb}= 165,7-23 = 142,7 °C

q_{amb}= α_{amb} πRL $\Delta T_{sur-amb}$=15*π*0,15*1,92*142,7 = 1936 W

This value is a little bit higher than what we calculated before, because the temperature on the roller surface is higher too.

The mean temperature on the workpiece side is almost equal to the required:

$T_{sur\_FEM\_wp}$ = 140,79 ≈ 140 °C.

According to the new analytical and numerical model, the final inlet oil temperature to be set in order to meet the requirements is:

T_{in} = 180,65 °C.

The temperature gradient on the workpiece side of the external surface is:

ΔT_{sur} = 6,46 °C. This value is higher than the maximum threshold, but we see in the figure 5.8 that the maximum temperature difference is placed on the two ends of the path. Hence, in the rest of the path a correct temperature distribution is ensured.

However, we can say that the new model provides a higher temperature gradient on the roller surface than the model described in the previous chapter (see Table 4.36 and q30).

The reason is that the heat flow rate is mainly concentrated in half of the outer surface, while previously it was uniform on the whole outer surface.

$T_{in\_new\_mod}$ = 180,65 °C > 165,12 °C = $T_{in\_old\_mod}$

The model used for the process simulation is very important because it influences the final results and, in turn, the project design.

5.3 Check the model

The last analyzed model seems to be suitable to simulate the process. However, one important aspect should be verified: to simulate the heat transfer coefficient and oil temperature distributions along the spires, we defined equations, which describe the parameters variation over the cylinder axial axis. We can state from the results (Table 5.4) that the oil temperature gradient is much higher in the pieces of tube on the workpiece side than on the ambient side. In our model, this difference is neglected because the oil temperature varies over the axis, doesn't matter the boundary condition.

Taking into account the last analytical analysis, we now want to create a new numerical model to simulate more properly the parameter variation.

We divide each turn in 50 parts: 25 of them are exposed to the ambient and 25 to the workpiece side. On the ambient side we set a constant value of oil temperature due to the very low oil temperature change. On the workpiece side, at each piece of tube we know the inlet and outlet oil temperature; we can set a linear function of oil temperature over the position in relation to the cylinder axial axis. Since we divide the tube into a high number of divisions, we can assume a constant value of the heat transfer coefficient within every single element of the tube.

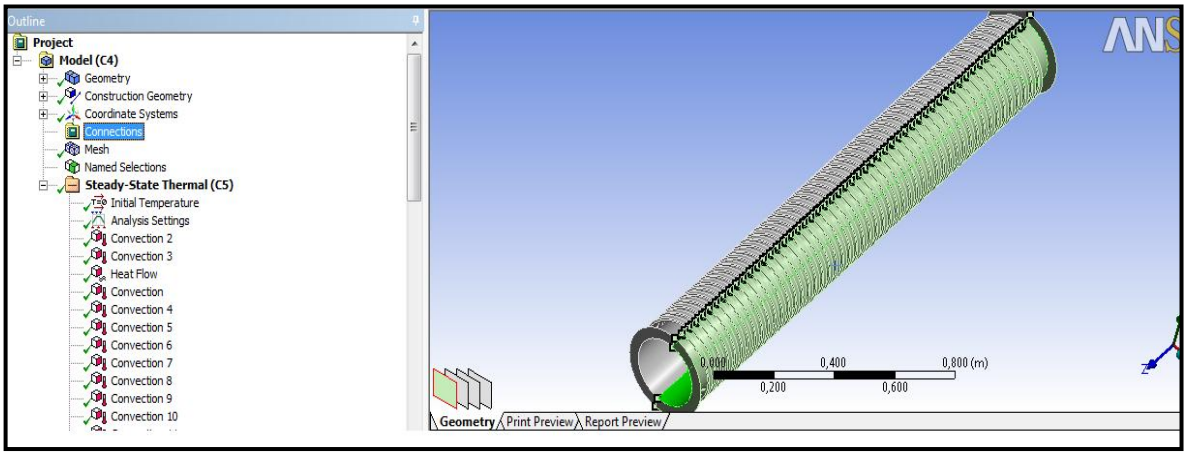

Figure 5.10 New numerical model. Each spire is divided into 50 parts to better simulate the oil temperature variations.

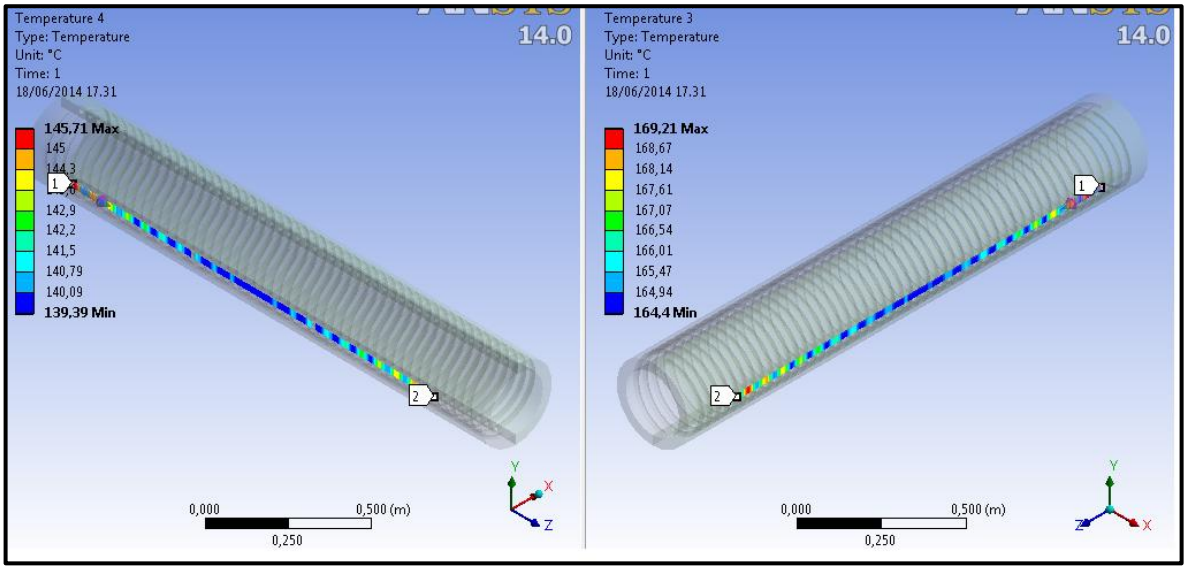

Figure 5.11 New numerical model. Paths on the two surfaces to evaluate the results.

Position	$\mathbf{T_{in}}$ [°C]	$\Delta\mathbf{T_{oil}}$ [°C]	**q** [W]	$\boldsymbol{\alpha_{oil}}$ [W m^{-2} K^{-1}]
1	180,7	1,60	1194	2122
2	179,1	0,04	31,76	2082
3	179,0	1,48	1100	2088
4	177,5	0,04	31,76	2052
5	177,5	1,36	1015	2057
6	176,1	0,04	31,76	2025
7	176,1	1,26	939	2030
8	174,8	0,04	31,76	2000
9	174,8	1,17	871	2005
10	173,6	0,04	31,76	1979
11	173,6	1,09	808	1984
12	172,5	0,04	31,76	1959
13	172,4	1,01	752	1964
14	171,4	0,04	31,76	1941
15	171,4	0,94	700	1946
16	170,4	0,04	31,76	1925
17	170,4	0,88	652	1929
18	169,5	0,04	31,76	1910
19	169,5	0,82	608	1914
20	168,6	0,04	31,76	1897
21	168,6	0,77	568	1900
22	167,8	0,04	31,76	1885
23	167,8	0,72	530	1888
24	167,1	0,04	31,76	1873
25	167,0	0,67	496	1876
26	166,4	0,04	31,76	1863
27	166,3	0,63	464	1865
28	165,7	0,04	31,76	1853
29	165,6	0,59	434	1856
30	165,1	0,04	31,76	1844
31	165,0	0,55	406	1846
32	164,5	0,04	31,76	1836
33	164,4	0,51	380	1838
34	163,9	0,04	31,76	1828
35	163,9	0,48	356	1830
36	163,4	0,04	31,76	1821
37	163,3	0,45	333	1823
38	162,9	0,04	31,76	1814
39	162,8	0,42	312	1816
40	162,4	0,04	31,76	1808
41	162,4	0,40	293	1809
42	162,0	0,04	31,76	1802
43	161,9	0,37	274	1803
44	161,6	0,04	31,76	1796
45	161,5	0,35	257	1798
46	161,2	0,04	31,76	1791
47	161,1	0,33	241	1792
48	160,8	0,04	31,76	1786
49	160,8	0,31	225	1788
50	160,5	0,04	31,76	1782

Table 5.14 Analytical results of the last analysis, in which the new wall temperature is set.

workpiece or ambient side	**inlet surface axial position** [m]	**linear equation T** [°C]
w-p	0,050	182,85-43,99*z
amb	0,086	179,02
w-p	0,123	183,93-40,55*z
amb	0,159	177,51
w-p	0,196	184,81-37,47*z
amb	0,232	176,10
w-p	0,268	185,39-34,70*z
amb	0,305	174,79
w-p	0,341	185,75-32,19*z
amb	0,378	173,58
w-p	0,41	185,94-29,91*z
amb	0,450	172,45
w-p	0,487	185,97-27,83*z
amb	0,523	171,39
w-p	0,560	185,87-25,92*z
amb	0,596	170,40
w-p	0,632	185,67-24,17*z
amb	0,669	169,48
w-p	0,705	185,37-22,55*z
amb	0,742	168,62
w-p	0,778	184,99-21,06*z
amb	0,814	167,81
w-p	0,851	184,54-19,69*z
amb	0,887	167,05
w-p	0,924	184,03-18,41*z
amb	0,960	166,34
w-p	0,996	183,48-17,23*z
amb	1,033	165,67
w-p	1,069	182,88-16,12*z
amb	1,106	165,04
w-p	1,140	182,26-15,10*z
amb	1,178	164,44
w-p	1,215	181,60-14,14*z
amb	1,251	163,89
w-p	1,288	180,92-13,25*z
amb	1,324	163,36
w-p	1,360	180,23-12,41*z
amb	1,397	162,87
w-p	1,433	179,52-11,63*z
amb	1,470	162,40
w-p	1,506	178,80-10,90*z
amb	1,542	161,96
w-p	1,579	178,07-10,22*z
amb	1,615	161,54
w-p	1,652	177,34-9,58*z
amb	1,688	161,15
w-p	1,724	176,60-8,97*z
amb	1,761	160,78
w-p	1,797	175,87-8,41*z
amb	1,834	160,43

Table 5.15 Oil temperature function over the axial coordinate at each piece of the first spire.

Table 5.14 shows the final analytical results: inlet oil temperature, oil temperature change, and heat transfer coefficient on each section of tube. We can see the difference between the temperature changes on the ambient side and on the workpiece side.
The table 5.15 shows the linear equations used to describe the oil temperature variation at each element of the first spire. The zero coordinate system is placed in the middle of one cylinder base.

- Workpiece side tube, example of the first half a turn:
  - T_{in} = 180,65 °C
  - ΔT_{oil} = 1,6 °C
  - Position of the inlet cross-area, z_{in} = 0,05 m
  - Position of the outlet cross-area, z_{out} = 0,0864 m

$$T_{oil} = T_{in} + \frac{\Delta T_{oil}}{z_{out} - z_{in}} (z_{in} - z)$$

$$T_{oil\_first\_part\_wp} = 180{,}65 + \frac{1{,}6}{0{,}0864 - 0{,}05} (0{,}05 - z) = 182{,}85 - 43{,}99 * z$$

- Ambient side tube, example of the first part (second half of the first turn):
  - T_{in} = 179,045 °C
  - ΔT_{oil} = 0,0426 °C

$$T_{oil} = T_{in} - \frac{\Delta T_{oil}}{2}$$

$$T_{oil\_first\_part\_amb} = 179{,}045 - \frac{0{,}0426}{2} = 179{,}02 \text{ °C}$$

Using the derived equations, we set the numerical model, keeping the same boundary conditions. We evaluate the results in the same manner: two paths placed on the two outer surfaces and subdivided by 202 points.

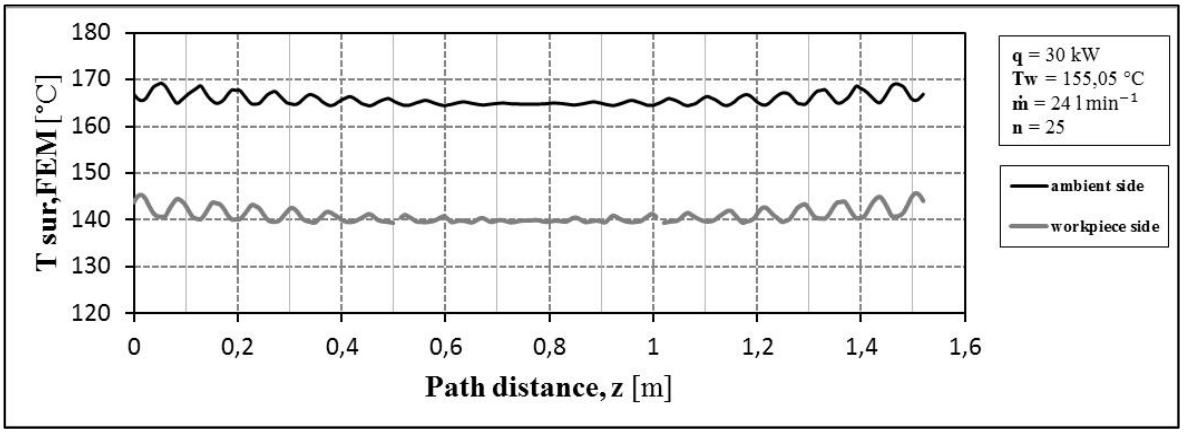

Figure 5.12 Temperature distribution on the outer surface: workpiece and ambient sides. The oil temperature is set at each part of the two spires.

- Temperature at the path points on the workpiece side

T_{in} [°C]	T_{min_sur} [°C]	T_{max_sur} [°C]	ΔT_{sur} [°C]	average T [FEM] [°C]	T_{mean} of 202 values [°C]
180,7	139,4	145,7	6,32	142,6	141,0

Table 5.16 Temperature values on the workpiece-side path. The oil temperature is set at each part of the two spires.

- Temperature at the path points on the ambient side

T_{min_sur} [°C]	T_{max_sur} [°C]	ΔT_{sur} [°C]	average T [FEM] [°C]	T_{mean} of 202 values [°C]	$\Delta T_{sur-amb}$ [°C]	q [W]
164,4	169,2	4,81	166,8	165,7	142,7	1936

Table 5.17 Temperature values on the ambient-side path. The oil temperature is set at each part of the two spires.

The results show that the temperature distribution on outer roller surface is almost the same in both models (see figure 5.13 and 5.14). Therefore, we can continue to consider

the previous simpler model to make the next simulations. In fact, in the next paragraph we adopt the same model configuration to develop a new final analysis.

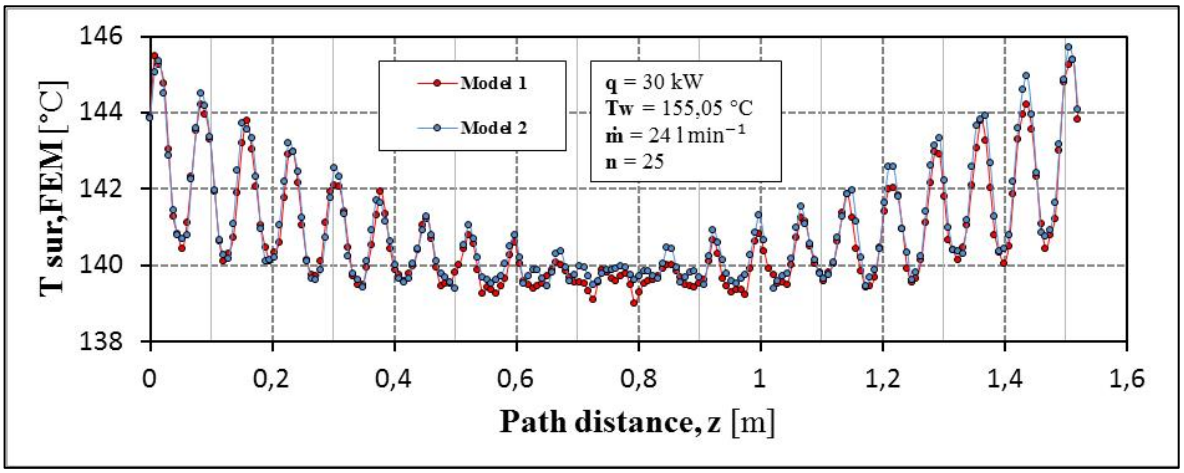

Figure 5.13 Temperature distribution on the external surface on workpiece side, in case of first and second model.

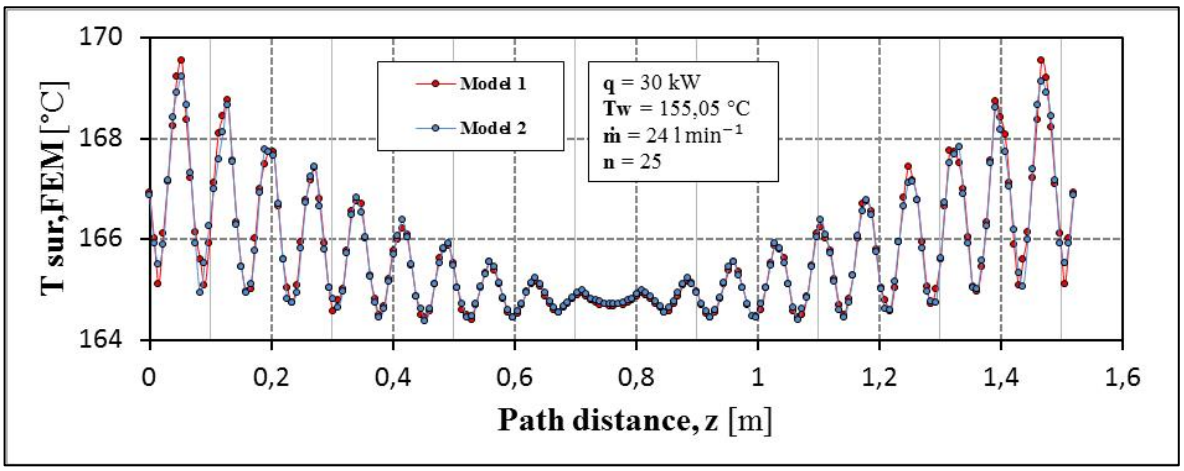

Figure 5.14 Temperature distribution on the external surface on ambient side, in case of first and second model.

5.3 Variation of heat flow rate with fixed number of turns.

In this chapter we want to repeat what was done in the paragraph 4.6.2. The main difference is represented by the model used to simulate the process. In fact, we saw that the same set of input parameters leads to different results due to two different applied models. We want to analyze how the inlet oil temperature should be set while the required heat flow rate is changed during the process or in case of a roller involved in different applications. The steps are followed:

9) Four values of heat flow rate: q = 10, q = 20, q = 30, q = 40 kW. For the calculation we start with the initial T_w calculated in the last analysis: T_w = 155,05 °C, which is the value in case of q = 30 kW. At the beginning, we use this value even for the other three cases: q = 10, q = 20, and q = 40 kW.

10) Analysis of the analytical results. For each case of study we enter the Excel file "Analysis 2_bis", set wall temperature and vary the inlet oil temperature till the heat flow rate reaches the required value.

q [kW]	10
$\mathbf{T_{in}}$ [°C]	163,356
$\mathbf{T_{out}}$ [°C]	156,56
$\Delta\mathbf{T_{oil}}$ [°C]	6,76
$\boldsymbol{\alpha_{oil}}$ **first spire** [W m^{-2} K^{-1}]	α_{oil} = -6,8495 z^3 + 39,138 z^2 - 98,691 z + 1826,8
$\boldsymbol{\alpha_{oil}}$ **second spire** [W m^{-2} K^{-1}]	α_{oil} = 6,8495 z^3 - 0,3146 z^2 + 24,15 z + 1733,1
$\mathbf{T_{oil}}$ **first spire** [°C]	T_{oil} = -0,3875 z^3 + 2,4788 z^2- 7,0546 z + 163,6
$\mathbf{T_{oil}}$ **second spire** [°C]	T_{oil} = 0,3875 z^3 + 0,2468 z^2+ 1,8214 z + 156,45

Table 5.18 Analytical results with q10 kW and setting the old wall temperature.

q [kW]	20
$\mathbf{T_{in}}$ [°C]	172,16
$\mathbf{T_{out}}$ [°C]	158,63
$\Delta\mathbf{T_{oil}}$ [°C]	13,53
$\boldsymbol{\alpha_{oil}}$ **first spire** [W m^{-2} K^{-1}]	α_{oil} = -22,129 z^3+ 113,8 z^2- 247,85 z + 1968,6
$\boldsymbol{\alpha_{oil}}$ **second spire** [W m^{-2} K^{-1}]	α_{oil} = 22,129 z^3- 13,659 z^2+ 55,579 z + 1755,6
$\mathbf{T_{oil}}$ **first spire** [°C]	T_{oil} = -0,9247 z^3+ 5,5431 z^2- 14,659 z + 172,63
$\mathbf{T_{oil}}$ **second spire** [°C]	T_{oil} = 0,9247 z^3+ 0,2171 z^2+ 3,6 z + 158,38

Table 5.19 Analytical results with q20 kW and setting the old wall temperature.

q [kW]	40
$\mathbf{T_{in}}$ [°C]	188,83
$\mathbf{T_{out}}$ [°C]	161,94
$\Delta\mathbf{T_{oil}}$ [°C]	26,9
$\boldsymbol{\alpha_{oil}}$ **first spire** [W m^{-2} K^{-1}]	α_{oil} = -104,91 z^3+ 466,27 z^2- 801,79 z + 2348,8
$\boldsymbol{\alpha_{oil}}$ **second spire** [W m^{-2} K^{-1}]	α_{oil} = 104,91 z^3- 137,99 z^2+ 171,5 z + 1785,7
$\mathbf{T_{oil}}$ **first spire** [°C]	T_{oil} = -2,634 z^3+ 13,992 z^2- 31,922 z + 189,71
$\mathbf{T_{oil}}$ **second spire** [°C]	T_{oil} = 2,634 z^3- 1,1795 z^2+ 7,3213 z + 161,36

Table 5.20 Analytical results with q30 kW and setting the old wall temperature.

11) Numerical results: once the oil temperature and heat transfer coefficient equations are developed, we can set the finite element model and run the simulations. Temperature at the path points on the workpiece side

q [kW]	$\mathbf{T_{in\_oil}}$ [°C]	$\mathbf{T_{min\ \_sur}}$ [°C]	$\mathbf{T_{max\ \_sur}}$ [°C]	$\Delta\mathbf{T_{sur}}$ [°C]	**average T [FEM]** [°C]	$\mathbf{T_{mean}}$ **of 202 values** [°C]
10	163,4	150,4	152,2	1,76	151,3	150,9
20	172,2	144,8	148,7	3,90	146,8	145,9
30	180,7	139,0	145,5	6,46	142,3	140,8
40	188,8	133,0	142,5	9,50	137,8	137,0

Table 5.21 Temperature values on the workpiece-side path with four different heat flow rates.

Temperature at the path points on the ambient side

q [kW]	$\mathbf{T_{min\ \_sur}}$ [°C]	$\mathbf{T_{max\ \_sur}}$ [°C]	$\Delta\mathbf{T_{sur}}$ [°C]	**average T [FEM]** [°C]	$\mathbf{T_{mean}}$ **of 202 values** [°C]
10	157,1	158,7	1,57	157,9	157,5
20	161,0	164,3	3,27	162,7	161,9
30	164,4	169,6	5,13	167,0	165,7
40	167,6	174,8	7,14	171,2	166,9

Table 5.22 Temperature values on the ambient-side path with four different heat flow rates.

12) Find the function between the wall temperature and the heat flow rate.

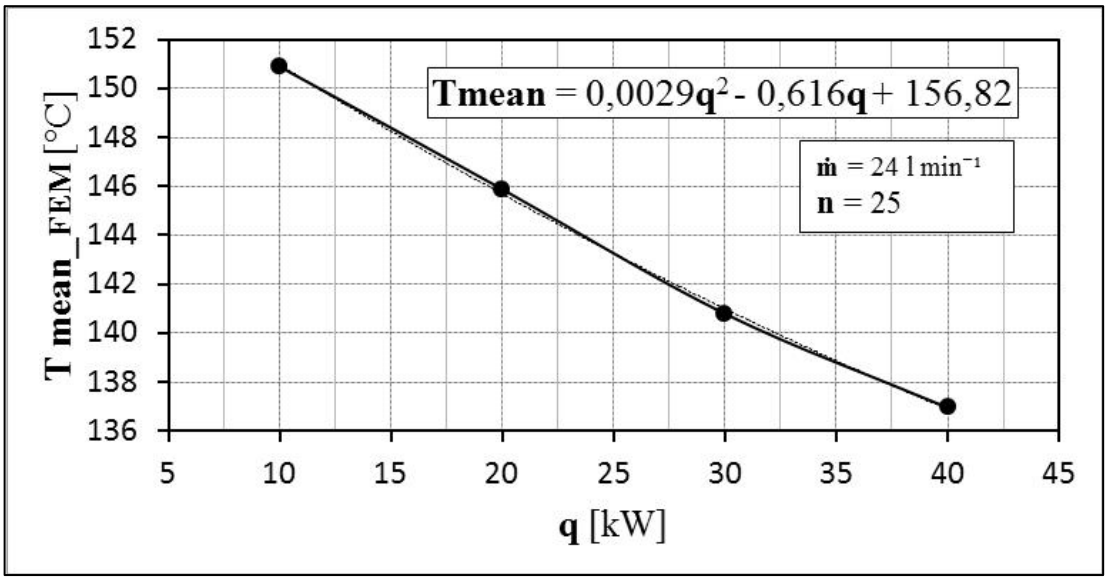

Figure 5.15 Mean surface temperature against the heat flow rate by setting the old wall temperature in the analytical calculation.

The figure 5.15 shows the variation of the average temperature on the outer roller surface over the heat flow rate. We can derive the following function:

$$\mathbf{T_{sur,FEM}\ (q)} = 0.0029*\mathbf{q}^2 - 0{,}616*\mathbf{q} + 156{,}82\mathbf{.}$$

13) Choose of other values of q to be analysed in order to create the final map.
The following values of heat flow rate are chosen [kW]:

10; 12,5; 15; 17,5; 20; 22,5; 25, 27,5; 30; 32,5; 35; 37,5; 40.

14) Calculation of $T_{sur,FEM}$ and $T_{w,new}$.

Adopting the derived equation, we can calculate the $T_{sur,FEM}$ for each number of turns. Afterwards we can make a simple proportion and, finally, obtain the $T_{w,new}$ to be set in the analytical calculation ($T_{w,old}$= 155,05 °C)

$$T_{w,new} = \frac{T_{w,old}}{T_{sur,FEM}} * 140$$

We obtain in the end the following values:

q [kW]	10	12,5	15	17,5	20	22,5	25	27,5	30	32,5	35	37,5	40
$\mathbf{T_{sur,FEM}}$	151,0	149,6	148,2	146,9	145,7	144,5	143,3	142,1	141,0	139,9	138,9	137,9	136,9
$\mathbf{T_{w,new}}$	143,9	145,2	146,5	147,8	149,1	150,4	151,6	152,8	154,4	155,2	156,4	157,5	158,7

Table 5.23 First row: Outer roller temperature from FEM simulations; second row: re-calculated wall temperature.

15) Set the input parameters in the "Analysis 4" and find out the analytical results.

q [kW]	10
$\mathbf{T_{in}}$ [°C]	152,524
$\mathbf{T_{out}}$ [°C]	145,68
$\mathbf{\Delta T_{oil}}$ [°C]	6,844
$\mathbf{\alpha_{oil}}$ **first spire** [W m^{-2} K^{-1}]	α_{oil} = -4,9646 z^3 + 29,06 z^2 - 76,971 z + 1694,4
$\mathbf{\alpha_{oil}}$ **second spire** [W m^{-2} K^{-1}]	α_{oil} = 4,9646 z^3 + 0,464 z^2 + 20,285 z + 1618,6
$\mathbf{T_{oil}}$ **first spire** [°C]	T_{oil} = -0,3445 z^3 + 2,287 z^2- 6,8714 z + 152,76
$\mathbf{T_{oil}}$ **second spire** [°C]	T_{oil} = 0,3445 z^3 + 0,3028 z^2+ 1,8989 z + 145,56

Table 5.24 Analytical results with q = 10 kW and the old wall temperature.

q [kW]	12,5
$\mathbf{T_{in}}$ [°C]	156,12
$\mathbf{T_{out}}$ [°C]	147,58
$\Delta\mathbf{T_{oil}}$ [°C]	8,54
$\boldsymbol{\alpha_{oil}}$ **first spire** [W m^{-2} K^{-1}]	α_{oil} = -7,2417 z^3 + 41,06 z^2- 104,16 z + 1736,5
$\boldsymbol{\alpha_{oil}}$ **second spire** [W m^{-2} K^{-1}]	α_{oil} = 7,2417 z^3 - 0,6516 z^2 + 26,571z + 1636,6
$\mathbf{T_{oil}}$ **first spire** [°C]	T_{oil} = -0,4543 z^3 + 2,9576 z^2 - 8,6834 z + 156,42
$\mathbf{T_{oil}}$ **second spire** [°C]	T_{oil} = 0,4543 z^3 + 0,3406 z^2 + 2,3509 z + 147,43

Table 5.25 Analytical results with q = 12.5 kW and the old wall temperature.

q [kW]	15
$\mathbf{T_{in}}$ [°C]	159,662
$\mathbf{T_{out}}$ [°C]	149,44
$\Delta\mathbf{T_{oil}}$ [°C]	10,22
$\boldsymbol{\alpha_{oil}}$ **first spire** [W m^{-2} K^{-1}]	α_{oil}= -10,095 z^3 + 55,64 z^2 - 135,46 z + 1781,1
$\boldsymbol{\alpha_{oil}}$ **second spire** [W m^{-2} K^{-1}]	α_{oil} = 10,095 z^3 - 2,5062 z^2 + 33,447 z + 1654,7
$\mathbf{T_{oil}}$ **first spire** [°C]	T_{oil} = -0,5759 z^3 + 3,6749 z^2 - 10,539 z + 160,02
$\mathbf{T_{oil}}$ **second spire** [°C]	T_{oil} = 0,5759 z^3 + 0,3578 z^2 + 2,7962 z + 149,25

Table 5.26 Analytical results with q = 15 kW and the old wall temperature.

q [kW]	17,5
$\mathbf{T_{in}}$ [°C]	163,151
$\mathbf{T_{out}}$ [°C]	151,24
$\Delta\mathbf{T_{oil}}$ [°C]	11,911
$\boldsymbol{\alpha_{oil}}$ **first spire** [W m^{-2} K^{-1}]	α_{oil}= -13,677 z^3 + 73,376 z^2 - 171,59 z + 1828,6
$\boldsymbol{\alpha_{oil}}$ **second spire** [W m^{-2} K^{-1}]	α_{oil} = 13,677 z^3 - 5,4029 z^2 + 41,087 z + 1672,9
$\mathbf{T_{oil}}$ **first spire** [°C]	T_{oil} = -0,7105 z^3 + 4,444 z^2 - 12,443 z + 163,56
$\mathbf{T_{oil}}$ **second spire** [°C]	T_{oil} = 0,7105 z^3 + 0,3513 z^2 + 3,2363 z + 151,02

Table 5.27 Analytical results with q17.5 kW and the old wall temperature.

q [kW]	20
$\mathbf{T_{in}}$ [°C]	166,584
$\mathbf{T_{out}}$ [°C]	153
$\Delta\mathbf{T_{oil}}$ [°C]	13,584
$\boldsymbol{\alpha_{oil}}$ **first spire** [W m^{-2} K^{-1}]	α_{oil}= -18,149 z^3 + 94,91 z^2 - 213,36 z + 1879,3
$\boldsymbol{\alpha_{oil}}$ **second spire** [W m^{-2} K^{-1}]	α_{oil} = 18,149 z^3 - 9,6293 z^2 + 49,623 z + 1691,1
$\mathbf{T_{oil}}$ **first spire** [°C]	T_{oil} = -0,8596 z^3 + 5,269 z^2 - 14,399 z + 167,05
$\mathbf{T_{oil}}$ **second spire** [°C]	T_{oil} = 0,8596 z^3 + 0,3177 z^2 + 3,6722 z + 152,75

Table 5.28 Analytical results with q = 20 kW and the old wall temperature.

q [kW]	22,5
$\mathbf{T_{in}}$ [°C]	169,963
$\mathbf{T_{out}}$ [°C]	154,71
$\Delta\mathbf{T_{oil}}$ [°C]	15,253
$\boldsymbol{\alpha_{oil}}$ **first spire** [W m^{-2} K^{-1}]	α_{oil}= -23,708 z^3+ 120,98 z^2- 261,67 z + 1933,4
$\boldsymbol{\alpha_{oil}}$ **second spire** [W m^{-2} K^{-1}]	α_{oil} = 23,708 z^3 - 15,575 z^2 + 59,279 z + 1709,2
$\mathbf{T_{oil}}$ **first spire** [°C]	T_{oil} = -1,0248 z^3 + 6,1558 z^2 - 16,411 z + 170,49
$\mathbf{T_{oil}}$ **second spire** [°C]	T_{oil} = 1,0248 z^3 + 0,2531 z^2 + 4,1063 z + 154,42

Table 5.29 Analytical results with q = 22.5 kW and the old wall temperature.

q [kW]	25
$\mathbf{T_{in}}$ [°C]	173,286
$\mathbf{T_{out}}$ [°C]	156,36
$\Delta\mathbf{T_{oil}}$ [°C]	16,926
$\boldsymbol{\alpha_{oil}}$ **first spire** [W m^{-2} K^{-1}]	α_{oil}= -30,623 z^3 + 152,6 z^2 - 317,65 z + 1991,4
$\boldsymbol{\alpha_{oil}}$ **second spire** [W m^{-2} K^{-1}]	α_{oil} = 30,623 z^3 - 23,786 z^2 + 70,324 z + 1727,3
$\mathbf{T_{oil}}$ **first spire** [°C]	T_{oil} = -1,2077 z^3 + 7,1095 z^2 - 18,484 z + 173,87
$\mathbf{T_{oil}}$ **second spire** [°C]	T_{oil} = 1,2077 z^3 + 0,1532 z^2 + 4,5401 z + 156,04

Table 5.30 Analytical results with q = 25 kW and the old wall temperature.

q [kW]	27,5
$\mathbf{T_{in}}$ [°C]	176,554
$\mathbf{T_{out}}$ [°C]	157,97
$\Delta\mathbf{T_{oil}}$ [°C]	18,584
$\boldsymbol{\alpha_{oil}}$ **first spire** [W m^{-2} K^{-1}]	α_{oil}= -39,18 z^3 + 190,79 z^2 - 382,49 z + 2053,5
$\boldsymbol{\alpha_{oil}}$ **second spire** [W m^{-2} K^{-1}]	α_{oil} = 39,18 z^3 - 34,887 z^2 + 83,152 z + 1745,1
$\mathbf{T_{oil}}$ **first spire** [°C]	T_{oil} = -1,4103 z^3 + 8,1366 z^2 - 20,624 z + 177,19
$\mathbf{T_{oil}}$ **second spire** [°C]	T_{oil} = 1,4103 z^3 + 0,0133 z^2 + 4,9764 z + 157,6

Table 5.31 Analytical results with q = 27.5 kW and the old wall temperature.

q [kW]	30
$\mathbf{T_{in}}$ [°C]	180,76
$\mathbf{T_{out}}$ [°C]	160,53
$\Delta\mathbf{T_{oil}}$ [°C]	20,23
$\boldsymbol{\alpha_{oil}}$ **first spire** [W m^{-2} K^{-1}]	α_{oil}= -51,889 z^3 + 246,19 z^2 - 472,39 z + 2141,9
$\boldsymbol{\alpha_{oil}}$ **second spire** [W m^{-2} K^{-1}]	α_{oil} = 51,889 z^3 - 52,696 z^2 + 100,89 z + 1775,2
$\mathbf{T_{oil}}$ **first spire** [°C]	T_{oil} = -1,6601 z^3 + 9,3453 z^2 - 22,93 z + 181,45
$\mathbf{T_{oil}}$ **second spire** [°C]	T_{oil} = 1,6601 z^3 - 0,2167 z^2 + 5,4031 z + 160,12

Table 5.32 Analytical results with q = 30 kW and the old wall temperature.

q [kW]	32,5
$\mathbf{T_{in}}$ [°C]	182,919
$\mathbf{T_{out}}$ [°C]	161,02
$\Delta\mathbf{T_{oil}}$ [°C]	21,899
$\boldsymbol{\alpha_{oil}}$ **first spire** [W m^{-2} K^{-1}]	α_{oil}= -62,785 z^3+ 292,6 $z^{2\,2}$ - 545,14 z + 2192,3
$\boldsymbol{\alpha_{oil}}$ **second spire** [W m^{-2} K^{-1}]	α_{oil} = 62,785 z^3 - 69,04 z^2 + 115,9 z + 1779,9
$\mathbf{T_{oil}}$ **first spire** [°C]	T_{oil} = -1,8824 z^3 + 10,435 z^2 - 25,118 z + 183,66
$\mathbf{T_{oil}}$ **second spire** [°C]	T_{oil} = 1,8824 z^3 - 0,4078 z^2 + 5,8667 z + 160,57

Table 5.33 Analytical results with q = 32,5 kW and the old wall temperature.

q [kW]	35
$\mathbf{T_{in}}$ [°C]	186,015
$\mathbf{T_{out}}$ [°C]	162,46
$\Delta\mathbf{T_{oil}}$ [°C]	23,56
$\boldsymbol{\alpha_{oil}}$ **first spire** [W m^{-2} K^{-1}]	α_{oil}= -78,796 z^3 + 359,65 z^2 - 646,68 z + 2270,1
$\boldsymbol{\alpha_{oil}}$ **second spire** [W m^{-2} K^{-1}]	α_{oil} = 78,796 z^3 - 94,21 z^2 + 137,03 z + 1796,6
$\mathbf{T_{oil}}$ **first spire** [°C]	T_{oil} = -2,1562 z^3 + 11,719 z^2 - 27,482 z + 186,8
$\mathbf{T_{oil}}$ **second spire** [°C]	T_{oil} = 2,1562 z^3 - 0,7008 z^2 + 6,3272 z + 161,98

Table 5.34 Analytical results with q = 35 kW and the old wall temperature.

q [kW]	37,5
$\mathbf{T_{in}}$ [°C]	189,055
$\mathbf{T_{out}}$ [°C]	163,85
$\Delta\mathbf{T_{oil}}$ [°C]	25,205
$\boldsymbol{\alpha_{oil}}$ **first spire** [W m^{-2} K^{-1}]	α_{oil}= -98,461 z^3 + 440,44 z^2 - 764,85 z + 2354,3
$\boldsymbol{\alpha_{oil}}$ **second spire** [W m^{-2} K^{-1}]	α_{oil} = 98,461 z^3 - 126,7 z^2 + 162,47 z + 1812,5
$\mathbf{T_{oil}}$ **first spire** [°C]	T_{oil} = -2,4585 z^3 + 13,103 z^2 - 29,931 z + 189,88
$\mathbf{T_{oil}}$ **second spire** [°C]	T_{oil} = 2,4585 z^3 - 1,0577 z^2 + 6,8032 z + 163,32

Table 5.35 Analytical results with q = 37.5 kW and the old wall temperature.

q [kW]	40
$\mathbf{T_{in}}$ [°C]	192,037
$\mathbf{T_{out}}$ [°C]	165,19
$\Delta\mathbf{T_{oil}}$ [°C]	26,847
$\boldsymbol{\alpha_{oil}}$ **first spire** [W m^{-2} K^{-1}]	α_{oil}= -122,5 z^3+ 537,46 z^2- 902,26 z + 2445,7
$\boldsymbol{\alpha_{oil}}$ **second spire** [W m^{-2} K^{-1}]	α_{oil} = 122,5 z^3 - 168,14 z^2 + 193,17 z + 1827,6
$\mathbf{T_{oil}}$ **first spire** [°C]	T_{oil} = -2,7917 z^3 + 14,595 z^2 - 32,468 z + 192,9
$\mathbf{T_{oil}}$ **second spire** [°C]	T_{oil} = 2,7917 z^3 - 1,4855 z^2 + 7,2988 z + 164,61

Table 5.36 Analytical results with q = 40 kW and the old wall temperature.

16) Run the simulations and obtain the mean temperature on the surface for each case of study.

The numerical model is prepared as explained in chapter 5.2.3. However, each case of study we keep the same heat transfer coefficient for the convective term on the ambient surface and change the heat flow rate set on the workpiece surface as:

$q_{w-p} = q_{tot} - q_{amb}$ [W]

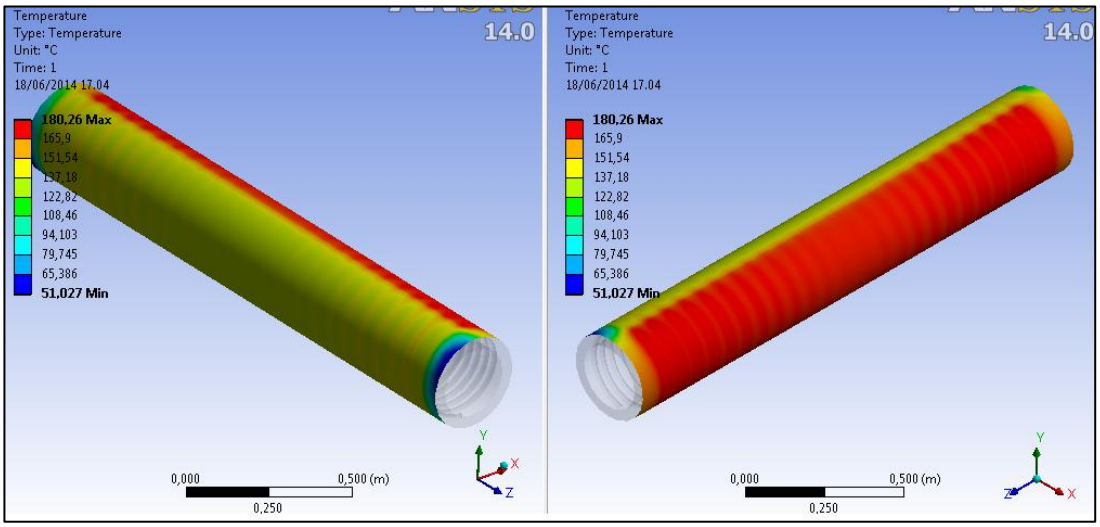

Figure 5.16 Temperature distribution on the outer roller surface, workpiece (left) and ambient (right) sides.Case of study: q = 40 kW.

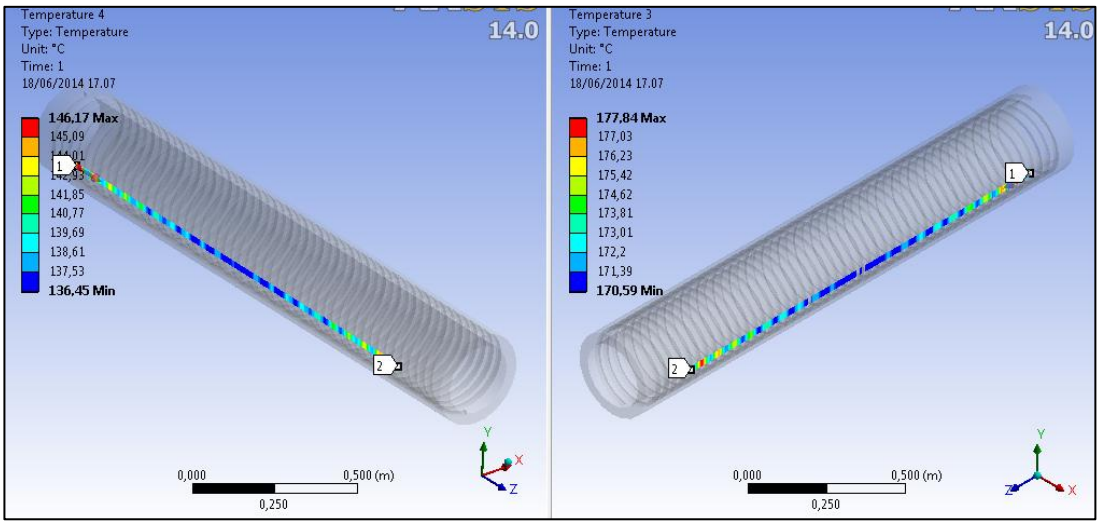

Figure 5.17 Temperature distribution on the two paths. Case of study: q = 40 kW.

q [kW]	**T_{in_oil}** [°C]	**$T_{min\ \_sur}$** [°C]	**$T_{max\ \_sur}$** [°C]	**ΔT_{sur}** [°C]	**average T [FEM]** [°C]	**T_{mean} of 202 values** [°C]
10	152,5	139,2	140,8	1,68	140	139,6
12,5	156,1	139,1	141,3	2,16	140,2	139,7
15	159,7	139,0	141,7	2,67	140,4	139,8
17,5	163,2	138,9	142,1	3,21	140,5	139,8
20	166,6	138,8	142,6	3,78	140,7	139,8
22,5	17,00	138,6	143,0	4,39	140,8	139,8
25	173,3	138,4	143,5	5,02	140,9	139,8
27,5	176,6	138,2	143,9	5,7	141,1	139,8
30	180,8	139,0	145,5	6,46	142,3	140,8
32,5	182,9	137,6	144,8	7,17	141,2	139,6
35	186,0	137,3	145,3	7,97	141,3	139,5
37,5	189,1	136,9	145,7	8,82	141,3	139,3
40	192,0	136,5	146,2	9,72	141,3	139,1

Table 5.37 Temperature values on the workpiece-side path against the heat flow rate. The simulation is made adopting results calculated with the new wall temperature.

q [kW]	**$T_{min\ \_sur}$** [°C]	**$T_{max\ \_sur}$** [°C]	**ΔT_{sur}** [°C]	**average T [FEM]** [°C]	**T_{mean} of 202 values** [°C]
10	146,3	147,8	1,51	147,0	146,6
12,5	148,6	150,6	1,91	149,6	149,1
15	151,0	153,3	2,32	152,1	151,6
17,5	153,2	156,0	2,75	154,6	153,9
20	155,4	158,6	3,18	157,0	156,3
22,5	157,6	161,2	3,65	159,4	158,5
25	159,6	163,8	4,12	161,7	160,7
27,5	161,6	166,2	4,6	163,9	162,8
30	164,4	169,6	5,13	167,0	165,7
32,5	165,4	171,1	5,61	168,3	166,9
35	167,2	173,4	6,14	170,3	168,8
37,5	168,9	175,6	6,69	172,3	170,7
40	170,6	177,8	7,25	174,2	172,5

Table 5.38 Temperature values on the ambient-side path against the heat flow rate. The simulation is made adopting results calculated with the new wall temperature.

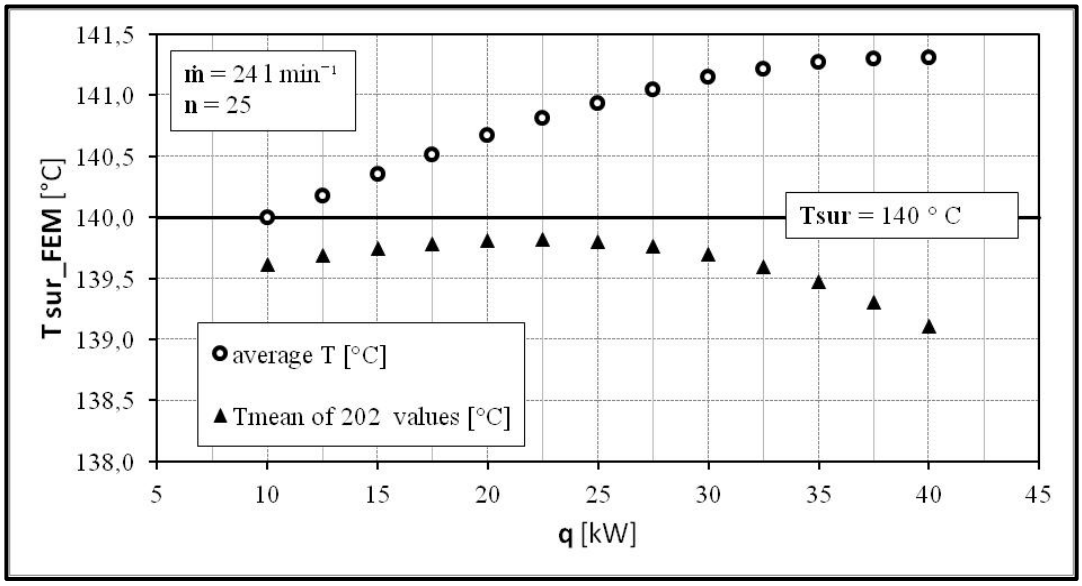

Figure 5.18 Average and mean surface temperature over the heat flow (see table 5.37).

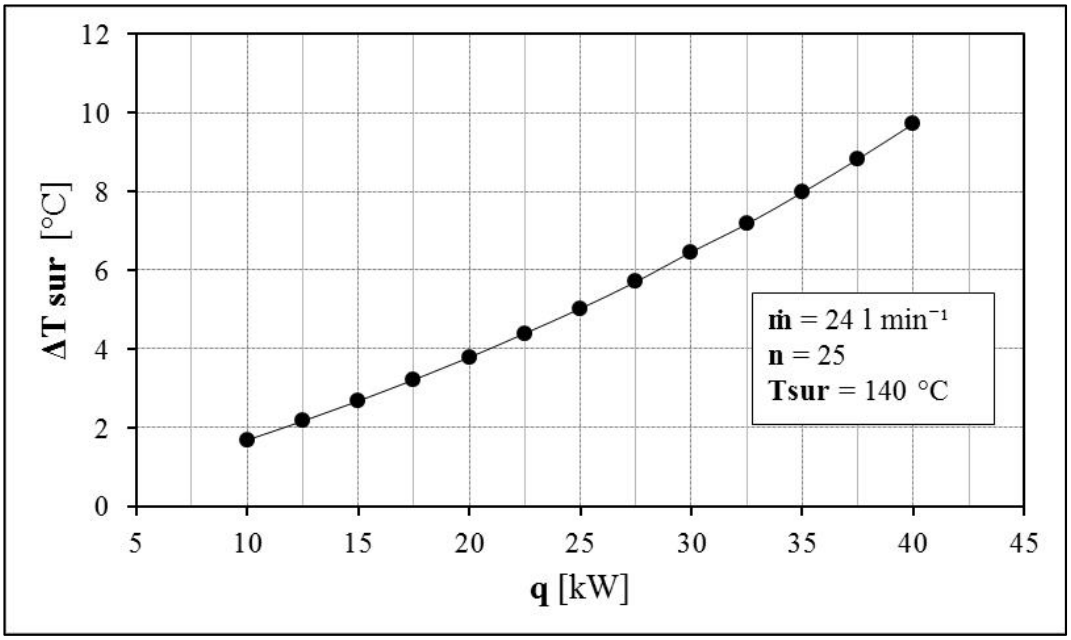

Figure 5.19 External temperature gradient from FEM simulations against the heat flow rate (see table 5.37).

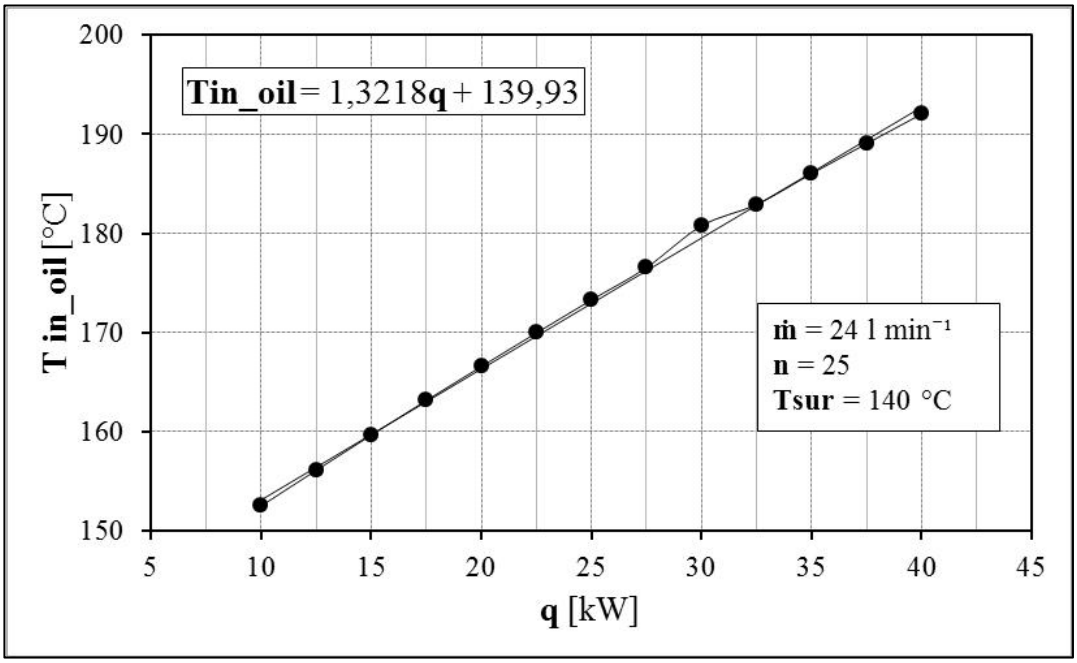

Figure 5.20 Inlet oil temperature to be set while the heat flow rate varies (see table 5.37).

The Figure 5.18 shows the variation of mean temperature calculated with all the points of the external path. The graph confirms an almost constant value of mean temperature with different heat flow rates involved in the model. This values has to be closed to the one required by the customer, T_{sur} = 140 °C.

The Figure 5.19 shows the variation of external temperature gradient over the heat flow rate. The relationship is almost linear and when the heat flow rate becomes greater than 25 kW the temperature variation overcomes the required threshold of 5 °C. With q=30 kW the temperature variation is higher but just because of the temperature distribution on the path ends.

The figure 5.20 shows how the inlet oil temperature should be set in order to obtain a certain amount of heat flow rate from the process. The relationship is almost linear and the oil temperature increases with the heat flow rate. The final function is:

$\mathbf{T_{in\_oil}\ (q)}$ = 1,3218 **q** +139,93 [°C],

where q is the heat flow rate [kW].

CHAPTER 6: Rolling roller

6.1 Step description

In this chapter we finally take into account the effects of the roller rotation and of the web while it moves around the roller. In fact we consider a variation of temperature and heat flow rate during the heating up period. In the previous chapter we just modeled the roller, neglecting the rotation and adopting an uniform heat flow rate over the whole surface, which was supposed to simulate the textile effect. During the process, the roller provides heat flow rate as:

- 1Amount absorbed by the textile during the contact period.
- 2Amount exchanged with the surroundings not-working side.
- 3Amount exchanged with the surroundings through the workpiece side.

The second and the third amounts are calculated by an analytical formula, which provides an average heat transfer coefficient over the outer surface of the workpiece and another one over the outer roller surface on the ambient side. The first amount provides a temperature increasing on the textile over the cylindrical coordinate. The temperature also changes along the textile thickness. In fact, the internal layer of the textile is supposed to reach immediately the outer surface temperature of the roller, whereas the outer layer needs more time because it is exposed to the ambient. The heat flow rate absorbed by the textile is even not constant over the cylindrical coordinate and it affects the temperature on the outer roller surface. Therefore it could lead to a non-uniform temperature distribution on the same surface and a different model could be defined.
The textile material taken into account is cotton with a surface density of 200 $\mathrm{g\,m^{-2}}$ (see paragraph 4.3.1). The material properties used for the model are:

- Thermal conductivity, λ_c = 0,04 $\mathrm{W\,m^{-2}\,K^{-1}}$;

- Density, ρ_c = 400 kg m^{-3};
- Specific heat capacity, c_{p_c} = 1300 J kg^{-1} K^{-1}.

6.2 External heat transfer coefficient.

As already mentioned, the natural convection is supposed to be the main heat transfer mechanism on the external roll surface. However, we don't consider a stationary cylinder anymore, but a rotating one. In a heated rotating system the buoyancy and the centrifugal forces are important. The combination of these determines the flow regime and the heat transfer mechanism. In the mixed convection system the flow and heat transfer characteristics are determined by the buoyancy and the centrifugal forces, which are characterized by Grashof number and Reynolds number, respectively. Of particular relevance is the ratio Gr/Re^2, which indicates the relative importance of buoyance and rotational effects. The heat transfer coefficient has to be calculated. Therefore, the following model can be applied to derive the Nusselt number [8]:
The Nusselt number is roughly independent on the Reynolds number up to critical value where $Gr/Re^2 = 1$. I.e. the Nusselt number is constant or slightly decreases with the increasing of the Reynolds number up to this critical value, beyond which Nu increases with Re. For Re above 8000, the heat transfer coefficients are independent from Grashof number (for Gr ≤ 100.000), they are correlated as:

$$Nu = 0{,}022Re^{0{,}821} = \frac{\alpha_{free} D}{\lambda}$$

For Re below 500 the Nusselt number depends almost entirely from the Grashof number (for Gr > 100) and in the intermediate between 500 and 8000 both Gr and Re influence the heat transfer coefficient as:

$$Nu = 0{,}11(Pr(0{,}5\ Re^2 + Gr))^{0{,}35}$$

- Grashof number: $Gr = \frac{D^3 \beta g (T_{sur} - T_\infty)}{\nu^2}$

- Prandtl number: $\mathrm{Pr} = \frac{c_p\,\mu}{\lambda}$
- Reynolds number: $\mathrm{Re} = \frac{\rho\omega D^2}{2\mu}$.

6.2.1 Cotton side

We have to take into account the external layer of the textile. The thermophysical properties of the air are calculated at the average temperature between the surface and the ambient. The surface temperature increases during the rotation starting from the ambient temperature. The final temperature of the outer layer is still unknown, but we assume a guess value to start with the calculation: T_{out_cotton} = 60 °C. Hence the average temperature of the cotton is: $T_{sur} = (T_{out\_cotton} + T_{in\_cotton})/2 = (23+60)/2 =$ 41,5 °C. The average one between the surface and the ambient is: $T_m = (T_{sur} + T_\infty)/2 =$ (41,5+20)/2 = 32,25 °C. Air properties at this temperature:

T [°C]	$\boldsymbol{\beta}$ [K^{-1}]	**ρ** [kg m^{-3}]	$\mathbf{c_p}$ [kJ $kg^{-1}K^{-1}$]	**λ** [10^{-3}W $m^{-1}K^{-1}$]	**μ** [μPas]	**Pr** [-]
32,25	0,0033	1,156	1,0069	26,59	18,84	0,71

Table 6.1 Thermo-physical properties of the air at the average temperature.

We obtain : Gr = 6,03 10^7 , Re = 12˙260, $\mathrm{Gr/Re^2}$= 0,4.

Re is higher than 8000, and the $\mathrm{Gr/Re^2}$ ratio indicates the rotational effects are more relevant than the buoyance ones. We adopt the equation that combines both effects (Gr > 100˙000):

$\mathrm{Nu} = 0{,}11(\mathrm{Pr}(0{,}5\,\mathrm{Re}^2 + \mathrm{Gr}))^{0{,}35} = 68{,}6.$

Finally, $\alpha_{free} = \frac{\mathrm{Nu}\,\lambda}{D} = \frac{68{,}6*0{,}0266}{0{,}3} = 6{,}08$ W $m^{-2}K^{-1}$..

Since the surface of the roller is hot, a non-negligible part of the heat is transferred by radiation:

$\alpha_r = 4\,\sigma\,T_m^3 = 4 * 5{,}67\,10^{-8} * 305{,}4^3 = 6{,}46$ W $m^{-2}K^{-1}$.,

Adding the two coefficients, we obtain:

$$\alpha_{ext} = \alpha_{free} + \alpha_r = 6{,}08 + 6{,}46 = 12{,}54 \text{ W m}^{-2}\text{K}^{-1}.$$

With this value is possible now to derive the total heat flow involved in the process:

$$q_{cot} = \alpha_{ext} \frac{A_{ext}}{2} \Delta T_{sur-amb} = 12{,}54 * \frac{1{,}81}{2} * 18{,}5 = 210 \text{ W}$$

where A_{ext} is the whole outer roller surface $A_{ext} = \pi D * l = 3{,}14 * 0{,}3 * 1{,}92 = 1{,}81$ m^2; but we take only half of it, that covered by the textile.

6.2.2 Ambient side

We have to take into account the average temperature of the external surface on the ambient side: T_{sur} = 166 °C (see table 5.13). The average temperature between the surface and the ambient is: $T_m = (T_{sur} + T_\infty)/2 = (166+20)/2 = 94{,}5$ °C. Air properties at this temperature:

T [°C]	$\boldsymbol{\beta}$ [K^{-1}]	**ρ** [kg m^{-3}]	$\mathbf{c_p}$ [kJ $kg^{-1}K^{-1}$]	**λ** [10^{-3}W $m^{-1}K^{-1}$]	**μ** [μPas]	**Pr** [-]
94,5	0,0027	0,972	1,011	30,48	21,73	0,72

Table 6.2 Thermo-physical properties of the air at the average temperature.

We obtain: Gr = 2,06 10^8 , Re = 8933, Gr/Re^2= 2,58.

Re is higher than 8000 but the Gr/Re^2 ratio indicates the buoyance effects are more relevance than the rotational ones. We adopt the equation that combines both effects:

$\text{Nu} = 0{,}11(\text{Pr}(0{,}5\ \text{Re}^2 + \text{Gr}))^{0{,}35} = 84{,}8.$

Finally, $\alpha_{free} = \frac{\text{Nu}\,\lambda}{D} = \frac{84{,}8 * 0{,}0305}{0{,}3} = 8{,}61$ W m^{-2}K^{-1}.

Since the surface of the roller is hot, a non-negligible part of the heat is transferred by radiation:

$\alpha_r = 4\,\sigma\,T_m^3 = 4 * 5{,}67\ 10^{-8} * 367{,}65^3 = 11{,}3$ W m^{-2}K^{-1},

Adding the two coefficients, we obtain:

$$\alpha_{ext} = \alpha_{free} + \alpha_r = 8{,}6 + 11{,}3 = 19{,}9 \text{ W m}^{-2}\text{K}^{-1}.$$

With this value is possible now to derive the total heat flow involved in the process:

$$q_{amb} = \alpha_{ext} \frac{A_{ext}}{2} \Delta T_{sur-amb} = 19{,}9 * \frac{1{,}81}{2} * 143 = 2.572 \text{ W}$$

where A_{ext} is the whole outer roller surface $A_{ext} = \pi D*l = 3{,}14*0{,}3*1{,}92 = 1{,}81$ m^2; but we take only half of it, exposed to the ambient.

6.3 Heating up of the textile.

As already mentioned, before the cotton gets in contact with the outer roller surface, its temperature can be assumed equal to the ambient one over the entire thickness and width. During the rotation it increases its temperature. We can now make the following assumptions:

- There isn't relative movement between the textile and the outer roller surface; no slip condition at the interface.
- The roll reaches stationary conditions, after the starting transient period.

If we consider the roller geometry characterized by the two spires, it is possible to state that the process is periodic with a constant period of $2\pi/\omega$ because the rotational speed of the cylinder is constant too. In fact, after one roller rotation, the internal geometry and conditions are the same. If we consider mean values for the parameters of the roller and we focus our attention only to the textile, we can simulate the heating up of the textile. Therefore, we start deriving the time of the heating up period as:

$$t = \frac{\pi R}{v} = \frac{\pi\ 0{,}15\ 60}{40} = 0{,}707 \text{ s.}$$

where πR is the semicircumference that is the contact length [m], and v is the textile velocity [m s^{-1}].

6.3.1 Piece of textile

Taking into account a piece of cotton, the average boundary conditions during the process are:

- Temperature of the outer roller surface in contact with the cotton.
- Heat transfer coefficient on the external surface.

We now want to model this piece of textile in order to derive the final temperature gradient along the thickness at the end of the heating up process. At first we derive the textile thickness and we fix also the width:

$h = \frac{w_c}{\rho_c} = \frac{0,2}{400} = 0,0005$ m = 0,5 mm,

w = 1,52 m

where ρ_c the density [kg m^{-3}] and w_c the weighing [kg m^{-2}].

Numerical model: we are going to run a transient thermal analysis in order to obtain the temperature variation of the textile over the time.

Geometry: the piece of cotton is modeled as a rectangular parallelepiped (see figure 6.1); its height is set equal to the thickness calculated above.

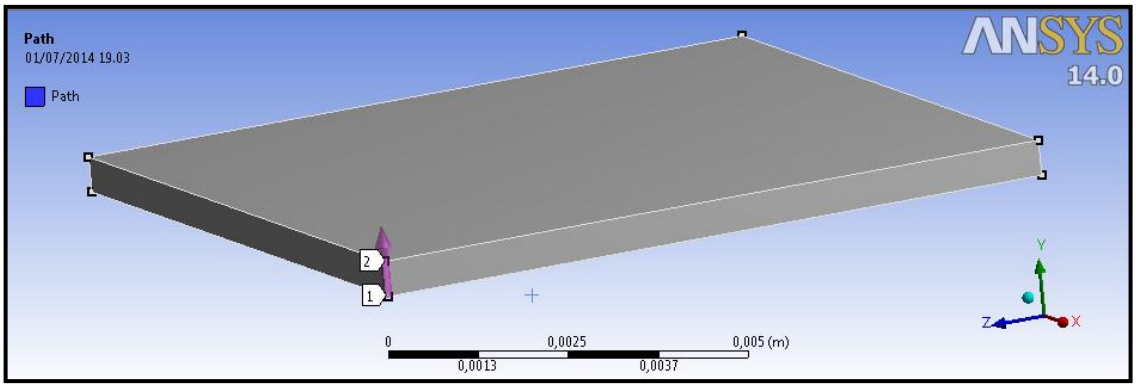

Figure 6.1 Geometry and path of the piece of cotton.

Material properties: The material properties of the cotton are listed above (see paragraph 6.1).

Boundary conditions: as already mentioned, the average parameters values are set:

- Temperature of the inner surface: T = 140 °C. This is an assumption because the temperature on the outer roller surface doesn't remain constant during the rotation, because the heat flux varies during this time and also the total heat flow rate provided by the roll depends on the properties of the textile. We start by setting constant surface temperature.
- Heat transfer coefficient on the external surface of the textile: α_{ext} = 13 $W\,m^{-2}K^{-1}$.

Analysis Settings: in the "Step controls" toolbox, we set one step lasting the heating up period time and we divide it into 6 substeps. The software computes the simulation for each substep:

- Number of steps = 1
- Step end time = 0,707 s
- Auto time stepping = off (the starting substep size is used throughout the load step, or the precise number of substeps can be set)
- Defined by = substeps
- Number of substeps = 6.

Numerical results: a path on the thickness is created in order to evaluate the results (see figure 6.1). After running the simulation we obtain the following distributions of temperature over the thickness at different time steps related to the six substeps:

Time [s]	0	0,11	0,24	0,35	0,47	0,59	0,707
Length [m]	**Tin** [°C]	**Tstep1** [°C]	**Tstep2** [°C]	**Tstep3** [°C]	**Tstep4** [°C]	**Tstep5** [°C]	**Tout** [°C]
0	22	140	140	140	140	140	140
0,03	22	110,1	123,0	127,2	129,4	130,7	131,8
0,06	22	87,9	107,1	114,7	118,9	121,6	123,6
0,08	22	71,2	92,7	102,9	108,8	112,7	115,6
0,11	22	58,7	80,2	91,9	99,1	104,1	107,9
0,14	22	49,4	69,5	82,0	90,1	96,0	100,5
0,17	22	42,5	60,5	73,0	81,8	88,3	93,5
0,19	22	37,4	53,1	65,2	74,2	81,2	86,9
0,22	22	33,5	46,9	58,3	67,4	74,7	80,8
0,25	22	30,6	42,0	52,5	61,4	68,8	75,2
0,28	22	28,4	37,9	47,5	56,1	63,6	70,1
0,31	22	26,8	34,8	43,4	51,5	59,0	65,6
0,33	22	25,7	32,2	39,9	47,7	55,0	61,7
0,36	22	24,8	30,3	37,2	44,5	51,6	58,3
0,39	22	24,2	28,8	35,0	41,9	48,8	55,6
0,42	22	23,7	27,7	33,4	39,9	46,7	53,3
0,44	22	23,4	27,0	32,2	38,4	45,1	51,7
0,47	22	23,3	26,5	31,5	37,5	44,1	50,6
0,50	22	23,2	26,3	31,2	37,1	43,6	50,1

Table 6.3 Temperature distribution over the web thickness, at each substep.

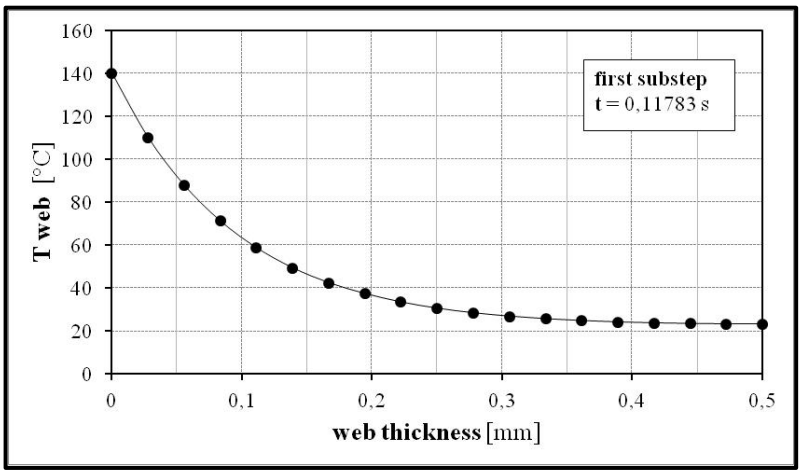

Figure 6.2: Temperature distribution over the web thickness; first substep

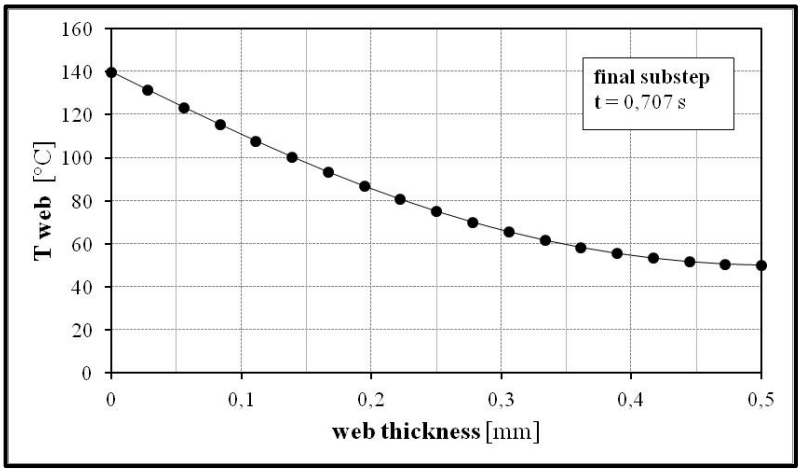

Figure 6.3: Final temperature distribution over the web thickness; last substep.

The figures show that the temperature on the inner layer is constant over the time and equal to 140 °C because of the set boundary condition. We can state that:

- the temperature on outer layer of the piece increases.
- the temperature gradient at the inner layer decreases, due to the heat absorbed. In fact, at the beginning of the heating period, the temperature distribution is constant and equal to the outer surface one, with a high slope coming up to the inner surface.

At each substep, it is possible to calculate the energy absorbed by the cotton as following explained for the first one:

- total mass of the cotton: M = $\rho V = \rho\pi Rwh = 400*\pi*0{,}15*1{,}52*0.0005 = 0{,}143$ kg
- mass flow at each substep: m = $\frac{M}{n} = \frac{0{,}143}{6} = 23{,}9$ g
- specific heat, $c_{p\_c} = 1300$ J kg^{-1} K^{-1}.
- Time substep, $t_{sub} = 0{,}117$ s

Dividing the thickness into 18 parts, with the evaluated results it is possible to calculate:

1) average inlet and outlet temperature at each slice of cotton: T_{in_i} and T_{out_i} (19 values of temperature along the thickness are available, both at the starting and the end of the substep),
2) temperature change at each slice of cotton: $\Delta T_i = T_{in\_i} - T_{out\_i}$,
3) absorbed heat at each slice of cotton: $H_i = \frac{m}{18} c_{p\_c} \Delta T$

part	**length** [mm]	**average T_{in}** [°C]	**T_{out}** [°C]	**average T_{out}** [°C]	**ΔT** [°C]	**absorbed heat** [J]
1	0	22	140	125,06	103,06	177,71
2	0,03	22	110,11	98,98	76,98	132,74
3	0,06	22	87,85	79,53	57,53	99,21
4	0,08	22	71,21	64,98	42,98	74,11
5	0,11	22	58,74	54,07	32,07	55,31
6	0,14	22	49,41	45,94	23,94	41,27
7	0,17	22	42,47	39,93	17,93	30,93
8	0,19	22	37,40	35,44	13,44	23,17
9	0,22	22	33,47	32,03	10,03	17,29
10	0,25	22	30,58	29,50	7,50	12,94
11	0,28	22	28,42	27,63	5,63	9,71
12	0,31	22	26,84	26,25	4,25	7,33
13	0,33	22	25,66	25,23	3,23	5,57
14	0,36	22	24,80	24,48	2,48	4,28
15	0,39	22	24,17	23,95	1,95	3,35
16	0,42	22	23,73	23,58	1,58	2,72
17	0,44	22	23,43	23,35	1,35	2,32
18	0,47	22	23,26	23,23	1,23	2,12
	0,50		23,20			

Table 6.4 Absorbed heat along the thickness after the first substep.

4) heat absorbed at the substep: $H_{sub} = \sum_i H_i = 702{,}1$ J
5) heat flow rate at the substep: $q_{sub} = \frac{H_{sub}}{t_{sub}} = \frac{702{,}1}{0{,}117} = 5962$ W

It is possible to repeat the calculations for each substep and, finally, obtain the total heat absorbed by the cotton and the amount of heat flow rate required in order to increase its temperature.

part	$\mathbf{H_{sub}}$ [J]	$\mathbf{q_{sub}}$ [W]
1	702	5962
2	345	2932
3	259	2196
4	213	1813
5	184	1562
6	162	1377
tot	1865	15842

Table 6.5 Absorbed heat and heat flow rate required at each substep.

It is now possible to calculate approximately the total heat flow rate that has to be provided by the roller:

q = q_{abs} + q_{amb} + q_{cot} = 15842 + 2572 + 210 = 18624 W,

where q_{amb} and q_{cot} are the heat flow rates transferred to the surroundings through the ambient and the cotton side.

The value isn't the real one due to the critical assumption made for the new model, but we have an order of magnitude. It is possible to state that the roller has been designed with the input heat flow rate data equal to q = 30 kW. Therefore, a reducing of the required one surely leads to better temperature distribution over the outer roller surface.

Approximating the value to q = 20 kW and looking at the results calculated and written in the previous chapter (paragraph 5.4), the inlet oil temperature must be set at:

T_{in} = 166,6 °C, this value should guarantee an outer surface roller temperature mostly equal to 140 °C on the web side.

The oil temperature change will be: ΔT_{oil} = 13,6 °C (table 5.28).

Whether the heat flow rate remains the same, higher value of inlet oil temperature leads to lower oil temperature change and, in turn, higher outer roller surface temperature that exceeds the requirement. However, that leads to higher absorbed heat by the cotton (the assumption of constant heat flow rate is not valid anymore) and an increasing of temperature on the outer layer of the web at the end of the process. This means that all the parameters are strictly linked one to each other.

6.3.2 Optimization of temperature on the outer layer

An important value that has to be taken into account is the final temperature on the outer layer of the cotton. Adopting this model we calculated:

$$T_{out\_final} = 50{,}1\ °C.$$

If the application requires different value of final temperature on the outer layer, it is possible to proceed by:

1) modify the average temperature on the outer roller surface: this solution forces to a re-designing of the project due to the fact that it was an input data: T_{sur} = 140 °C;
2) modify the rotational speed of the roller in order to increase or decrease the heating up process time.

We select six values of surface temperature : T_{sur} = 100, 120, 140, 160, 180, 200 °C; for each one we run a simulation setting:

- end time = 5 s
- number of substeps = 10

Finally we obtain the results shown in the see table 6.6 and plotted in the figure 6.4. It is now possible to state:

- the higher the surface temperature, the higher the final temperature on the outer web layer after a certain heating up period, and the lower the time required to reach a certain value of temperature.
- the higher the heating up period, the higher the final temperature on the outer web layer and the value increases with the outer roller surface.

n substep	Time [s]	100 [°C]	120 [°C]	140 [°C]	160 [°C]	180 [°C]	200 [°C]
0	0	22	22	22	22	22	22
1	0,5	33,4	36,3	39,2	42,2	45,1	48,0
2	1	47,4	53,9	60,5	67,0	73,5	80,0
3	1,5	59,2	68,8	78,3	87,9	97,4	107,0
4	2	68,0	79,8	91,6	103,4	115,2	127,0
5	2,5	74,3	87,7	101,1	114,6	128,0	141,4
6	3	78,7	93,3	107,8	122,4	136,9	151,5
7	3,5	81,8	97,2	112,5	127,9	143,2	158,6
8	4	84,0	99,9	115,8	131,7	147,6	163,5
9	4,5	85,5	101,9	118,1	134,4	150,7	167,0
10	5	86,6	103,2	119,7	136,3	152,8	169,4

Table 6.6 Final temperature on the outer cotton layer against the process time, varying the outer roller surface temperature.

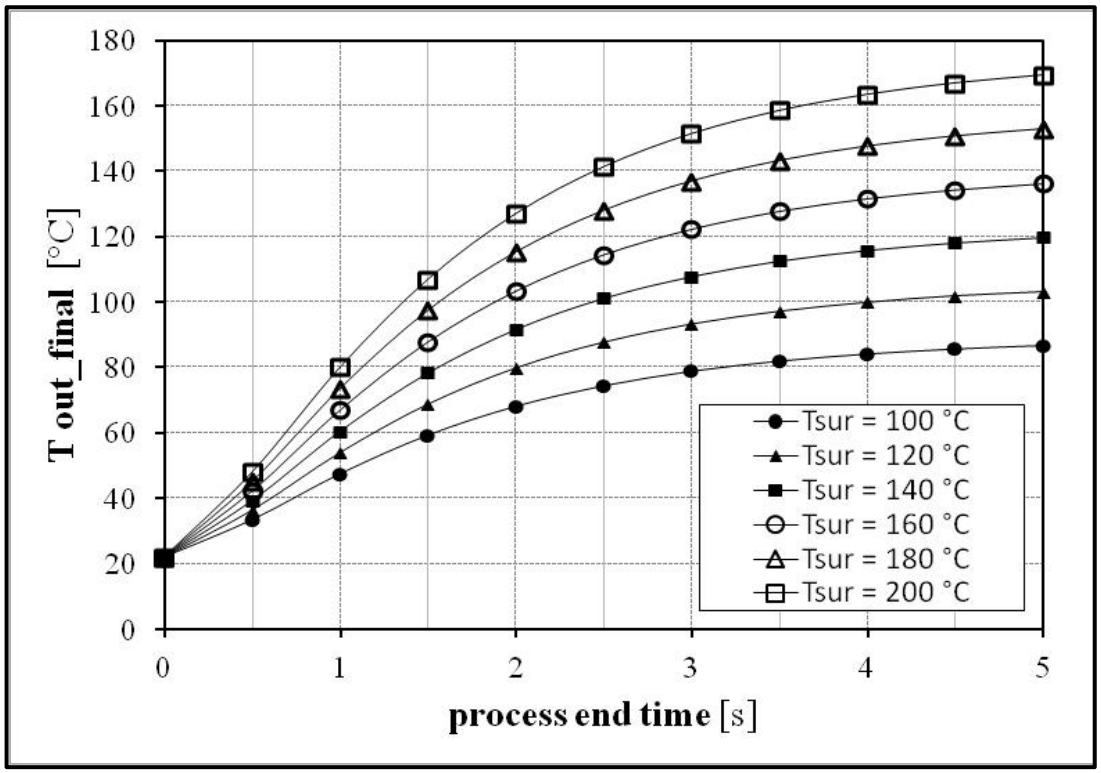

Figure 6.4 Final temperature on the outer cotton layer against the process time; the curves are parametric with the temperature on the outer roller surface.

Example:

1) considering the rotational roller velocity remain the same as before, we derive T_{sur} required to reach T_{out_final} = 70 °C.

Setting the end time = 0,707 s, and varying the T_{sur}, we obtain:

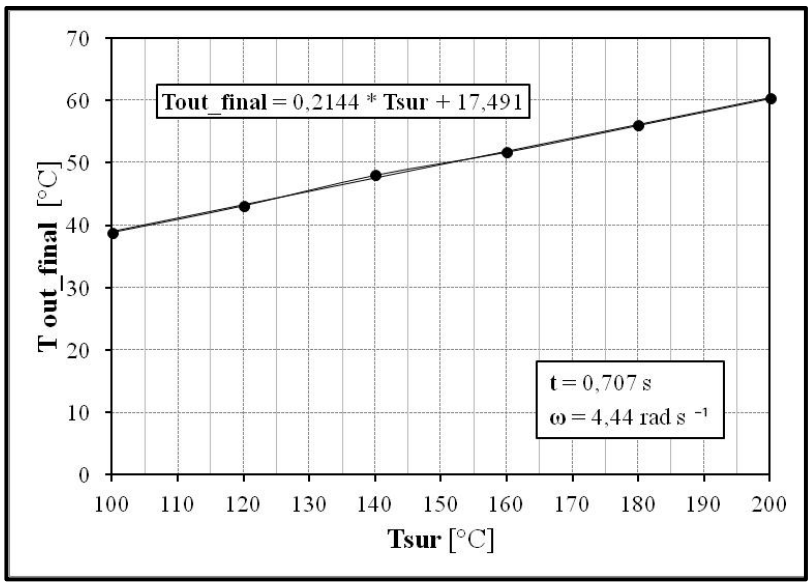

Figure 6.5 Final temperature on the outer cotton layer against the temperature on the outer roller surface.

And the temperature on the outer roller surface is:

$$T_{sur} = \frac{T_{out\_final} - 17,491}{0,2144} = \frac{70 - 17,491}{0,2144} = 245\ °C.$$

2) We fix the outer roller temperature at 140 °C, and derive the process end time required to reach T_{out_final} = 70 °C in order to calculate the new rotational speed. Looking to the table 6.6 and the figure 6.4 we can derive the following end time: t = 1,25 s; therefore:

$$\omega = \frac{v}{R} = \frac{\pi R}{t}\frac{1}{R} = \frac{\pi}{1,25} = 2,51\ \text{rad s}^{-1}.$$

CONCLUSIONS

We have been studied the roller behaviour at different process conditions:

- Roll exposed to the ambient; low value of heat flow rate.
- Full web covering; high heat flow rate.
- Partial web covering; high heat flow rate.

For each one we created a model in order to simulate the real conditions. We made also some assumptions that have to be experimentally verified.
With the results obtained we can state that the increasing of required heat flow rate leads to different parameter selections, such as oil flow rate (connected to the cross-section area) and number of turns.

By going to analyze the roller in case of high heat flow rate, with the same geometry and oil flow rate, the full or partial covering have a strong influence on the final results.
The thermal load placed on the roller by a **full covering** will result in a fairly uniform temperature on the entire roller surface (this condition has been studied and discussed in chapter 4).

If the web does not cover the entire heated roller surface, the temperature uniformity of the roller can be drastically altered. With a **partial covering**, heat is being removed mostly from the web area (this condition has been studied and discussed in chapter 5). The results show that, if the thermal load on the roller is significant, the roller surface temperature will have a big gap from the oil temperature in the web are, whereas the temperature on the roller surface outside the web area is close to the oil temperature.

In both full and partial covering the final most important result was the map of the inlet oil temperature against the heat flow rate. Comparing the two maps, it is possible to state that the partial web leads to higher required inlet oil temperature with a certain heat flow rate. That is basically due to the fact that the heat has to be provided through an internal pipe area which is half of the previous one.

In the last chapter of the thesis, the way to calculate the input project data to design the roller has been proposed. In fact, an example of external textile has been taken into account. The two values of heat flow rate and average surface temperature of the roller are important results that influence the roller angular speed and the final outer temperature of the workpiece. With these two values it is possible to start a new project following the steps and the pattern proposed in this work, choosing the model depending on the boundary conditions.

Further work:

The models been used in this work may be considered as a first attempt, due to the several assumptions involved, such as:

- Uniform heat flow rate over the heat transfer surfaces,
- Not rotating roller,
- Constant heat transfer coefficient in the simulations made in case of full web,
- Constant wall temperature (analytical calculations),
- Others....

The best way to verify the model quality is with an experimental analysis, which includes: creating a prototype of the roller and varying the external conditions as we have done theoretically.
Considering a specific case of study or application, e.g. partial web made by cotton and described in chapter 6, the procedure which has to be adopted may be:

- Make the calculations, as explained in chapter 6, in order to obtain approximately the heat flow rate to be provided by the roller; q_{1_model}.
- Set the inlet oil temperature as calculate in this project (figure 7.2; $T_{in\_oil\_model\_1}$.
- Measure the outlet oil temperature $T_{out\_oil\_process\_1}$.
- Calculate the real heat flow rate provided by the oil. $q_{2\_process}$ =2 $\dot{m}\ c_p\ \Delta T_{oil}$.

- Set the inlet oil temperature as calculate in this project (figure 7.2) related to the new heat flow rate. $T_{in\_oil\_model\_2}$.
- Verify if the outlet oil temperature is almost the same as calculated in this work.
- Measure the temperature on the outer roller surface on the web side, in many points and check if:
    - The values of measured temperature are actually close to the required one.
    - The temperature gradient is less than the maximum threshold required by the customer or by the process.

REFERENCES

[1] http://www.shell.com/

[2] Cesare Bonacina, Alberto Cavallini, Lino Mattarolo, “Trasmissione del Calore”, 3rd ed., CLEUP editor , Padova, 1989.

[3] Volker Gnielinski, “VDI Heat Atlas”, 2nd ed. (VDI-Buch), Springer editor, 2010.

[4] Ansys 14.0 Help.

[5] http://www.linn-pumpen.de/com/Zahnradpumpen.php.

[6] Luisa Rossetto, “Dispensa di Termodinamica Applicata” , Padova, 2007.

[7] http://www.efunda.com/materials/alloys/alloy_home/steels_properties.cfm.

[8] Reda I. Elghnam. Experimental and numerical investigation of heat transfer from a heated horizontal cylinder rotating in still air around its axis. Ain Shams Engineering Journal (2014); 5: 177-185.

[9] Youqi Wang, Xuekun Sun. Digital-element simulation of textile processes. Composites Science and Technology (2001), 61: 311-319.

[10] Byung Chul Ji, Young A Han, and Jietae Lee. Sequential Relay Autotuning Method for the temperature Control of Multizone Heated Rollers. International Journal of Control, Automation, and System (2009); 7(6): 918-921.

[11] Walter Fung. Coated and Laminated Textiles. Woodhead Publishing, 2002.

[12] D. Veit. Simulation in Textile Technology: theory and applications. Woodhead Publishing, 2012.

[13] Dr. Ing. Andreas Giessmann. Coating Substrates and Textiles; A Practical Guide to Coating and Laminating Technologies. Springer editor, 2012.

[14] http://www.mengesroller.com/

[15] http://www.americanroller.com/

[16] http://www.fourwents.com/

[17] http://www.van-baal.com/

[18] http://www.macroeng.com/

[19] http://www.ptonline.com/

[20] http://haehl.com/

[21] http://www.dotcoat.com/

[22] http://www.ar-walzen.de/

[23] http://www.gmp.com/

[24] http://www.blackbros.com/

[25] http://www.comaintel.com/

[26] http://www.pcmc.com/

[27] http://www.wumag-texroll.de/